Characterization and Modeling of the Channel and Noise for Indoor MIMO PLC Networks

Rehan Hashmat

N° d'ordre : 2012telb0230

Sous le sceau de l'Université européenne de Bretagne

Télécom Bretagne

En habilitation conjointe avec l'Université de Rennes 1

Ecole Doctorale – MATISSE

Caractérisation et modélisation du canal et du bruit pour les réseaux CPL MIMO domestiques

---

Thèse de Doctorat

Mention : Traitement du signal et télécommunications

Présentée par **Rehan Hashmat**

Département : Signal et communication

Laboratoire : Lab-STICC

Directeur de thèse : Thierry Chonavel

Soutenue le 21 juin 2012

Jury :

Mme Fabienne Nouvel	Professeur	INSA de Rennes
Mme Martine Lienard	Professeur	Université de Lille
M. Raymond Quéré	Professeur	Université de Limoges
M. Andréas Schwager	Ingénieur	EUTEC-SONY Deustchland
M. Pascal Pagani	Ingénieur	Orange Labs, Lannion (Co-encadrant de thèse)
M. Thierry Chonavel	Professeur	Télécom Bretagne, Brest (Encadrant de thèse)

Dedication

To my Parents and Teachers

Thanks

The doctoral thesis work presented in this document was performed at Orange Labs with the collaboration of Telecom Bretagne. I am cordially grateful to all the people who helped and encouraged me during the course of my Ph.D. work.

First of all, I am extremely thankful to the director of my thesis Mr. Thierry Chonavel, professor at Telecom Bretagne, for his availability and guidance during my thesis. I also offer my heartiest gratitude to the co-director of the thesis Mr. Pascal Pagani, R&D engineer at Orange Labs, for supervising my research work and sparing time for me whenever I needed his help.

I express thanks to Mr. Yvon Guedes, chief of the laboratory DEAN, and Mr. Benjamin Barlaud, head of the EMC unit at France Telecom R&D Lannion for permitting me to conduct my research work at the hi-tech facilities under their charge, and providing me an excellent working environment.

I am equally grateful to all the colleagues for their memorable company and encouragement especially Fabienne, Farah, Hassina, Raluca, Ahmed, Brice, Rolland, Mohamed T, Alain, Michel, Adil, Slim, Amilcar, Rabah, Fred, Sylvain, Pascal B., Francis, Hakim, Pierre, Mohamed B, Philippe, Bezeid, David, Hervé …

Table of contents

List of figures

List of tables

Glossary

ADSL	Asymmetric Digital Subscriber Line
AWG	Arbitrary Waveform Generator
AWGN	Additive White Gaussian Noise
BER	Bit Error Rate
BPL	Broadband over Power Line
CDF	Cumulative Distribution Function
CM	Common Mode
CSI	Channel State Information
CTF	Channel Transfer Function
DM	Differential Mode
DSL	Digital Subscriber Line
DSO	Digital Sampling Oscilloscope
EMC	Electromagnetic Compatibility
EVD	Eigen Value Decomposition
FDM	Frequency Division Multiplexing
FFT	Fast Fourier Transform
FIR	Finite Impulse Response
FTTH	Fiber To The Home
HPAV	HomePlug AV
IEEE	Institute of Electrical and Electronics Engineers
IFFT	Inverse Fast Fourier Transform
IP	Internet Protocol
ISI	Inter Symbol Interference
ITU	International Telecommunication Union
MAC	Media Access Control
MIMO	Multiple Input Multiple Output
MMSE	Minimum Mean Square Error
MTL	Multiconductor Transmission Line
MTS	Multivariate Time Series
OFDM	Orthogonal Frequency Division Multiplexing
OMEGA	hOME Gigabit Access
OQAM	Orthogonal Quadrature Amplitude Modulation
PE	Protective Earth
PL	Power Line
PLC	Power Line Communication

PLT	Power Line Telecommunications
PSD	Power Spectral Density
QAM	Quadrature Amplitude Modulation
RMSE	Root Mean Square Error
SA	Simulated Annealing
SISO	Single Input Single Output
SMX	Spatial Multiplexing
SNR	Signal to Noise Ratio
STBC	Space Time Block Code
SVD	Singular Value Decomposition
TTS	Trivariate Time Series
VAR	Vector Auto-Regressive
VDSL	Very high bit rate Digital Subscriber Line
VNA	Vector Network Analyzer

Introduction Générale

Durant les dernières décennies, l'industrie des télécommunications a évolué très rapidement. Cette évolution a engendré l'invention de téléphone mobile, de la technologie *Digital Subscriber Line* (DSL), des services *Internet Protocol* (IP), etc. Il y a une demande incessante pour des débits plus élevés, et de services dans la garantie d'une haute Qualité de Service (QoS). Satisfaire ces demandes est un véritable défi pour les fournisseurs des services de télécommunications. Les réseaux mobiles permettent principalement la mobilité des clients, mais ils ne peuvent pas assurer de très hauts débits. Le Wi-Fi est également une solution sans fil très commune pour l'accès aux services. Il offre des débits de l'ordre de quelques dizaines de mégabits par seconde (Mbps) avec une mobilité limitée. L'inconvénient principal des réseaux sans fil est la variation inconnue de la stabilité du lien radio. D'autre part, la performance des réseaux sans fil est affectée par l'interférence électromagnétique. En conséquence, les services demandant des débits importants sont fournis par les réseaux filaires.

Actuellement, les services à haut débit sont délivrés aux clients via des liens optiques, Ethernet et la technologie *Very High Speed DSL* (VDSL). Le déploiement d'un réseau filaire est onéreux car il demande des travaux d'installation de l'infrastructure. Généralement, les fibres optiques qui servent comme un réseau d'accès sont déployés sous terre, et nécessitent une planification à long terme. La technologie *Fiber To The House* (FTTH) prolonge les fibres optiques jusqu'à la maison du client. Mais, pour profiter des avantages de la fibre optique, il faut installer une infrastructure supplémentaire jusqu'à la maison du client. Les technologies VDSL et Ethernet souffrent de la même contrainte. La plupart des services de télécommunication et de loisirs, comme par exemple l'Internet, la voix, la télévision et les jeux vidéo, sont fournis via la technologie IP. Pour profiter de ces services dans la maison, les différentes pièces sont équipées de terminaux, comme par exemple un ordinateur, un téléviseur ou une console de jeu. Cependant, les terminaisons de connectivité à haut débit ne sont pas disponibles dans chaque pièce. Par exemple, la technologie ADSL utilise la ligne téléphonique existante pour délivrer les services à haut débit. Généralement, une maison est équipée d'une ou deux prises téléphoniques, donc la connectivité Internet n'est pas omniprésente dans la maison. De plus, on ne trouve pas les câbles Ethernet préinstallées dans une maison commune. Ainsi, l'installation de nouveaux câbles dans la maison peut être prohibitive pour les clients pour des raisons pratiques ou esthétiques.

Les clients ont besoin d'un réseau haut débit omniprésent et fiable dans la maison. La technologie Courants Porteurs en Ligne (CPL) répond à ce besoin de couverture des services à haut débit sans nécessiter l'installation de nouvelle infrastructure. En effet, les circuits électriques, initialement installés pour délivrer l'énergie électrique à la maison, sont utilisés par la technologie CPL comme un canal de transmission. Les circuits et les prises électriques sont généralement présents dans chaque pièce de la maison. Ainsi, la technologie CPL peut fournir la portée maximale des services de télécommunication à haut débit et atteindre l'ensemble de la surface de la maison. Actuellement, des débits de plusieurs centaines de Mbps sont atteints en utilisant la technologie CPL.

En France, les circuits électriques domestiques délivrent généralement un courant de secteur sur une phase, à une tension de 230 Volts et une fréquence de 50 Hz. Ainsi, les câbles utilisés pour construire le réseau électrique domestique sont conçus pour délivrer des courants à basse fréquence et haute tension. Ces câbles ne sont pas construits pour transporter des signaux de télécommunication à haute fréquence. En conséquence, le réseau d'énergie électrique offre un environnement très défavorable pour les signaux de télécommunication. D'autre part, la présence des appareils électriques domestiques aggrave les conditions de transmission sur ce canal, en raison des bruits électromagnétiques qu'ils génèrent par eux. Pour garantir un accès à haut débit fiable via la technologie CPL, il est nécessaire d'étudier le canal de transmission et le bruit électromagnétique liés à cette technologie.

Dans la plupart des pays développés, le câble utilisé pour construire le réseau domestique d'énergie est constitué de trois fils : le fil de Phase (P), le fil de Neutre (N) et le fil de Terre (en anglais, *Protective Earth*, PE). Les systèmes CPL actuels utilisent les fils P et N (que l'on notera port P-N) pour émettre et recevoir des signaux de manière différentielle. Typiquement, il s'agit d'un mode transmission utilisant un capteur à l'émission et un capteur à la réception, ce que l'on nomme généralement transmission *Single Input Single Output* (SISO). Dans le domaine de la communication sans fil, les techniques *Multiple Input Multiple Output* (MIMO) sont largement employées pour augmenter la capacité du canal. Elles consistent à utiliser plusieurs antennes à l'émission et plusieurs antennes à la réception et bénéficier ainsi de la diversité du canal. Dans le contexte CPL, la présence du fil PE dans les prises électriques de transmission et de réception permet d'envisager la possibilité d'utiliser plusieurs ports d'émission et de réception, ce qui constitue un canal de communication MIMO. Des mesures et des simulations réalisées pour les canaux de

transmission CPL ont montré une nette augmentation de la capacité du canal en utilisant les techniques MIMO par rapport aux systèmes traditionnels SISO.

1. Objectifs de la thèse

L'objectif principal de cette thèse est l'étude et l'exploration des canaux CPL domestiques dans le contexte MIMO. Il s'agit d'une étude détaillée des technologies CPL existantes et d'une investigation des caractéristiques des canaux CPL MIMO. Les objectifs principaux de la thèse sont :

- Le développement d'un protocole de sondage afin de réaliser des mesures intensives du canal de transmission et du bruit électromagnétique sur les réseaux CPL domestiques. L'objectif est de générer une base de données riche et réaliste. La base de données obtenue par les mesures permettra d'évaluer la capacité du canal CPL MIMO.
- La caractérisation et la modélisation du canal de transmission CPL MIMO domestique via un ensemble de paramètres, en utilisant les mesures de canal obtenues par la campagne de mesure. La performance du modèle de canal sera évaluée par la comparaison entre les canaux simulés et les canaux mesurés.
- La caractérisation et la modélisation du bruit électromagnétique CPL MIMO via plusieurs paramètres, en utilisant les mesures de bruit obtenues par la campagne de mesure. La performance du modèle de bruit sera évaluée par la comparaison entre le bruit simulé et le bruit mesuré.

2. Organisation de la thèse

Le premier chapitre de la thèse présente l'état de l'art de la technologie CPL. Ce chapitre décrit brièvement l'histoire de technologie CPL. Nous présentons également une vue globale des acteurs principaux du développement de cette technologie, notamment les groupes industriels et les groupes de normalisation. Nous décrivons les normes principales développées pour la technologie CPL. Par ailleurs, les projets internationaux traitant de l'exploration et de la caractérisation des systèmes CPL sont présentés. Les réseaux CPL SISO domestiques et leur caractérisation sont décrits brièvement, avec un focus particulier sur les études sur le canal de transmission et le bruit. Finalement, ce chapitre donne une introduction aux particularités des canaux de transmission et du bruit pour le CPL MIMO.

Le deuxième chapitre de la thèse s'intéresse aux campagnes de mesures que nous avons réalisées. Nous présentons les mesures des canaux de transmission et du bruit

électromagnétique sur les réseaux CPL dans le contexte MIMO. La méthodologie de mesure est d'abord discutée, et l'équipement utilisé ainsi que les dispositifs de mesure sont détaillés. Par la suite, les observations expérimentales et les résultats obtenus à partir des données mesurées sont présentés. Enfin, nous décrivons les statistiques des capacités de transmission en modes SISO et MIMO, et nous évaluons le gain obtenu par l'utilisation de la technique MIMO. Ce chapitre présente également nos résultats sur la corrélation des bruits MIMO.

Dans le troisième chapitre, on procède à la caractérisation des canaux CPL MIMO via plusieurs paramètres, comme par exemple la corrélation des canaux, l'étalement des retards et la bande de cohérence du canal. A partir de cette caractérisation, nous présentons un modèle du canal CPL MIMO basé sur le formalisme de trajets multiples. Les paramètres du modèle sont obtenus à partir des données mesurées en utilisant des techniques d'optimisation. Finalement, le modèle proposé est validé par la comparaison entre les canaux simulés et les canaux mesurés.

Le quatrième chapitre de cette thèse se concentre sur la caractérisation et la modélisation du bruit de fond dans les canaux CPL MIMO. Tout d'abord, on propose deux modèles de bruit de fond dans le domaine fréquentiel, basés sur deux modèles de la littérature : le modèle du projet OMEGA et le modèle d'Esmailian. Les paramètres des deux modèles sont obtenus à partir des données mesurées, en utilisant une technique d'ajustement de courbes. Dans la dernière partie de ce chapitre, nous proposons un modèle détaillé du bruit de fond dans le domaine temporel, permettant de conserver les propriétés de corrélation du bruit CPL MIMO. Ce modèle est basé sur un formalisme de filtrage par auto-régression vectorielle (en anglais *Vector Auto-Regressive*, VAR). Enfin, on présente un modèle global de canal de transmission CPL MIMO, en incorporant le modèle de canal proposé dans le chapitre 3 et le modèle de bruit proposé dans le chapitre 4. Le canal MIMO global est validé en comparant les statistiques d'étalement des retards des canaux simulés avec les canaux mesurés.

General introduction

During the recent decades the telecommunication industry has gone through a rapid evolution. This has led to the advent of mobile phones, DSL technology, IP services etc. There is an ever increasing demand of data rates, services and of guaranteed Quality of Service (QoS). The telecom service providers face a challenge to fulfill the requirements of the customers. The mobility needs of the customers are satisfied through the mobile phone networks. However, the mobile phone networks provide a limited data through put. The other wireless solutions which is popular for data services access is the Wi-Fi. The Wi-Fi offers data rates of the order of some tens of Mbps with the facility of limited mobility. The major drawback of the wireless networks is the variable link reliability. Moreover, the performance of a wireless network is affected by the electromagnetic interference as well. Therefore, high speed services rely mostly on the wired networks.

Currently, high data rate services such as the high speed internet are provided through optical fiber links, Ethernet and VDSL technology. The deployment of a wired network is costly and demands physical effort. The optical fibers generally serve as a backbone access networks and are deployed underground with long term planning. The fiber to the house (FTTH) technology stretches the optical fibers to the customer premises but to reap the benefits of the fiber supported high through put additional infrastructure should be installed within the house. Same is the case with VDSL technology. Most telecom and entertainment services, for example the Internet, voice, TV and live video games, are provided through IP technology. In many houses more than one room are equipped with the terminals, for example a computer, a television and a play station, to access such services. However, high data rate terminals are not available in each room. ADSL technology uses the existing telephone line to deliver the high bit rate services. Generally, a house is equipped with one or two telephone outlets so the internet connectivity based on VDSL is not ubiquitous within the house. Similarly, one does not find preinstalled Ethernet cables in a common house. Installation of the new cables in the house may be prohibitive for the customers for esthetic reasons as well.

The customers require a ubiquitous, high speed and reliable data network within the house. The Power Line Communication (PLC) technology provides the omnipresence of high speed data services without requiring the installation of new infrastructure. The existing household electrical wiring which is basically used to deliver the

electrical energy to the house is used by the PLC technology as a transmission channel. The electrical wiring and the power outlets are generally present in every room of the house. Therefore, the PLC technology can provide the maximum reach of the high speed telecom services in every corner of the house. The data rates of several hundreds of Mbps are realized by the PLC technology.

The household electrical wiring is usually a single phase power delivery network which carries the 230 volts of AC mains at 50 Hz. The cables used to construct the wiring network are originally designed to carry low frequency, high voltage electrical power. They are not intended to transport high frequency telecom signals with guaranteed fidelity. In fact the electrical power network offers a harsh environment for telecom signals. Moreover, the presence of electrical appliances further aggravates the channel conditions because of various types of noises generated by them. Therefore, in order to guarantee a reliable and high speed access via the PLC technology, it becomes necessary for the telecom service providers not only to study the PLC channel and noise but to explore new communication strategies over the power lines as well.

In most developed countries the cable used for household electrical wiring consists of three wires: Phase (P), Neutral (N) and Protective Earth (PE). The existing PLC systems use the P-N port to transmit and receive the signals. It is a typical single input single output (SISO) transmission. In the field of wireless communications the multiple input multiple output (MIMO) techniques are used to increase the link capacity. In the PLC context the inclusion of the PE wire at transmit and receive outlets leads to the availability of multiple transmit/receive ports which in turn leads to the realization of a MIMO communication channel. It has been shown through measurements and simulations over the PLC channels that the MIMO techniques can achieve more channel capacity compared to the existing SISO systems.

3. Thesis objectives

The principle objective of this thesis is to study and explore the inhome PLC channels in the MIMO context. This includes a thorough study of existing PLC technologies and the investigation of the character of MIMO PLC channels. The main objectives of the thesis are categorized as the following:

- Development of a channel sounding protocol to perform extensive channel and noise measurements on the inhome PLC networks, with the objective of generating a rich and realistic database. Evaluation of the MIMO PLC channel capacity by utilizing the database obtained from the measurements.

- Characterization and modeling of the inhome MIMO PLC channel through a set of parameter by utilizing the measured channel data. Evaluation of the performance of the channel model by comparing the simulated channels parameters with the measured ones.
- Characterization and modeling of the MIMO power line noise through various parameters by utilizing the measured noise data. Evaluation of the performance of the noise model by comparing the simulated noise characteristics with the measured noise.

4. Organization of the thesis

The first chapter of the thesis is about the state of the art of the PLC technology. This chapter describes a brief history of the PLC technology. A global picture of various major players in the domain of PLC is presented. It consists of the industrial groups, the standardization bodies, etc. We have also stated the main standards framed for the PLC technology. The international projects launched to explore and characterize the PLC technology are also added. A brief account of indoor SISO PLC networks and their characterization is provided by including various studies on the PLC channel and noise. The chapter finally introduces the MIMO PLC channels and noise.

The second chapter of the thesis is dedicated to various measurement campaigns that we performed. It includes the MIMO PLC channel and noise measurements. We discuss the measurement methodology, the equipment and the measuring instruments. The observations, findings and results obtained from the measured data are included in this chapter. We present statistics of the SISO and MIMO capacities and the MIMO capacity gains. Results obtained about MIMO noise correlation are also added.

In the third chapter we demonstrate the characterization of the MIMO PLC channels through various parameters such as channel correlation, RMS delay spread and coherence bandwidth. A MIMO PLC channel model is presented, based on the multipath formalism. The model parameters are extracted from the measured data via curve fitting. The proposed model is validated by comparing the simulated channels with the measured ones.

The fourth chapter of this thesis concentrates on the characterization and modeling of the MIMO power line background noise. First we propose two frequency domain background noise models based on the Omega Project model and the Esmailian model. The parameters of the two proposed models are extracted from the measured noise data via curve fitting. In the second half of this chapter we propose a complete time

domain model of the background noise by using the formalism of the vector autoregressive (VAR) model. In the end a global MIMO channel model is described by incorporating the channel model proposed in chapter 3 and the noise model proposed is chapter 4. The global MIMO channel model is validated by comparing the delay spread statistics of the simulated channels to the measured ones.

Chapter .1
State of the art

1. Introduction

Power Line Communication (PLC) is a system for carrying information on a conductor which is primarily used for electrical power transmission. Electrical power is transmitted over high voltage transmission lines, distributed over medium voltage and used inside buildings at lower voltages. Power line communications can be applied at each stage for various applications.

The evolution of PLC spans more than one hundred years. The technology of information transfer over the power lines was first employed for exchange of telemetry and telecommand of the power grid system. In the later years, many inhome applications emerged, for example, the automation of domestic appliances and security of buildings, homes etc. The Power Line Communication, like any technology, has covered certain stages to attain its present day form. Having started from very low data rate applications, today PLC is promising to deliver broadband services at customer premises. As early as 1838, remote electricity supply metering was proposed for the purpose of checking the voltage levels of the batteries at unmanned sites. In 1897 a power line signalling electricity meter was patented. From 1900's to 1970's, following the evolution in electronics, many developments were made for remote reading of electricity meters [Brow99].

The first major application involving data transmission over power lines was for the protection of power distribution system in the case of fault. In fact, telemetry or telecommand for power distribution network on high voltage power lines is still one of the primary functions of power line communications [Gall11]. When a fault occurs, the exchange of information is necessary between power plants, substations and distribution centres so as to avoid or minimize the damage. The robustness of the power lines and their ready connectivity and availability make the PLC technique an

optimal solution. Narrowband power line communications started soon after the beginning of wide-spread electrical power supply. Around the year 1922 the first carrier-frequency systems began to operate over high-voltage lines in the frequency range from 15 to 500 kHz for telemetry purposes, and this continues to the present time [Yous08].

The primary motivation for the development of power line communications is the load management of the grid system. Considering that data transmission over the power lines has been around for quite some time, one might wonder why it is receiving such renewed attention recently especially considering the data rate for protection and telemetry purposes is at most a few kb/sec and is not comparable to the Mb/sec data that needs to be supported for multimedia applications? The answer is a combination of effects that took place during the 1990s, namely, the explosive growth of the Internet and the gigantic leaps in VLSI (Very Large Scale Integration) and DSP (Digital Signal Processing) technology. In addition, the telecommunication market was deregulated, first in the US and then in Europe and Asia. All these events have made power line communications a viable technology for numerous applications necessitating high data rates in the 1 to 100 Mbps bandwidth.

2. Standards, major players and projects

2.1. PLC ecosystem

There are various manufacturers, operators and standardization groups in the domain of PLC technology. Some groups are chip manufacturers such as Gigle and Spidcom. Some groups are large telecom operators such as France Telecom and British Telecom.

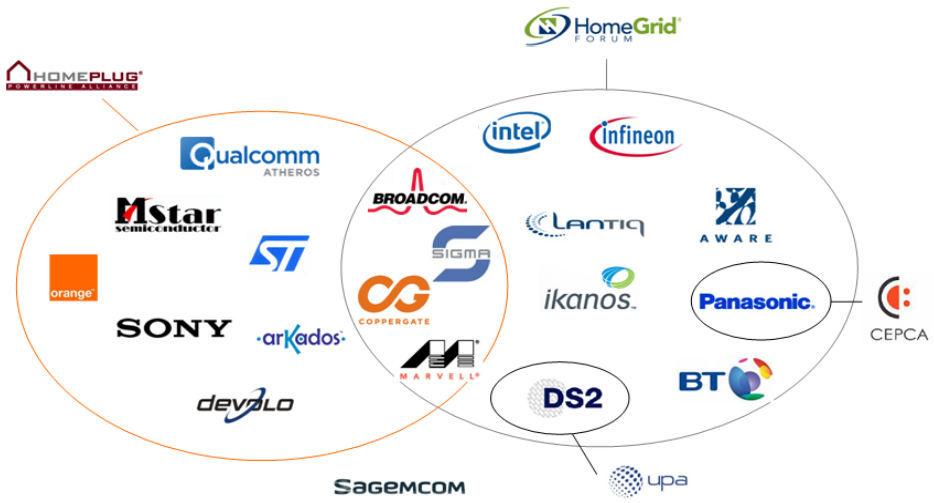

Figure 1.1. Major industrial groups and consortiums in the PLC technology

The PLC ecosystem is shown in Figure 1.1. The major consortiums are HomePlug Powerline Alliance and Home Grid Forum.

2.2. Standards

Standardization bodies for telecommunications are involved in many discussions regarding the possible evolution of PLC systems. The standards are proposed to meet the following major targets:

- General requirements
- Safety
- Electromagnetic compatibility
- Performance & interoperability

The PLC standardisation is performed by different Standard Definition Organizations (SDO) such as ETSI PLT, IEEE P1901, and ITU G.hn. In addition, numerous industrial consortiums are active in the development of PLC technology, such as the HomePlug Powerline Alliance and the Home Grid Forum.

2.2.1. ETSI

ETSI standards have a significant importance as far as the overall interoperability with the Electricity standards in Europe is concerned. ETSI TC (Technical Committee) PLC aims to develop high quality standards and specifications to provide telecommunication services via the existing public and private mains power networks. Standards are developed in sufficient details to allow interoperability between equipments from different manufactures and co-existence of multiple PLC systems within the same environment [Omega08a]. ETSI TC PLT is publishing and developing the necessary standards to make sure that the PLC successfully coexists with other technologies and services [ETSI].
The ETSI PLT requirements are given in:

- TR 102049 "Quality of Service (QoS) requirements for in-house systems": this document lists the categories of home application, home devices, service classes, traffic classes and QoS requirements.

- TR 102494 "Technical requirements for In-House PLC modems": for the moment, almost no technical specification is given on PHY and MAC layers.

ETSI has set up a Special Task Force STF 410 to study and compare MIMO characteristics of the Low Voltage Distribution Networks (LVDN). The STF 410

members are from Sony, France Telecom, Marvell, Spidcom, Devolo, JobAssist and the University of Duisberg-Essen. The STF 410 has performed MIMO channel and noise measurements in various European countries In addition, the task force has devised measurement setups, designed MIMO couplers and surveyed the existence of Protective Earth (PE) wire in many countries [ETSIa], [ETSIb], [ETSIc].

2.2.2. IEEE P1901

IEEE P1901 Standard has been officially published in January 2011. This standard is developed by IEEE working group and its objective is to achieve high capacity power line communication with PHY data rates of more than 100 Mbps. The standard covers the frequency band up to 100 MHz and it covers the access part (up to 1.5 Km from the user) as well as the local network part (up to 100 m from the terminals) [1EEE].The chipsets AR7400 compatible with IEEE P1901 have already been proposed by Qualcomm Atheros.

2.2.3. ITU G.hn

The G.hn working group is devoted to a new recommendation defining transceivers for in-premises networking over metallic conductors such as phone-line, co-axial, data and power cables. The IUT G.9960 standard has been released in 2009. It is expected that the first chipsets employing this standard will be available by early 2012. The maximum data rate and the QoS are defined to address the Triple Play (Internet, video over IP, telephone over IP). Though the announced data rates go up to 1 Gbps but this is probably true only for the coaxial cables. The original approach of the G.hn working group is to jointly address different types of existing wires in the home environment. This innovative approach should enable the deployment of a unique network using any wired medium available in the customer premises. In September 2011, ITU has released G.9963 standard which covers the MIMO functionality for PLC [ITU].

2.3. Major players

Thanks to the potential advantages associated with the PLC technology, it has caught the attention of various enterprises and research groups in the telecom community. Some major players are described here.

2.3.1. HomePlug power alliance (HPA)

The HomePlug Powerline Alliance, Inc. is an industry-led initiative. It was established to create specifications for inhome high-speed powerline networking

products and command & control among platforms. HPA formalises the broadband access services to the home as well. The Alliance accelerates demand for HomePlug-enabled products and services worldwide through the sponsorship of market and user education programs. Membership in the Alliance has grown to include more than 75 industry-leading companies. France Telecom is also participating as a telecom operator. HomePlug Powerline Alliance created several specifications for PLC standards such as HomePlug 1.0, HomePlug AV, HomePlug BPL, HomePlug Green PHY and HomePlug Command and Control. The latest HPAV 2.0 employs the MIMO functionality [HPA].

2.3.2. UPA

UPA (Universal PowerLine Association) is an international organization. UPA promotes DS2 chipsets and has created the Digital Home Standard (DHS), whose purpose is to provide a complete specification for the silicon vendors for designing integrated circuits for voice, video and data distribution using power lines [Omega08a], [UPA].

2.3.3. CEPCA

CEPCA (Consumers Electronics Powerline Communication Alliance) is another alliance that works to promote PLC. Its fourteen members are mainly Japanese manufacturers (Sony, Mitsubishi, Panasonic, etc.). The aim of CEPCA is to enable the different PLC systems to coexist. Panasonic (i.e. Matsushita Electric Industrial) promotes the HD-PLC (High Definition Power Line Communication) chipset, that uses a high frequency efficient Wavelet-OFDM modulation method, and a programmable notch filter that prevents from interference with other radio frequency transmissions such as amateur radio. The theoretical maximum data transmission rate is up to 190 Mbps [Omega08a], [CEPC].

2.4. Projects

2.4.1. OMEGA

The OMEGA project is dedicated to develop a user friendly home access network capable of delivering high bandwidth services and content at a transmission speed of one Gigabit per second. The interdisciplinary project consortium consists of 20 European partners from industry and academia. The project started in January 2008 and finished in December 2010. OMEGA is an Integrated Project in the ICT area co-funded by European Commission under EU Framework Program 7 (FP7). Given that the fiber to the house (FTTH) access promises symmetric data rates of at least 100

Mbit/s, this implies a home network supporting Gbit/s data transmission and a latency time in the millisecond regime. It implies that the performance of the home network must be high enough to maintain several services simultaneously, each with different requirements. Furthermore, it must be low-cost and easy to manufacture in at an industrial scale. The OMEGA home network aims to deliver Gbit/s capacity and low latency within the home and to the access network, with either wireless transmission or transmission using existing wired home infrastructure, thus enabling access to and the development of new and innovative services [Omega].

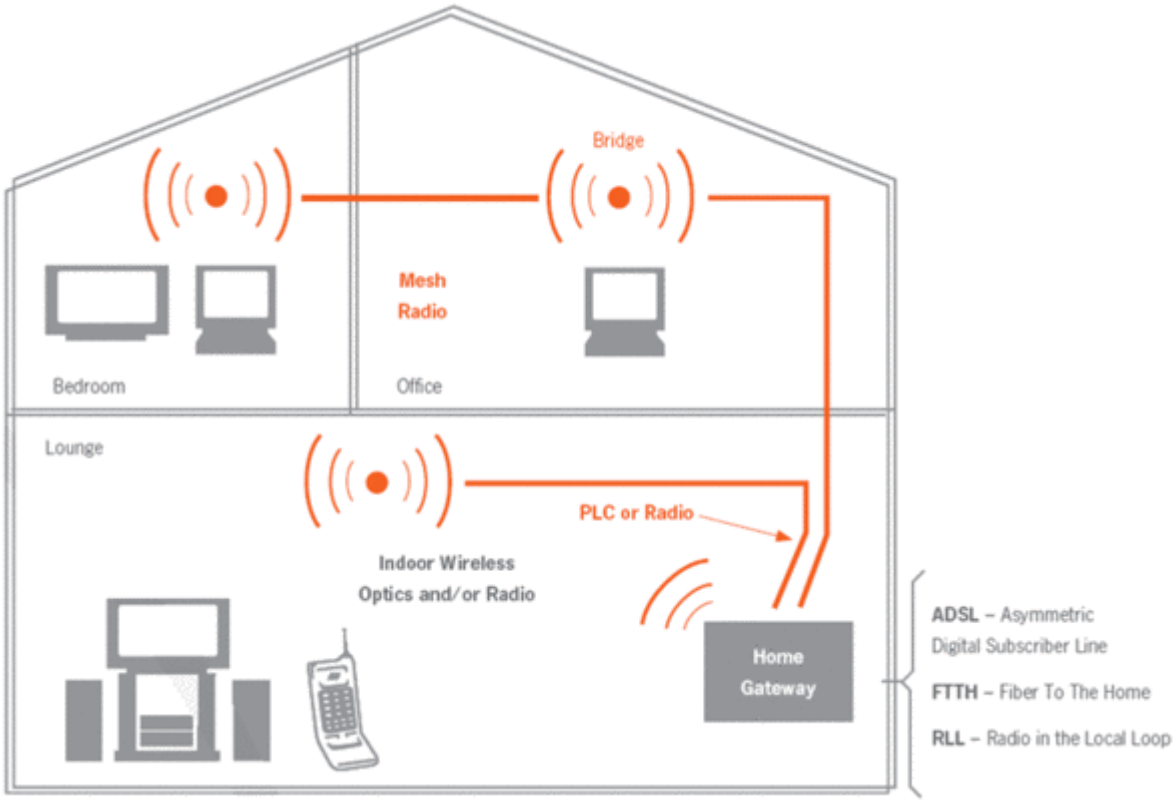

Figure 1.2. Inhome Gigabit network [Omega]

Figure 1.2 illustrates the network concept. Data enters the home and is routed by the home gateway. The gateway in turn is connected to OMEGA hardware, which can deliver Gbit/s data transmission. Room-area communications is provided through 60 GHz ultra wide band (UWB) radio or by the use of visible-light communications. To extend ultra broadband penetration, the gateway can also use lower frequency RF to connect to the terminals, or use power-line communications (PLC) beyond 100 Mbps to connect to OMEGA bridges within the house. Bridges can alternatively or complementarily be networked by means of high speed radio backbone, leading to the first hybridization of the wired and wireless connectivity.

2.4.2. Powernet

This project has been completed in 2008. The Powernet project has as a goal to demonstrate and validate the new cognitive broadband over power lines (CBPL) under real world conditions in field trials using a large number of CBPL equipment. This project was motivated because the technology has a big market potential. The main advantage of Broadband over Power Line (BPL) over the other broadband is that there are no new cables to be deployed as they are already in place. The new, cognitive BPL (CBPL) technology has been developed during the last two years, based on the detailed knowledge of the problems encountered in the previously conducted field trials. The CBPL technology has been successfully simulated using MATLAB. The results are very promising: higher data rates are achievable (up to 300 Mbps) with lower transmit power spectral density, e.g. lower electromagnetic radiations. The leakage energy in the frequency bands allocated to other users is as low as -100dBm/Hz so that CBPL do not interfere with other users [Powe].

2.4.3. OPERA

The strategic objective of the OPERA project was to push PLC technology in all relevant aspects (standardization, technology improvement, installation tools and processes, telecom services, intelligent grid services, dissemination) so as to allow it to become an alternative that offers broadband access to all European citizens using the most ubiquitous infrastructure. This development of the PLC technology will contribute to develop the European Information Society in full concordance with the proposed objectives in the plan eEurope 2005 by the means of:

- Increased competition in the broadband access: PLC networks can be quickly and easily deployed without large investments by using the existing electricity networks. PLC is a ubiquitous solution for access and in-home distribution that will contribute to have a real alternative last-mile access network.
- Fostering mass services availability: PLC features such as the transparent integration with different communication technologies (WiFi, etc.) and the complete end-user coverage will contribute to the deployment of value-added-services over broadband such as: smart home, video streaming, e-health, VoIP, etc.
- European industry leadership: PLC technology know-how and technical excellence are currently located in Europe. This represents an extraordinary opportunity for the development, competitiveness and leadership of European Broadband Industry that will contribute to the creation of employment, to the development of the information society technologies in Europe and to the socio-economic prosperity in EU [Oper].

The tasks related to the physical aspects, such as transmission and peripheral support for the deployment of PLC networks, were carried out in the OPERA project. The OPERA project had an estimated duration of 48 months.

2.5. Electromagnetic compatibility of PLC technology

From the Electromagnetic Compatibility (EMC) point of view, an equipment or system must neither be the source nor the victim of undesired electromagnetic noise in its operational frequency band. The transmission of the perturbations between a transmitter and a receiver is either through conduction or through radiation. In Europe, the PLC equipment must respect the CISPR22 standard which concerns the radio electric perturbations [CISP].

2.5.1. Limits of conducted perturbations

The EN55022 standard, the European adaptation of CISPR22, specifies the limits of conducted perturbations for 220 V Information Processing Equipment (IPE). The EN55022 standard divides the IPE's into two classes: Class A and Class B. The Class B is for the residential IPE's. As an example, we present perturbation limits defined for Class B equipment in Table 1.1 and Table 1.2 [Bric12].

Frequency Range MHz	***Limits of voltage dB(µV)***	
	Peak	***Mean value***
0,15 to 0,5	*66 to 56*	*56 to 46*
0,5 to 5	*56*	*46*
5 to 30	*60*	*50*

Table 1.1 Limits of conducted perturbations at 220 V power supply

Frequency Range MHz	***Limits of voltage dB(µV)***		***Limits of current dB(µA)***	
	Peak	***Mean value***	***Peak***	***Mean value***
0,15 to 0.5	*84 to 74*	*74 to 64*	*40 to 30*	*30 to 20*
0.5 to 30	*74*	*64*	*30*	*20*

Table 1.2 Limits of common mode (CM) conducted perturbations at telecom access

2.5.2. Limits of radiated perturbations

In the framework of OMEGA project which proposes to extend the PLC frequency band up to 100 MHz, it has been found useful to apply the limits stated in EN55022

standard. As an example, the perturbation limits for the Class B IPE's are mentioned as shown in Table 1.3 [Prah12]:

Frequency Range MHz	*Peak Limit dB(µV/m)*
30 to 230	*30*
230 to 1000	*37*

Table 1.3 Limits of radiated perturbations at a distance of 10 m

2.5.3. IEC/CISPR Project Team PLT

The activities of CISPR/I committee of International Electrotechnique Commission (IEC) are related to the EMC issues of the IPE's. The sub working group CISPR-22-PLT has been given the task to prepare an amendment to the CISPR22 standard. This amendment has the objective to define the test methods and emission limits for the PLC equipments. After ten years, this committee has abandoned its works after failing to find an accord on the standard it has developed. Since then, the task of preparing the amendment, at European level, has been handed over to the technical committee TC210 of Comité Européen de Normalisation Electrotechnique (CENELEC) [Prah12].

2.5.4. CENELEC TC210

After the failure of IEC/CISPR to propose an amendment, the CENELEC initiated a new project to formulate an independent standard. The other objective was to answer the question of the mark "CE" for the PLC equipment in Europe. It is worth mentioning that the European Commission had published a ruling which deferred the application of a harmonized EMC EN55022 Ed 6.0 standard up till October 2011. This delay allowed the publishing of a document specific to the PLC equipments. In fact, the limits defined by EN55022 standard in the frequency band below 30 MHz do not permit the PLC equipment to attain a high level performance. The final project of European Norm (NE) by CENELEC (EN 50561-1) for the EMC of indoor PLC equipment was proposed for a vote and was rejected in September 2011. The European Commission is planning to submit the document for a second vote after considering the comments of national committees. Today, no globally harmonized standard for EMC in the domain of PLC exists [Prah12].

3. Indoor PLC networks

3.1. Electrical wiring

An inhome electrical network is a 3-wire single phase network as shown in Figure 1.3. The electrical energy is conveyed to the lights, embedded appliances (consisting of immobile loads such as fans, refrigerator etc.) and various sockets or outlets.

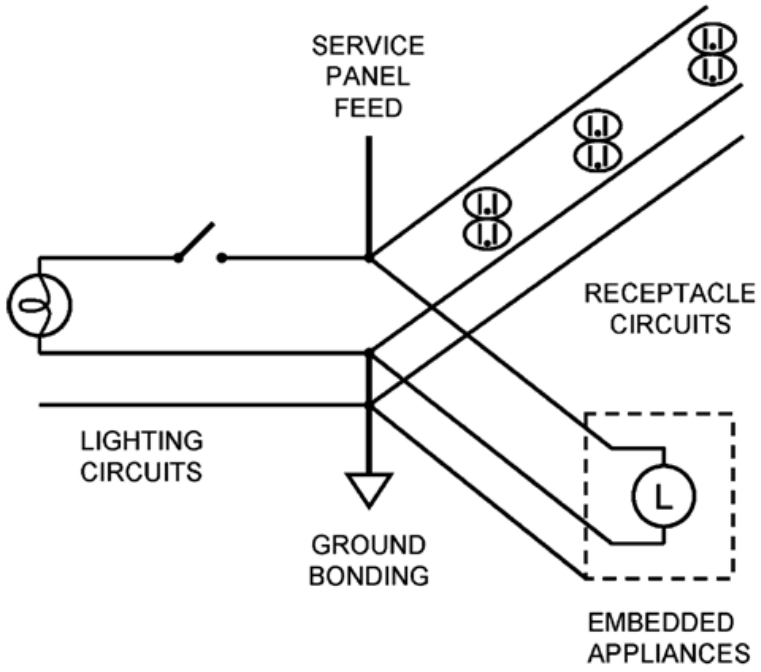

Figure 1.3. Inhome electrical network topology [Banw05a]

Three wires are: Protective Earth (PE), Neutral (N) and Phase (P). The circuit breakers act as a safety device against over currents or over voltages. The indoor PL network is distinguished from the outdoor distribution PL network in that cables are shorter but often less uniform in their geometry and the indoor PL network topology generally has more branches. The two networks overlap with the mains feed to the home. Commonly two voltage levels are found through out the world: 110 volts and 230 volts.

A typical indoor power-line network consists of a main service panel that contains the circuit breakers (Figure 1.4). The service panel feeds multiple branches that serve different rooms or appliances. Residential and commercial premises power-line networks usually comprise of a service panel feeding multiple branching paths that include outlet circuits, fixed or embedded appliances and lighting circuits. The resistance R_{SB} is a shunt resistance which connects the N and PE wires. L_2 and L_3 are

two loads. Different circuits have different balance/symmetry characteristics that affect the channel characteristics for the communications.

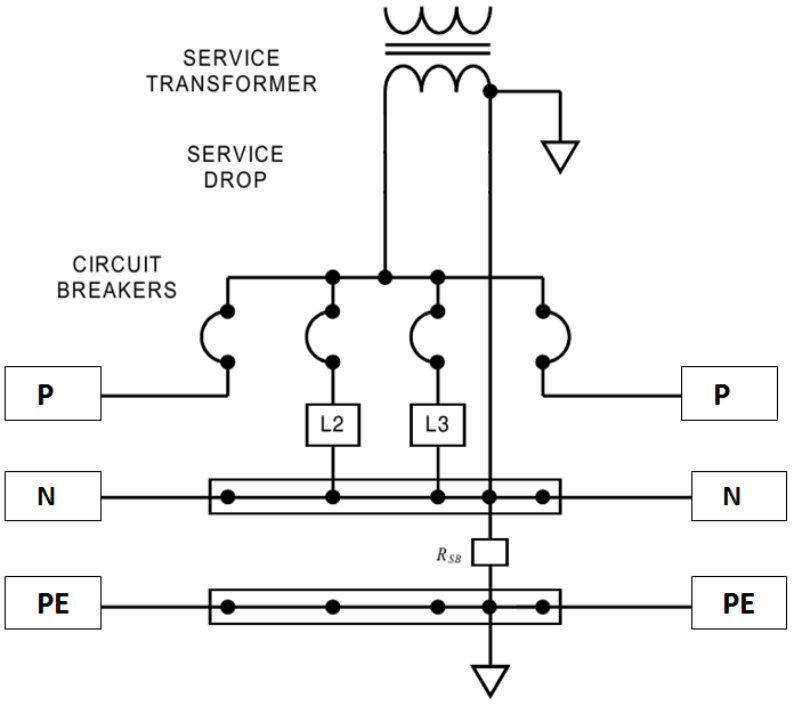

Figure 1.4. Indoor electrical network [Gall04]

There are a variety of configurations in different countries regarding how the power-line cables are shared among multiple devices. For example, some countries may have a tree or star configuration where a single cable feeds all the wall mounted power outlets (sockets) in a room. The ring configuration is also possible where a single cable runs around the house connecting different sockets and there may be multiple rings in the house. These configurations will determine the sharing of the cable (communication channel) among different devices. The sockets can be two-wire ungrounded outlets or three-wire grounded outlets - Some countries have a combination of the both [Jaga07].

3.2. SISO PLC channel model

The domestic wiring deployed for the supply of electricity in most modern day houses in Europe and United States consists of three wires: Phase (P), Neutral (N) and Protective Earth (PE). The existing PLC systems utilize only two wires (P and N) for signal transmission and reception. This is a typical single input single output (SISO) transmission between two P-N ports. The PLC channel consists of the channel transfer function (CTF) and the channel noise. In the PLC literature there are various

attempts to characterize and model the SISO PLC channels. However, till date no agreed upon channel model is available in the PLC domain.

The electrical cables are an unsuitable medium for the PLC signals which are low level, high frequency signals. Such cables are designed for the transfer of electrical energy to the household appliances. The norms of domestic wiring are different for different countries. It is almost impossible to predict the topology of the PLC network in a house with absolute precision. The household electrical appliances and loads attached to the PLC network create various types of noise on the PLC network which is not straightforward to model. The PLC channel models are broadly categorized as top-down models and bottom-up models. The top-down models rely heavily on the measurements while the bottom-up models are based on the transmission line theory. The details of these two modeling approaches will be discussed in Chapter 3. Some channel and noise modeling attempts are be discussed in the following sections.

3.2.1. Multipath model

In this section we will discuss various PLC channel models based on the multipath formalism. The multipath model is one of the most common types of the channel models in the PLC domain. Such models fall in the category of the top-down models.

A PLC multipath channel model was firstly formalized by Zimmerman [Zimm02]. The PLC channel, according to this model, is visualized as a tapped network. The transmitted signal experiences scattering and multiple reflections within the channel. Along with the original signal, the receiver gets delayed and distorted copies of the original signal. The channel shown in Figure 1.5 has only one tap and consists of three segments A-B, B-C and B-D with lengths l_1, l_2 and l_3 and characteristic impedances Z_{L1}, Z_{L2} and Z_{L3} respectively. In a typical impedance mismatch scenario (which is the case in practical networks), theoretically, an infinite number of propagation paths is possible due to the signal reflections.

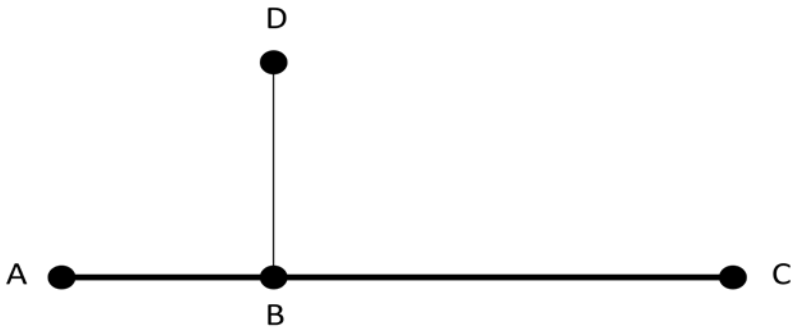

Figure 1.5. One tap power line network

Each path p has a weighting factor $g_p \leq 1$. The amplitude g_p reduces as the number of reflections increases. The physical length of a path also contributes to reduce the amplitude g_p. Therefore the infinite number of paths can be approximated to N_p dominant paths. The multipath model in [Zimm02] is defined as shown in Eq.1.1:

$$H(f) = A\sum_{p=1}^{Np} g_p e^{-j\frac{2\pi d_p}{v}f} e^{-(a_0 + a_1 f^K)d_p} \tag{1.1}$$

where H, f, g_p, N_p and d_p stand for the channel transfer function, frequency, path gain, the number of paths and path length respectively. In addition, $v=(2/3)c$ is the speed of electromagnetic waves in the cable material, where c is the speed of light in vacuum. It should be noted here A, a_0, a_1, and K are attenuation parameters. The same multipath channel model has been adopted in [He04], [Mell06], [Tlil03], [Roka05].

Using the multipath formalism, the impulse response of a PLC channel with 5 paths has been described in [Liu08]. The first path is considered to experience a Rician fading while for the later paths a Rayleigh fading has been noted. The model parameters have been extracted from measured channels.

In [Ma05], a time domain representation of the multipath model is described. It has been assumed that the channel does not change throughout the transmission of data. That is, the channel can be regarded as a time-invariant system. Such a system is defined by Eq. 1.2 in [Ma05].

$$h(t) = \sum_{n=1}^{N_p} \beta_n \delta(t - \tau_n) \tag{1.2}$$

where β_n and τ_n are the amplitude and arrival time of a multipath component respectively, and N_p is the number of paths.

Another time domain representation of the multipath model, which is similar to [Ma05] has been presented in [Zhan04]. It is a simple discrete time domain depiction of a channel impulse response based on the measurements on low voltage power lines.

3.2.2. **Model based on Transmission line theory**

This type of model falls in the category of the bottom-up models. This model is based on classical Multiconductor Transmission Line theory (MTL). The electrical wiring is studied as a network of transmission lines whose transmission properties can be fully characterized through the parameters like the transmission constant, attenuation constant, capacitance, inductance, resistance and conductance. Theoretically, given the topology of the PLC network, such a model can arrive at a very precise description of the channel. However, the exact topology of the PLC network is rarely known and this fact limits the utility of such models.

According to the two conductor transmission line theory, the paired power cables are regarded as networks of lumped circuit parameters, where voltages and currents can vary in magnitude and phase over its length. Hence, the PLC cable can be described by the lumped circuit parameters.

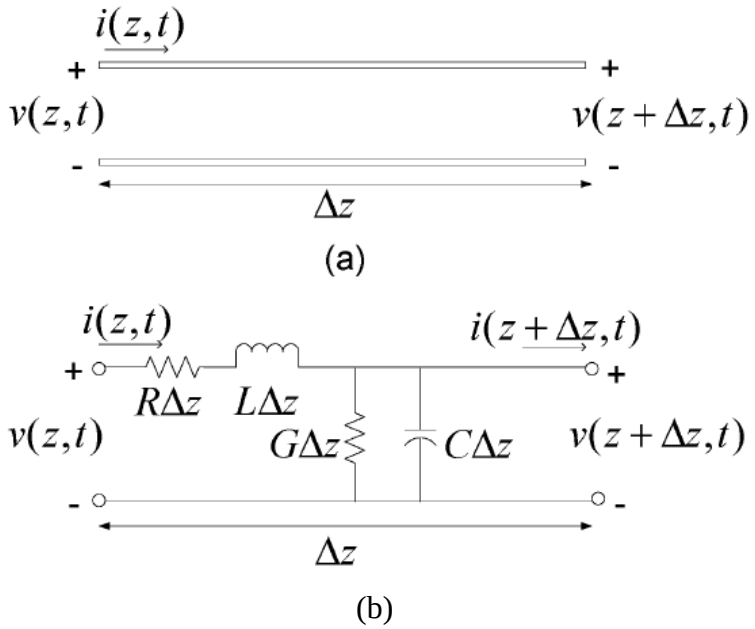

Figure 1.6. Two conductor transmission line (a), Equivalent lumped elements (b) [Meng04]

In Figure 1.6 (a), the quantities *v(z,t)* and *v(z+Δz,t)* denote the instantaneous voltages at location *z* and *z+Δz* respectively. Similarly *i(z,t)* and *i(z+Δz,t)* denote the instantaneous currents at *z* and *z+Δz* respectively. *R* defines the resistance per unit length (in *Ω/m*), *L* defines the inductance per unit length (in *H/m*), *G* is the conductance per unit length (in *S/m*), and *C* is the capacitance per unit length (in *F/m*). Based on the lumped-element circuit shown in Figure 1.6 (b), the two intrinsic parameters for the transmission line, i.e. *γ*, the propagation constant and *Zo* the characteristic impedance, can be written as shown in Eq. 1.3 and Eq. 1.4 respectively.

$$\gamma = \alpha + j\beta = \sqrt{(R + j\omega L)(G + j\omega C)} \tag{1.3}$$

$$Z_0 = \sqrt{\frac{R+j\omega L}{G+j\omega C}} \tag{1.4}$$

where ω is the angular frequency. The real part α and the imaginary part β of the propagation constant are the attenuation constant (in *Np/m*) and the phase constant (in *rad/m*) respectively. Note that both γ and *Zo* are characteristic properties of a transmission line even if the line is infinitely long. In other words, they depend on *R*, *L*, *G*, *C* and ω, but not the length of the line. As the power line has been modelled as a transmission line, its γ and *Zo* will dominate the wave behaviour along the line. In the model proposed in [Phil99], they serve as the parameters to model the transfer function of the channel.

The multiconductor transmission line (MTL) theory can be considered as a natural extension of the two-conductor modelling to include the presence of additional wires, for example, the PE wire. The PLC channel model based on the MTL theory is similar to the one based on two conductor transmission line theory. Therefore, the MTL theory approach has the advantages and the drawbacks similar to those of the two conductor model. However, the appealing feature of the MTL theory based model is that it is able to describe the PL channel more accurately than the one that ignores the presence of the PE wire [Gall06].

For the calculation of overall transfer function, the formalism of MTL theory is applied to each section of the network and the global CTF is obtained by cascading all the CTF's of all the sections [Robl07].

A SISO PLC channel model based on transmission line coefficients is described in [Kita08]. The model takes into account the network topology. It has been shown that the proposed model can efficiently generate the channel transfer function which is very similar to the measurements.

In [Tone10], a statistical bottom-up PLC channel model has been proposed in the 0-30 MHz range. In [Vers10] a statistical channel model based on transmission line theory has been considered. The approach allows maintain the connection between the physical topology and the theoretical formalism.

3.2.3. **Parametric characterization of the channel**

This channel modeling and characterization method is based on measurements. In this modeling methodology, first of all some key parameters are defined and they are extracted from the measured data. For example in [Tlic08], a SISO PLC channel characterization is described on the basis of channel capacity, coherence bandwidth and channel delay spread. The measurements are made in 7 houses and a total of 144 channels are measured. These channels are categorized on the basis of channel capacity. Figure 1.7 shows typical channels measured in the inhome environment. For us this approach is important because we use a similar methodology to characterize the MIMO PLC channels in chapter 3.

The channel capacity is evaluated by using Eq. 1.5. The parameters of Eq.1.5 are given in Table 1.4, the classification of the channels according to the capacity is shown in Table 1.5 and the class wise average attenuation models of the channels are shown in Table 1.6. Channels are generated through simulations and the accuracy of the model is validated by comparing the delay spread of modeled channels to the measured channels.

$$C = \Delta f \cdot \sum_{i=1}^{N} log_2\left(1 + \frac{P_e \cdot |H(f_i)|^2}{Pb}\right) \quad [bit/s] \tag{1.5}$$

Frequency Band	1 MHz – 100 MHz
Carrier spacing (Δf)	25 KHz
Number of carriers (N)	3960
Transmitted PSD (P_e)	-50 dBm/Hz
White noise PSD (P_b)	-140 dBm/Hz

Table 1.4 Channel capacity calculation parameters [Tlic08]

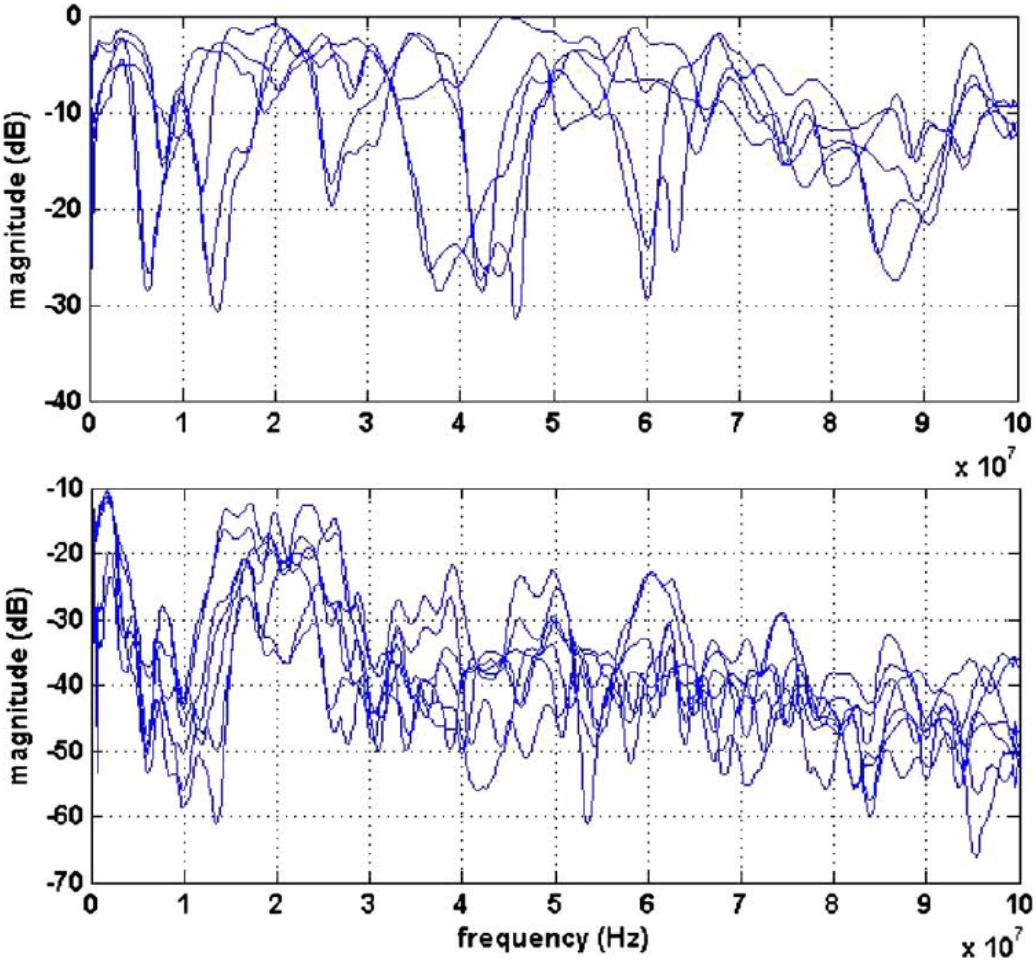

Figure 1.7. PLC channel measurements at the same site [Tlic08]

Classes	Percentage de channels (%)	Capacity interval (Mbit/s)	Capacity (Mbit/s)
1	3.49	1000 - 1200	1120
2	16.78	1200 – 1400	1307
3	18.18	1400 – 1600	1486
4	11.88	1600 – 1800	1687
5	11.88	1800 – 2000	1899
6	12.58	2000 - 2200	2098
7	9.79	2200 - 2400	2298
8	7.69	2400 - 2600	2499
9	7.69	2600 – 2800	2699

Table 1.5 Channel percentage and average capacity of class [Tlic08]

Classes	Average Attenuation Model
1	$-80 + 30\cos(\frac{f}{5.5x10^7} - 0.5)$
2	$-43 + 25exp(\frac{f}{3x10^6} - 0.5)$- $\frac{15}{10^8}f$
3	$-38 + 25\exp(\frac{f}{3x10^6} - 0.5)$ - $\frac{14}{10^8}f$
4	$-32 + 20\exp(\frac{f}{3x10^6} - 0.5)$ - $\frac{15}{10^8}f$
5	$-27 + 17\ \exp(\frac{f}{3x10^6} - 0.5)$ - $\frac{15}{10^8}f$
6	$-38 + 17\cos(\frac{f}{7x10^7})$
7	$-32 + 17\cos(\frac{f}{7x10^7})$
8	$-20 + 9\cos(\frac{f}{7x10^7})$
9	$-13 + 7\cos(\frac{f}{4.5x10^7} - 0.5)$

Table 1.6 Average attenuation model by class [Tlic08]

3.3. SISO PLC channel noise model

In contrast to many other communication channels the noise in a powerline channel can not be described by an additive white Gaussian noise (AWGN) model. SISO channel noise has been categorized into five major classes.

- Colored background noise, with a relatively low level of the power spectral density (PSD), varying with frequency. The colored background noise is stronger at the lower frequencies. This type of noise is mainly caused by summation of numerous noise sources with low power. Its PSD varies over time in terms of minutes or even hours. The background noise limits the channel capacity.

- Narrow-band noise, mostly sinusoidal signals, with modulated amplitudes caused by ingress of broadcast stations. The level is generally varying with daytime.

- Periodic impulsive noise asynchronous to the mains frequency with a repetition rate between 50 and 200 kHz, with a discrete line spectrum spaced according to the impulse repetition rate. This type of noise is mostly caused by switched power supplies.

- Periodic impulsive noise synchronous to the mains frequency with a repetition rate of 50 or 100 Hz. The impulses are of short duration (some microseconds) and have a PSD decreasing with frequency. This type of noise is caused by power supplies, mainly by switching of rectifier diodes, which occurs synchronously with the mains cycle.

- Asynchronous impulsive noise is caused by switching transients in the network. The impulses have durations of some microseconds up to a few milliseconds with random occurrence. The PSD of this type of noise can reach values of more than 50 dB above the background noise.

In the framework of this thesis we will study the background noise in detail. A MIMO PLC channel background model is presented in chapter 4.

3.3.1. Colored background noise

3.3.1.1. OMEGA model

The OMEGA model of the background noise is shown in Eq.1.6, where N_{bk} represents the background noise PSD in mW/Hz, and f is the frequency [Omega08]. This model is based on the measurements performed on the indoor SISO PLC channels. From the Figure 1.8 it is evident that this is a typical exponentially decreasing model. The spectral shape is defined with the $1/f^2$ term and the noise floor of -155 dBm/Hz is attained at the highest frequencies.

$$N_{bk}(f) = \frac{1}{f^2} + 10^{-\frac{155}{10}} \quad \text{mW/Hz} \tag{1.6}$$

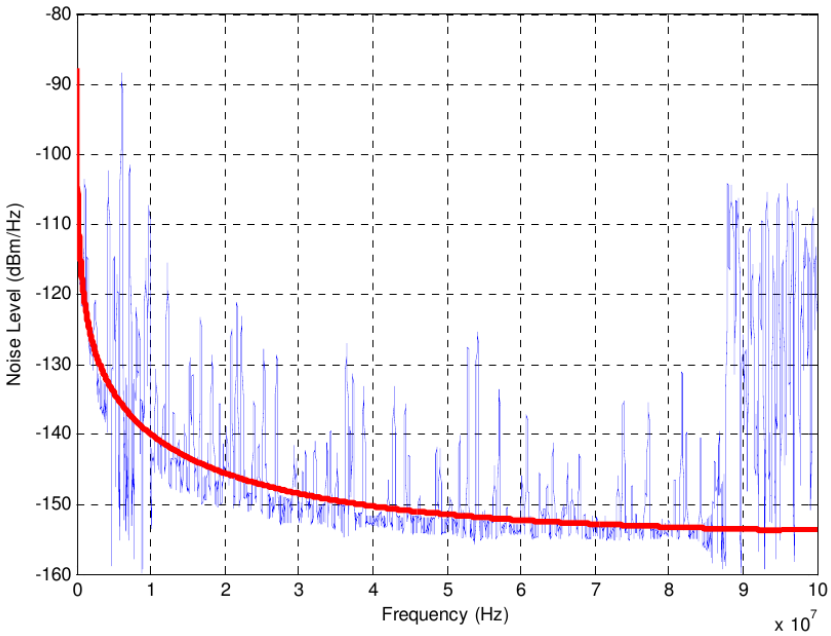

Figure 1.8. OMEGA background noise model [Omega08]

3.3.1.2. Esmailian model

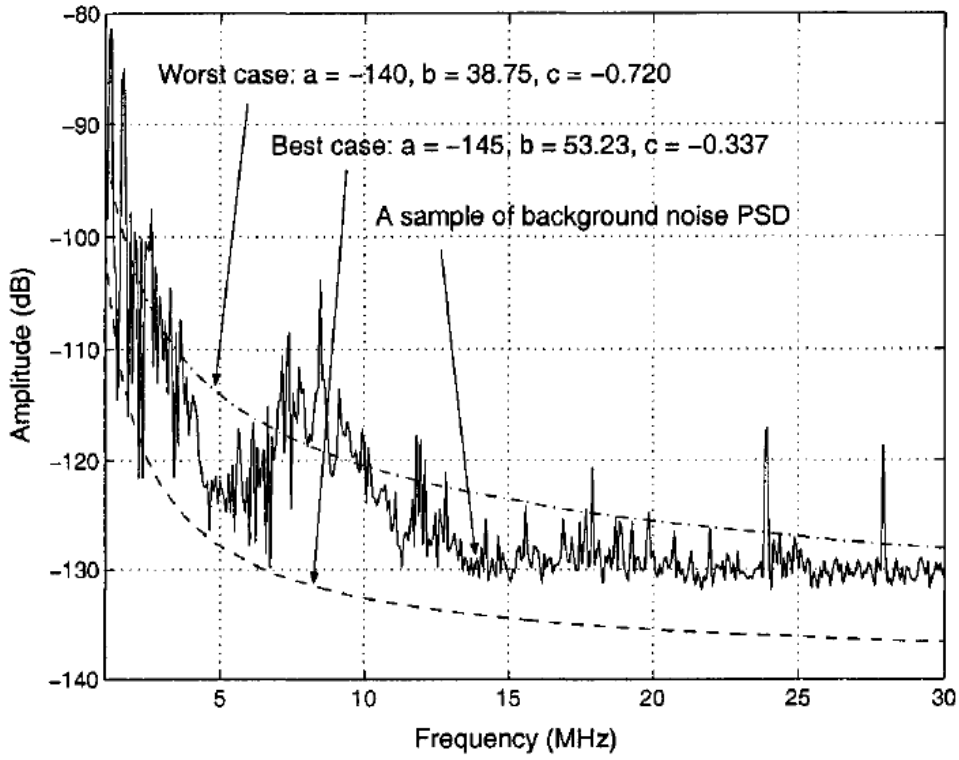

Figure 1.9. Esmailian background noise model [Esma03]

The Esmailian model shown in Eq.1.7 is also based on measurements [Esma03]. Figure 1.9 shows the plots of Esmailian model for two parameters sets (along with a measured noise PSD).

$$N_{ES} = a + b.\left|\frac{f}{10^6}\right|^c \tag{1.7}$$

where N_{ES} stands for noise PSD in dBm/Hz, f denotes the frequency in Hz and a, b and c are the model parameters. The accuracy of the OMEGA model and the Esmailian model to model the MIMO background noise will be discussed in detail in Chapter 4.

3.3.1.3. Guillet Model

This model presents new values of the estimated Esmailian model coefficients [Guil10]. The proposed values of the parameters, shown in Table 1.7, are extracted from the spectrum of the noise which is measured in time domain. These results and the underlying model are important in the context of this thesis because by using a similar technique we will propose two frequency domain models of MIMO PLC background noise in chapter 4.

Statistics	Background parameters		
	A	***B***	***C***
max	-128,6	29,1	-0,206
average	-129,6	22,7	-0,275
min	-134,3	18,3	-0,33
standard deviation	0,89	1,59	0,021

Table 1.7 Typical values estimated for the background noise [Guil10]

The periodicity of the background noise (Figure 1.10) has also been discussed. It is asserted that the periodicity can be attributed to the cycle of the AC mains. A new background noise has been proposed to encompass the periodicity (Eq.1.8).

$$P_{NOISE}(f,t) = A + \frac{\beta_1|Sin(2\pi 2 f_{MAIN} t)| + \beta_2}{\sqrt{f}} \quad \text{dBm/s/Hz} \tag{1.8}$$

β_2 *and* β_{21} are the scaling factors whose value is in the order of 7.5 and f_{MAIN} is 50 Hz.

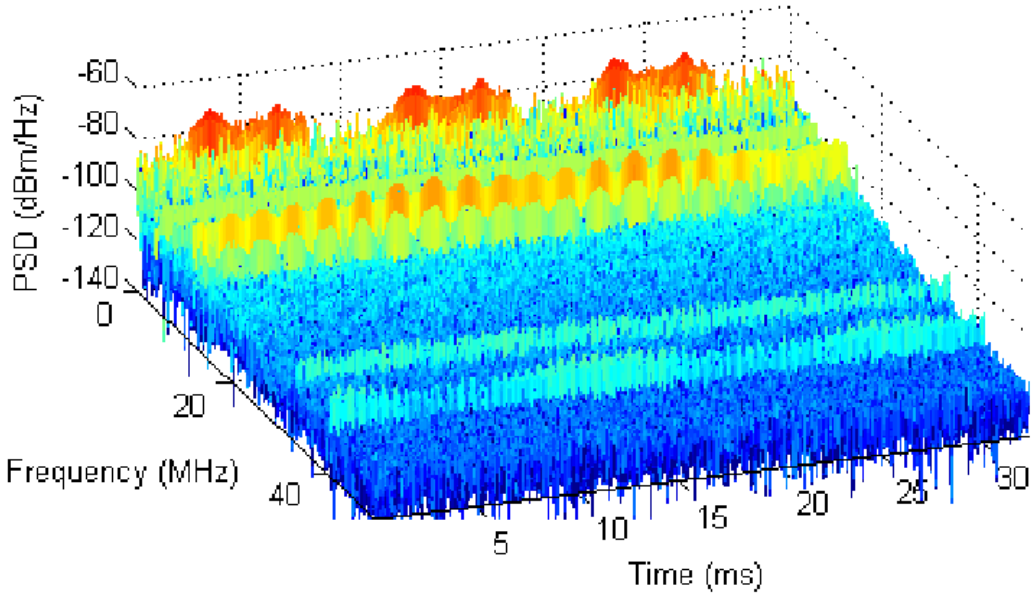

Figure 1.10. Time-frequency representation of measured noise [Guil10]

3.3.1.4. Other models for the background noise

Although in the framework of this thesis we will be using the measurements to extract the parameters of the background noise, it is worth mentioning some other techniques reported for the background noise model.

A closed form mathematical model of the power line background noise has been proposed in [Kim08]. The model is based on the Nakagami-m distribution. The simulation results have shown good agreement between the simulated noise and the one obtained from the closed form model.

A model for colored background noise has been derived with the help of the neural network technique [Ma10]. A finite impulse response (FIR) filter of order 85 is built where the filter coefficients are obtained from an artificial neural network. The noise is generated in time domain and its spectrum is reported to match closely to the measured background noise.

4. Orthogonal frequency division multiplexing (OFDM)

OFDM is a well proven multi carrier technique in applications such as digital audio broadcasting (DAB), terrestrial digital video broadcasting (DVBT) and asymmetric digital subscriber line (ADSL). Similar to band spreading, OFDM exhibits robustness against various kinds of interference and enables multiple-access. The spectrum used

by the OFDM transceiver is segmented into numerous narrow sub-channels. A data stream is transmitted by frequency-division multiplexing (FDM) using *N* orthogonal carriers, centred in the sub-channels. Due to the sub-channels' narrowband property, attenuation and group delay are constant within each channel. Consequently, in OFDM, the equalization is easy and can be performed by so-called one-tap techniques [Gotz04]. Figure 1.11 shows an OFDM transmission chain.

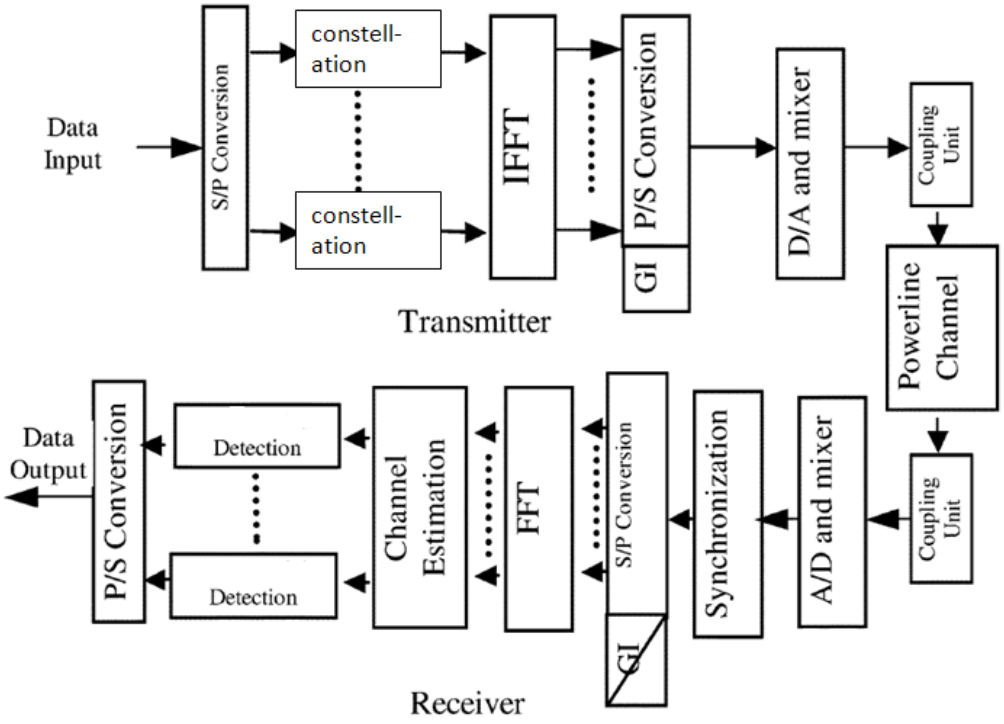

Figure 1.11. OFDM transmission chain [Luo05]

The HomePlug AV standard uses the OFDM technique. In the HomePlug AV specification the frequency of sampling is equal to 75 MHz (HPAV band= 2-30 MHz) and the symbol duration is 40.96 μsec. This leads to a carrier spacing of 24.14 KHz. Guard interval is used between successive symbols to avoid the Inter Symbol Interference (ISI). Three different guard intervals (durations 5.56, 7.56 and 47.12 μsec) are used in HPAV systems depending on the RMS delay spread of the channel.

A substantial advantage of OFDM is its adaptability. It is possible to choose the optimum modulation scheme individually for each sub channel. This process is called adaptive bit loading. In addition, frequency ranges excluded from use for PLC due to regulation or bad quality can easily be faded out by zeroing (or nothcing) the corresponding carriers. In future it is expected that OFDM will become the most favorable modulation scheme in all PLC applications. In [Giov05], a Space Frequency coded OFDM system for multi-wire differential signalling with receive diversity has

been proposed, which shows very good performance results in space and frequency selective power line channels.

Another variant of OFDM is the pre-coded OFDM. The precoding scheme is simply based on inserting one or more zeros between two sets of *K* consecutive information symbols. It has the advantage of removing the spectral nulls of an ISI channel without any need to channel response knowledge. A precoded OFDM systems implementation is much simpler than coded OFDM. The BER performance of precoded OFDM systems is better than conventional and coded ones [Tlil03].

An OFDM/OQAM modulation for PLC has been analysed in [Skrz07]. OQAM stand for offset quadrature amplitude modulation. From the EMC point of view, masking the sub-carriers is necessary in OFDM to protect the existing services such as radio amateur band. However, the conventional OFDM only provides 13 dB of attenuation with its rectangular pulse shape and can hardly satisfy stringent specifications. This makes OFDM/OQAM a suitable candidate. A difference between OFDM/OQAM and OFDM is the transmission of real-valued coefficients instead of complex ones. Both systems contain the same number of carriers and the symbol duration of the OFDM/OQAM real symbols is half the one used for the complex ones in OFDM. Moreover, for OFDM/OQAM, there is no guard interval (GI), so a higher theoretical spectral efficiency can be achieved.

5. MIMO PLC

In the following part of this chapter we will concentrate on the works reported in the PLC literature where Multiple-Input Multiple-Output (MIMO) techniques have been applied to the PLC network. The increasing demand for high data rates and the limited available bandwidth motivates the investigation of the transmission systems which efficiently exploit the spatial domain. The use of spatial diversity both on the reception as well as the transmission can improve the throughput and coverage in addition to allowing a higher degree of spectral reuse and thereby increasing the system capacity. The channel capacity can be greatly increased by using feed array at both transmit and receive side, so-called MIMO systems, as long as the environment provides sufficient scattering [Yu02].

5.1. Theoretical background

In the general case of a MIMO system comprising of *M* emitter ports and *N* receiver ports, the channel matrix ***H(f)*** can be written as shown in Eq.1.9

$$H(f)=\begin{bmatrix} h_{1,1}(f) & h_{1,2}(f) & \cdots & h_{1,M}(f) \\ h_{2,1}(f) & h_{2,2}(f) & \cdots & h_{2,M}(f) \\ \vdots & \vdots & \ddots & \vdots \\ h_{N,1}(f) & h_{N,2}(f) & \cdots & h_{N,M}(f) \end{bmatrix} \tag{1.9}$$

where $h_{n,m}(f)$ represents the complex channel transfer coefficient from the mth emitter to the nth receiver, at frequency f. In the framework of this thesis, channels represented by $h_{n,m}$ with $m=n$ are called co-channels, and those with $m\neq n$ are called cross-channels. This distinction although not necessary in wireless systems, allows discrimination between the connected ports and coupled ports in wired communication systems. In the frequency domain, the signal y_n received at the nth receive port is given by Eq. 1.10

$$y_n=\sum_{m=1}^{M} h_{nm}x_m + w_n \tag{1.10}$$

where x_m is the signal sent by the m^{th} transmit port, M is the number of transmit ports and w_n is the noise received at the n^{th} receiver. In a matrix representation, and omitting the frequency index for simplicity, the channel input-output relationship can be described as in Eq.1.11.

$$\boldsymbol{y = Hx + w} \tag{1.11}$$

The described MIMO system is power constrained at the transmitter, that is, the total transmitted power is not more than P watts. The capacity C of a MIMO channel, represented by Eq. 1.12, is defined as the maximum data rate that can be transmitted over the channel with a probability of error arbitrarily close to zero [Xi03].

$$C = [\log_2 \det(I_M + \frac{\rho}{M} HH^{\dagger})] \tag{1.12}$$

where I_m is an identity matrix, ρ denotes the signal-to-noise ratio (SNR) at each receive antenna and the superscript † indicates a Hermitian transpose. For $M=N$, Eq. 1.12 simplifies to Eq. 1.13.

$$C = \sum_{i=1}^{r} \log_2 (1 + \frac{\rho}{M} \lambda_i) \tag{1.13}$$

where r is the rank of $\boldsymbol{HH}^\dagger$ and λ_i is the i^{th} eigenvalue of $\boldsymbol{HH}^\dagger$ obtained by eigenvalue decomposition (EVD) shown in Eq. 1.14.

$$\boldsymbol{HH}^\dagger \boldsymbol{A} = \boldsymbol{AD} \tag{1.14}$$

Here $\boldsymbol{A}$ is a unitary matrix composed of the eigenvectors of $\boldsymbol{HH}^\dagger$, and $\boldsymbol{D}$ is the matrix whose diagonal entries are its eigenvalues. For $M \neq N$, singular value decomposition (SVD) is used instead of EVD. The SVD of matrix $\boldsymbol{H}$ produces three matrices $\boldsymbol{U}$, $\boldsymbol{\Delta}$ and $\boldsymbol{V}$ which are related to each other by Eq. 1.15

$$\boldsymbol{H} = \boldsymbol{U\Delta V}^\dagger \tag{1.15}$$

where $\boldsymbol{U}$ and $\boldsymbol{V}$ are unitary matrices, and $\boldsymbol{\Delta}$ is the matrix whose diagonal entries are the singular values of $\boldsymbol{H}$. Singular values, denoted by δ, are related to the eigenvalues as shown by Eq. 1.16.

$$\delta = \sqrt{\lambda} \tag{1.16}$$

5.2. MIMO Multi-phase PLC networks

5.2.1. Space-time coded MIMO PLC communication

In a multi-phase power distribution system, for example a 3-phase system, there exist at least three lines corresponding to three phases and a fourth line for neutral, as depicted in Figure 1.12. Therefore, an analogy can be established between a phase and an antenna. These lines can be utilized as distinct feed points at the transmit and receive ends to achieve a MIMO performance. The Space Time Block Codes (STBC) have attracted the attention of the researchers for this application [Giov03].

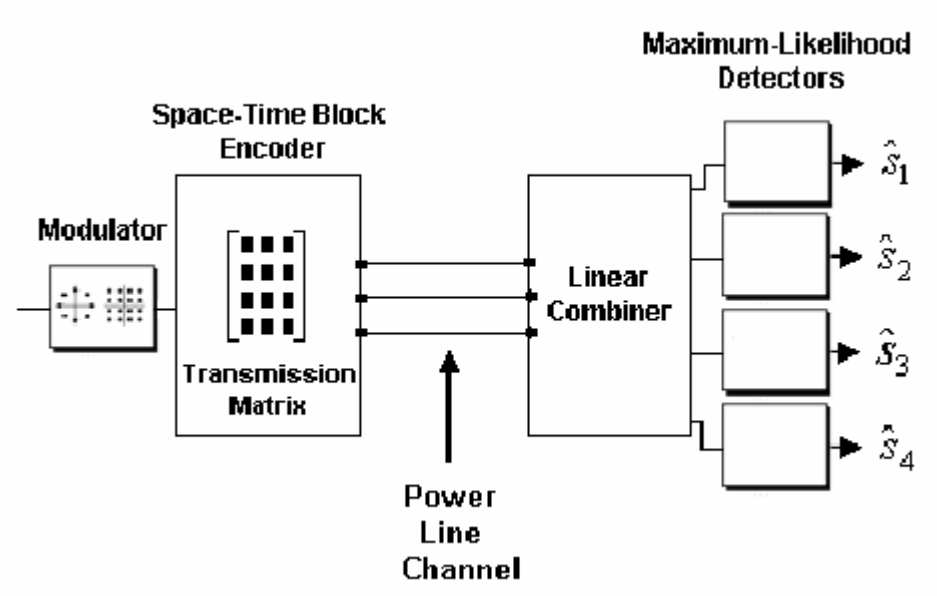

Figure 1.12. Powerline communication system using space-time block coding [Giov03]

5.2.2. **Space-frequency coded MIMO PLC communication**

The exploitation of the available diversity in PLC channel has been extended to space-frequency (SF) coding. It is achieved by transmitting the same data symbol over two uncoupled pair of wires and over two different carriers, with a frequency separation between carriers greater than the coherence bandwidth of the channel [Giov05].

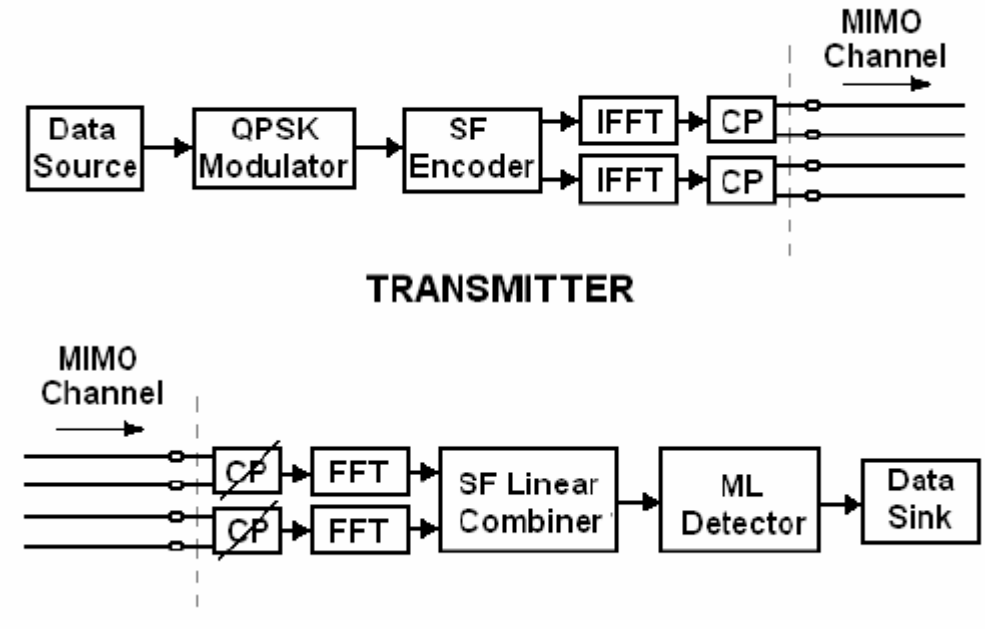

Figure 1.13. Space-frequency coded powerline network [Giov05]

In comparison to the space-frequency coded systems the space-time PLC systems were designed for single carrier (SC) modulation and the power line channel was modelled as a frequency flat multiple-input multiple output (MIMO) channel. Although SC modulation is an attractive proposition from the complexity point of view, the strong Inter Symbol Interference (ISI) caused by the PLC channel calls for powerful equalisation techniques, which exhibit a computational complexity that increases exponentially with the length of the impulse response. A typical SF coded OFDM system is shown in Figure 1.13.

A multi-carrier (MC) modulation scheme suitable for the frequency selective channels is OFDM. OFDM orthogonalises a time dispersive channel into *N* orthogonal flat fading single-input single-output (SISO) channels. OFDM modulation for SISO channels can be easily extended to the MIMO scenario. MIMO-OFDM techniques for frequency selective multi-phase power line channels offer a potentially convenient solution for control signalling and data transmission in the access domain, as well as in large buildings and industrial plants where power cables comprising four conductors (3 phases and 1 neutral) are available. As described above, the space diversity gain can be extracted by transmitting the OFDM signal vector over two uncoupled pairs of wires and if the frequency separation between the two carriers (tones) is made greater than the coherence bandwidth of the channel, the transmitted signals experience independent fading.

6. Inhome MIMO PLC networks

6.1. Physical channel

In this section we will present a brief bibliographic account of inhome MIMO PLC. It should be noted that inhome MIMO PLC is a relatively new domain of research. A limited number of publications are available in this field though the interest of PLC community is increasing in MIMO.

In most developed countries the inhome electrical wiring consists of three wires: Phase (P), Neutral (N) and Protective Earth (PE).The existing PLC systems utilize only P and N wires for signal transfer. However, MIMO PLC systems are envisaged to exploit the unused PE wire as well. This provides three possible ports, P-N, P-PE and N-PE for transmission and reception of differential signals between two given sockets or PLC outlets. Therefore, a MIMO PLC channel can be visualized as a classical MIMO system with three transmit and three receive antennas as shown in Figure 1.14.

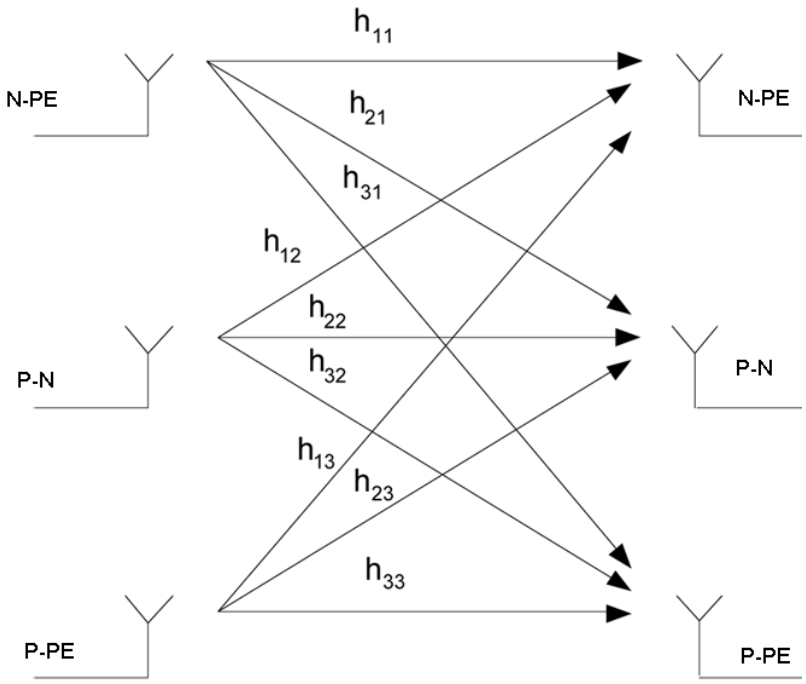

Figure 1.14. A 3x3 inhome MIMO PLC system (radio system analogy)

However, due to Kirchhoff's circuit law, simultaneous realization of three feed ports is not physically possible. However, 2x2 and 2x3 systems, with two feed and two or three receive ports are realizable. The 2x4 and 3x4 MIMO configurations are also possible if the common mode (CM) signal could be captured at the receiver [Stad08], [Schw11], [ETSIa]. Figure 1.15 shows a 2x2 MIMO PLC system constituted by using P-N and N-PE ports, represented by coaxial connectors. Similar configurations are possible with N-PE and P-PE (and P-N and P-PE ports respectively).

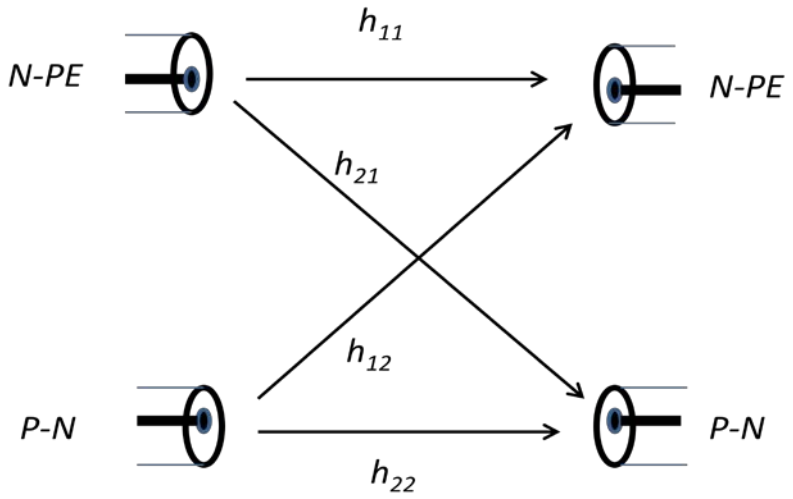

Figure 1.15. A 2x2 inhome MIMO PLC system

The indoor PLC channel, like the above mentioned 3-phase PLC channels, has been explored in the context of the MIMO techniques [Stad08]. Although today's PLC solutions theoretically offer data rates of up to 200 Mbit/s, measurements in private households have shown that in reality only much lower bitrates can be guaranteed due to high attenuation, frequency selective transfer functions and noise in the powerline channel. Typical inhome applications such as High Definition (HD) video streaming as a key application for the IP centric home network require data rates of around 20 Mbit/s with high reliability. Today's PLC systems use one transmit and one receive port for their data communication. However, in Europe and in the US 3-wire installations allow more feeding and receiving possibilities. Generally, in the presence of multiple feeding and receiving ports, MIMO principles can be used. In the currently available PLC modems the signal is symmetrically fed and received between P and N wires. Figure 1.16 shows a typical PLC MIMO configuration.

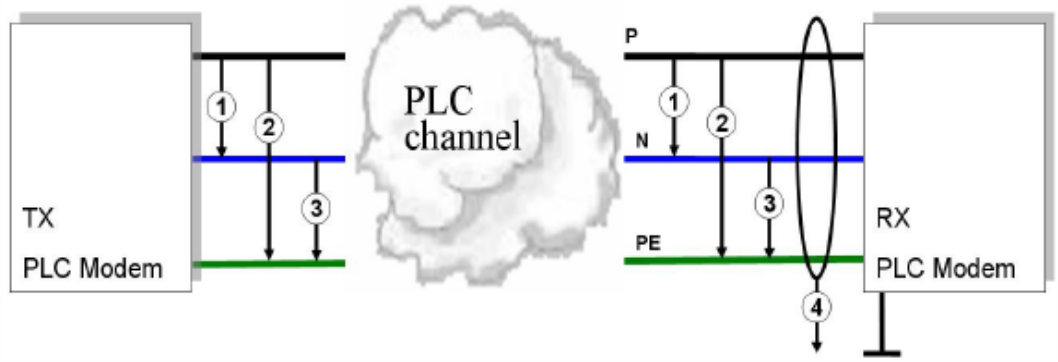

Figure 1.16. An inhome MIMO PLC channel [Stad08]

One key parameter is the optimum number of feeding and receiving ports to deliver the best trade-off between system complexity and throughput. Basically there are several MIMO arrangements, which differ by their number of transmit and receive ports (Table 1.8). In the absence of PE wire 1x2 MIMO can be used, but if PE wire is available 1x3 is also possible. Low impedance ground for High Frequency (HF) signals makes 1x4 MIMO possible. A second transmit port makes 2x3 and 2x4 MIMO realizable. 2x3 and 2x4 MIMO configurations exhibit considerable capacity gain compared to 1x2, 1x3 and 1x4 configurations [Stad08].

MIMO mode	Tx ports	Rx ports
1 x 2	P-N	P-N, CM
1 x 3	P-N	P-N, P-PE, N-PE
1 x 4	P-N	P-N, P-PE, N-PE, CM
2 x 3	2 best of: P-N, P-PE, N-PE	P-N, P-PE, N-PE
2 x 4	2 best of: P-N, P-PE, N-PE	P-N, P-PE, N-PE, CM

Table 1.8 PLC MIMO arrangements [Stad08]

A MIMO technique based on precoded spatial multiplexing has been presented in [Schn08]. Different MIMO schemes like spatial multiplexing (SMX), precoded spatial multiplexing (also referred to as Eigen beamforming) and the Alamouti scheme in conjunction with adaptive modulation have been compared in PLC system simulations. Eigen beamforming is considered to be the best choice in the PLC environment for several reasons, for example, it offers the highest bit rate of all investigated schemes. Especially in correlated channels the precoding still allows high bitrates while SMX without precoding faces strong throughput degradations. However, precoded SMX requires channel state information (CSI) at the transmitter (TX). Since the time variation of the PLC channel is rather low, the overall amount of feedback data can also be kept low.

The first stage of the physical layer of an OFDM based PLC-MIMO system comprises of the multiplexing of the incoming bits into two separate streams, as shown by a typical 2x4 MIMO system in Figure 1.17. The proposed scheme employs adaptive modulation, i.e. each of the N sub carriers uses a QAM constellation according to the instantaneous SNR of the related frequency (also referred to as adaptive OFDM). The lower the SNR, the smaller the chosen QAM constellation. The N complex symbols s_1 , s_2 , … s_N of each transmit path are multiplied by the matrix $\boldsymbol{F_i}$, OFDM modulated and sent via the two transmit ports over the PLC-MIMO channel $\boldsymbol{H}$. At the receiver each signal is OFDM demodulated and all four symbols of each subcarrier are detected with $\boldsymbol{W_i}$. In the case of eigen beamforming, the matrix $\boldsymbol{F_i}$ are equal to $\boldsymbol{V_i}$ and $\boldsymbol{W_i}$ equal to $\boldsymbol{U_i}^{\dagger}$.

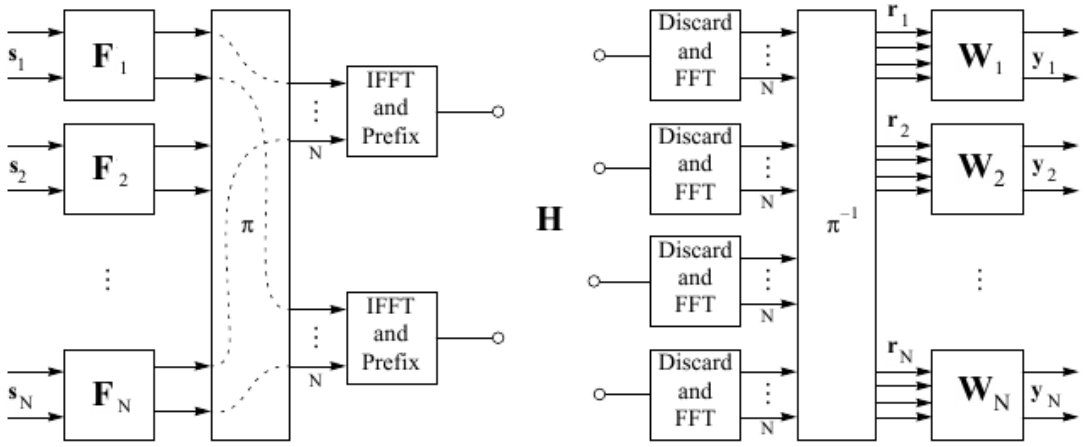

Figure 1.17. Precoded spatial multiplexing for MIMO-OFDM [Schn08]

6.2. Channel capacity

In [Stad08], the capacity of MIMO PLC channels capacity has been presented in the 0-30 MHz range. Channel capacity calculations are made for transmit power levels: -93 dBm/Hz as the lower level and -67 dBm/Hz as the higher level. A flat noise spectral density is considered with a level of -136 dBm/Hz. It can be noted in Table 1.9 that the average capacity gain of the MIMO channels is 2.2 and 2.6 for low transmit power level. The capacity gain is more effective for low transmit power levels as well as for difficult channels which exhibit high attenuation and frequency selectivity.

	Low transmit level *(-93 dBm/Hz)*			**High transmit level** *(-67 dBm/Hz)*		
	Average gain	**Min gain**	**Max gain**	**Average gain**	**Min gain**	**Max gain**
2x3 MIMO	2.2	1.3	4.9	1.8	1.2	2.9
2x4 MIMO (incl. CM)	2.6	1.5	5.2	2.1	1.3	2.9

Table 1.9 Channel capacity gain [Stad08]

In [Vers11a], the inhome MIMO PLC capacity is investigated in 2-100 MHz band. In this thesis, we have firstly extended the analysis of the MIMO capacity up to 100 MHz [Hash09] and [Hash10].

6.3. Channel transfer function model

A strategy for the simulations of MIMO PLC channels has been described in [Vers11]. This strategy is based on MTL theory. The mutual interactions between the three conductors (wires) Phase, Neutral and Protective Earth have been considered. In [Vers11], a typical 2x2 MIMO PLC system is defined on the basis of the coupling effects. The model thus obtained has been validated through the comparison of insertion loss for measured and modeled parameters.

In [Vero11], the characterization of inhome MIMO power line channels is presented. The analysis ranges from 0 to 100 MHz. Basically it is a statistical description of inhome MIMO PLC channels extracted from 96 channel measurements performed in North American houses. In this thesis, we have proposed a comprehensive inhome MIMO CTF model, in 2-150 MHz range [Hash11].

A detailed account of these channel models is described in chapter 3.

6.4. Noise model

Modeling and characterization of the MIMO PLC noise is a recent development. The interest of the PLC community is, however, increasing in this particular domain. In [Rend11], MIMO PLC noise correlation and its effect on the channel capacity have been discussed. The analysis is based on measurements performed on several US homes. The measurements are performed in time domain by transmitting two independent signals over two wire pairs and receiving on all three wire pairs. The strongest correlation is measured between P-PE and N-PE receive ports. This result is in accordance with [Hash10a]. It has been reported in [Rend11] that noise correlation helps to increase the MIMO channel capacity. On weaker channels, the correlation can increase the capacity by as much as 40 %. In the framework of this thesis, we firstly presented the characterization of the MIMO PLC channel noise in [Hash10a].

Two frequency domain models of the MIMO PLC background noise have been proposed in [Hash12]. These models are based on two existing SISO noise models: the Omega model and the Esmailian model. A detailed time domain model of the MIMO PLC background noise has been proposed in [Hash11a]. This model is based on a vector autoregressive model which is generally used for modeling the multivariate time series.

In [Paga12], a detailed analysis of the MIMO PLC noise is presented in 1-100 MHz range. This analysis is based on an extensive measurement campaign performed in 5 European countries in the framework of ETSI STF410. The noise PSD is reported between -168 dBm/Hz and -80 dBm/Hz. The common mode (CM) port is found more sensitive to noise with an approximate 5 dB increase in the noise PSD. An analysis of correlation between MIMO PLC noise sequences is also included in [Paga12].

7. Conclusions

In this chapter we have presented a comprehensive bibliographic study of the PLC domain. Power line communication is the technology which uses the existing power delivery network for data transmission. In its early days the power line communication was used for very low bit rate applications but with time it has become a potential competitor of VDSL for the accomplishment of high speed services.

This chapter covers important PLC standards, major industrial groups and European projects. We have briefly discussed various standards formalized by ETSI, IEEE and ITU. Among the major industrial players we have included HPA, UPA and CEPCA. The activities of three important European projects, Omega, Powernet and Opera have been described.

The inhome PLC networks have been discussed in detail. We have given a brief account of the physical aspects of the inhome PLC network. Some prominent SISO channel and noise models have been included. A very popular transmission scheme among the PLC systems, the OFDM, has been described concisely. Then we divert our attention towards the MIMO power line communication. First of all we give a brief theoretical background of the MIMO transmission. The initial application of the MIMO transmission techniques to the multi-phase power networks is discussed. In the last part of the chapter we have thrown light on the inhome MIMO PLC. We have presented a brief account of the physical MIMO PLC channel and the potential capacity gain compared to the existing SISO PLC systems. In the end some MIMO PLC channel and noise models have been discussed.

In the Chapter 2 of this document we will present the measurements performed during the thesis and the preliminary results extracted from the measured data. In Chapter 3 and 4 we will propose models of the MIMO PLC channel transfer function and noise.

Chapter .2
Measurements on PLC networks and preliminary results

1. Introduction

The purpose of this chapter is to describe the methodology of the measurements performed on the PLC channels in a MIMO context. Several channel measurement campaigns on SISO channels can be found in PLC literature [Tlic08], [Meng04], [Barm06], [Zimm02a], etc. To understand the significance of the measurements it is worth discussing their utility from the channel modeling point of view.

Most of the times the primary objective of the measurements is to gather data and information about PLC channels. The measured data is fitted to a mathematical function to extract various parameters on the basis of which statistical models for channel transfer function (CTF) and noise would be proposed. This approach is generally named as the top-down approach. Its counterpart is the bottom-up approach which is based on transmission characteristics of electrical wires. Both approaches have their pros and cons. For example, the top-down approach, which relies on measurements, views the PLC channel as a black box. The characteristics of the channel such as, the topology, the electrical loads, cable types, wiring norms etc. are fully captured in the measured data. The top-down approach is simple and generally does not require large computational resources; it is true especially when the network size and the number of channel parameters are not too large.

A channel model proposed on the basis of the top-down approach utilizes the data obtained from the measurements to estimate model parameters. Such a model is naturally limited to the measured channel. A slight change in the channel conditions will mean that the already measured data does not truly represent the present state of the channel. Nevertheless, this limitation of the model can be overcome by enriching

the measured database through extensive measurements on sufficiently large number of channels over longer periods of time [Zimm02a].

In contrast, the bottom-up approach is more systematic, and is generally based on the transmission line theory. This approach takes into account the characteristics of the PLC channel [Gall06]. Although a fully deterministic channel model can be realized by the bottom-up approach, it needs complete *a priori* knowledge of the network which includes many parameters such as topology, loads types, cable types etc. A thorough *a priori* information about the PLC networks is usually not available. Moreover, the bottom-up approach requires more computational resources. Consequently, the utility of bottom-up approach is severely hampered. For such reasons, till date, there exists no unanimous model even for SISO PLC channels, let alone the MIMO PLC channels.

Just like the channel measurements, there exist various PLC channel noise measurements methodologies. For example, noise can be measured in the time-domain as well as in the frequency-domain. One important aspect which needs to be respected while measuring MIMO PLC channel noise is the nature of the noise. The MIMO PLC channel noise is composed of simultaneous noise sequences which should be measured at the same instant.

Measurements have always played an important role in the process of scientific discovery. Many channel and noise models have been proposed in PLC domain through measured data. Moreover, measurements over PLC channels have been exploited as a touchstone to validate the proposed models and communication techniques. For example, methods of transfer function measurements for PLC channels have been discussed in [Meng04] and [Barm06]. Time-domain PLC channel measurements have been utilized for the extraction of the channel model parameters in [Oh08]. A propagation model for PLC channels is described on the basis of line impedance measurements in [Sabo05]. In [Tlic08], a PLC channel generator has been detailed in 30 KHz to 100 MHz range based on frequency-domain channel measurements. A model based on time-domain measurements, for impulsive noise in PLC channels up to 20 MHz has been presented in [Zimm02b]. Similarly, a method for impulsive noise detection in PLC channels has been proposed and validated through measurements in [Avri08]. All these examples show the importance and utility of the measurements on SISO PLC channels. In the context of MIMO PLC, [Stad08] shows the potential benefits of MIMO techniques for PLC systems in terms of increased capacity. The results presented in [Stad08] are based on measurements

performed in several flats and houses. All these research works indicate the significance of measurements in the domain of PLC research.

In this chapter various measurements on inhome MIMO PLC channels will be presented. First of all, MIMO channel measurements were performed on an experimental PLC network. Later, they were extended to a live laboratory network. And finally the MIMO channel measurements were performed in different houses. However, the MIMO PLC channel noise measurements were performed only in the houses. On the basis of the measurements performed in the houses, a complete MIMO PLC CTF model and background noise model will be presented in chapter 3 and 4 respectively.

2. Measurement techniques

In this section we discuss techniques for measuring PLC channel transfer function and noise. The focus will be on a comparison between time domain measurement techniques and frequency domain measurement techniques.

2.1. Channel measurements

A channel is the environment through which a transmitted signal has to pass before it reaches the receiver. Different channels exhibit different physical conditions for the signal. Channel measurements are performed to investigate the characteristics of a channel, for example, channel attenuation, frequency dependence, fading nature, etc.

2.1.1. Time domain channel measurements

Time domain channel measurements are performed by injecting a known signal into the channel. Generally an arbitrary waveform generator (AWG) is used to synthesize a signal in the time domain. At the receiver, the signal is captured by a digital sampling oscilloscope (DSO). The characteristics of the channel are investigated through off-line computations [Zimm02a].

2.1.2. Frequency domain measurements

Frequency domain channel measurements are performed by using a network analyzer. The channel is visualized as a typical 2-port network or filter. The channel characteristics are measured in the form of the scattering parameters (S-parameters). The parameter S_{21} represents the channel gain. Frequency domain channel measurement is a simpler and more direct way to investigate a channel. Therefore, we select this measurement technique in our channel measurement campaign.

2.2. Noise measurements

Noise is the contamination added to the signal while it passes through a channel. The level of noise power spectral density (PSD) plays an important role in evaluating the signal to noise ratio (SNR). Communication channels are hampered by different types of noise. Noise measurements provide an insight about the characteristics of the channel noise.

2.2.1. Time domain noise measurements

Time domain noise measurements are performed with a DSO. The DSO can display and capture instantaneous states of the noise. Modern DSOs are multiport devices which can measure more than one noise sequences simultaneously. The noise in a MIMO PLC channel consists of three sequences: N-PE, P-N and P-PE. Simultaneous measurement of the three sequences is important to capture their inter-dependence. Therefore, for our MIMO PLC noise measurements we have used a DSO to perform time domain noise measurements.

2.2.2. Frequency domain noise measurements

Frequency domain noise measurements are performed with a spectrum analyzer. A spectrum analyzer displays the frequency domain picture of a signal. Frequency domain noise measurements on the PLC networks have been discussed in [Mesc10]. The background noise in the PLC channels is generally considered to be a colored noise whose level depends on the frequency. The frequency domain noise measurements provide a direct picture of the background noise spectrum. However, due to the duration of a frequency sweep, spectrum analyzers are not able to capture transient phenomena, such as the presence of impulsive noise.

3. Devices used in the measurements

3.1. Coupling devices

Coupling devices provide an interface between the PLC network and the measuring instrument such as a DSO or a network analyzer. In our measurements we have used various couplers during different measurements.

3.1.1. SISO coupler

The SISO couplers used in our measurements are passive devices developed at Orange Labs. The schematic diagram of a SISO coupler is shown in Figure 2.1. This coupler is essentially a means to provide protection to the sensitive (and costly) measuring instrument. The RC filters block the 230 Volts, 50 Hz AC mains and the

transformer provides necessary isolation between the AC mains and the measuring instrument. The coupler does not present attenuation to the high frequency signals. The impedance of the BNC port is adapted to 50 ohms [Avri08a].

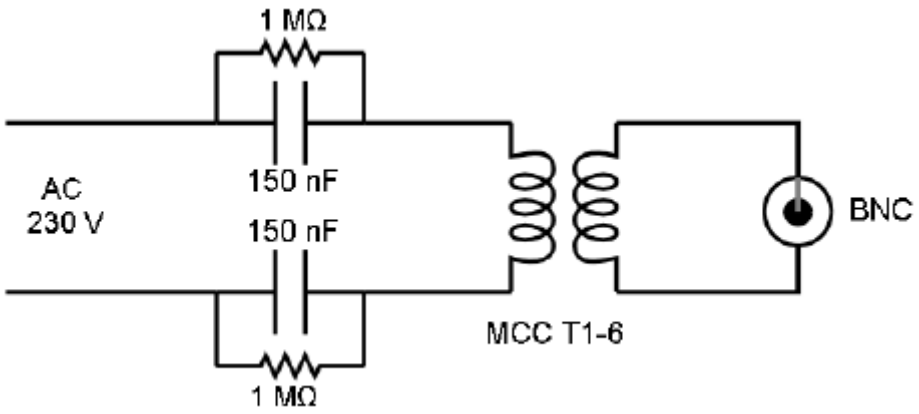

Figure 2.1. Schematic diagram of the SISO PLC coupler developed at Orange Labs [Avri08a]

3.1.2. MIMO couplers

Simple MIMO coupler

The MIMO PLC coupler shown in Figure 2.2 is a very simple device. It is merely a wire splitter. The electronic components to block the 230 volts AC mains are not required because this coupler is exclusively used for the channel measurements on an experimental PLC network which is not connected to the 230 Volts AC mains. This MIMO coupler performs the important task of pairing the P, N and PE wires into three BNC ports: P-N, P-PE and N-PE.

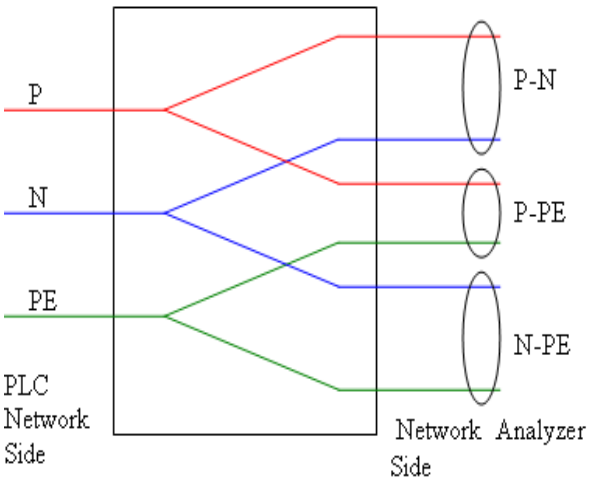

Figure 2.2. Schematic diagram of a simple MIMO PLC coupler

Hybrid MIMO coupler

The hybrid MIMO coupler is an arrangement designed at Orange Labs to implement the MIMO functionality for live PLC networks connected to 230 Volts AC mains. It comprises of two parts: one SISO coupler and one wire-selecting coupler. A hybrid MIMO coupler is shown in Figure 2.3. The SISO coupler provides the necessary protection and isolation from AC mains while the wire selector provides connectivity to two wires. The wire selector units select from P, N and PE wires to form a P-N, N-PE and P-PE ports, as shown in Figure 2.4.

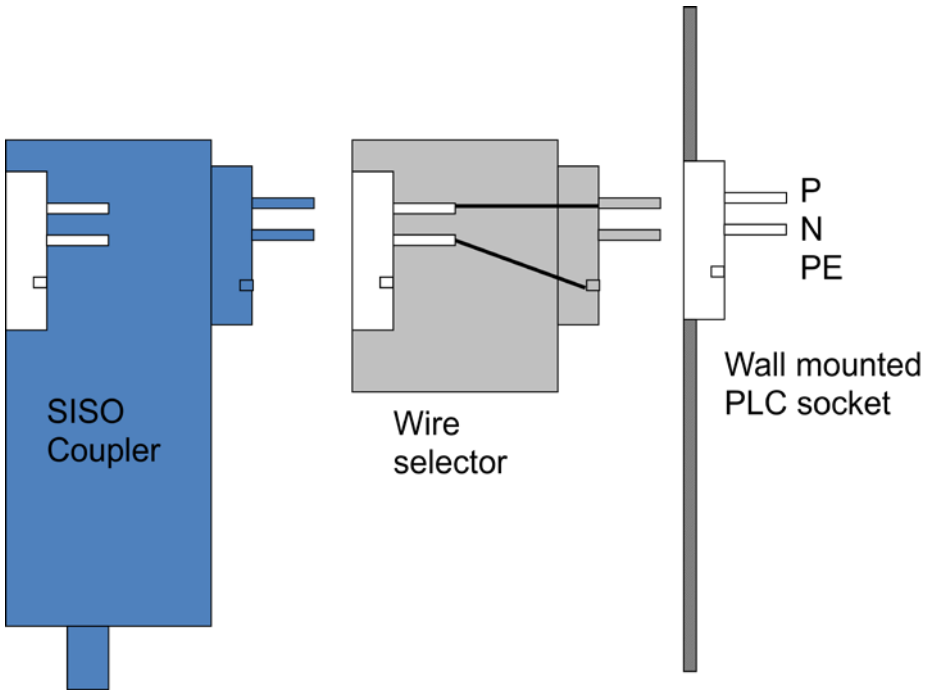

Figure 2.3. A hybrid MIMO PLC coupler designed at Orange Labs

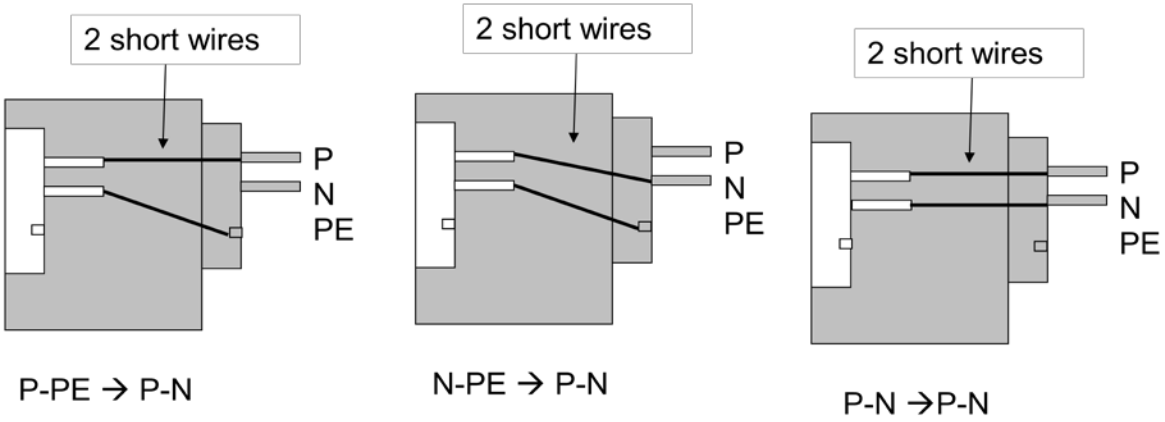

Figure 2.4. Function of the wire selectors in the hybrid MIMO PLC coupler

Compact MIMO coupler

A compact MIMO coupler is a device which provides the protection and the MIMO functionality in one single unit. A compact MIMO coupler is made up of three interconnected circuits. Each circuit is very similar to the one used in the SISO coupler. Such a MIMO coupler has three BNC or SMA ports: P-N, N-PE and P-PE. The schematic diagram of a compact MIMO PLC coupler is shown in Figure 2.5.

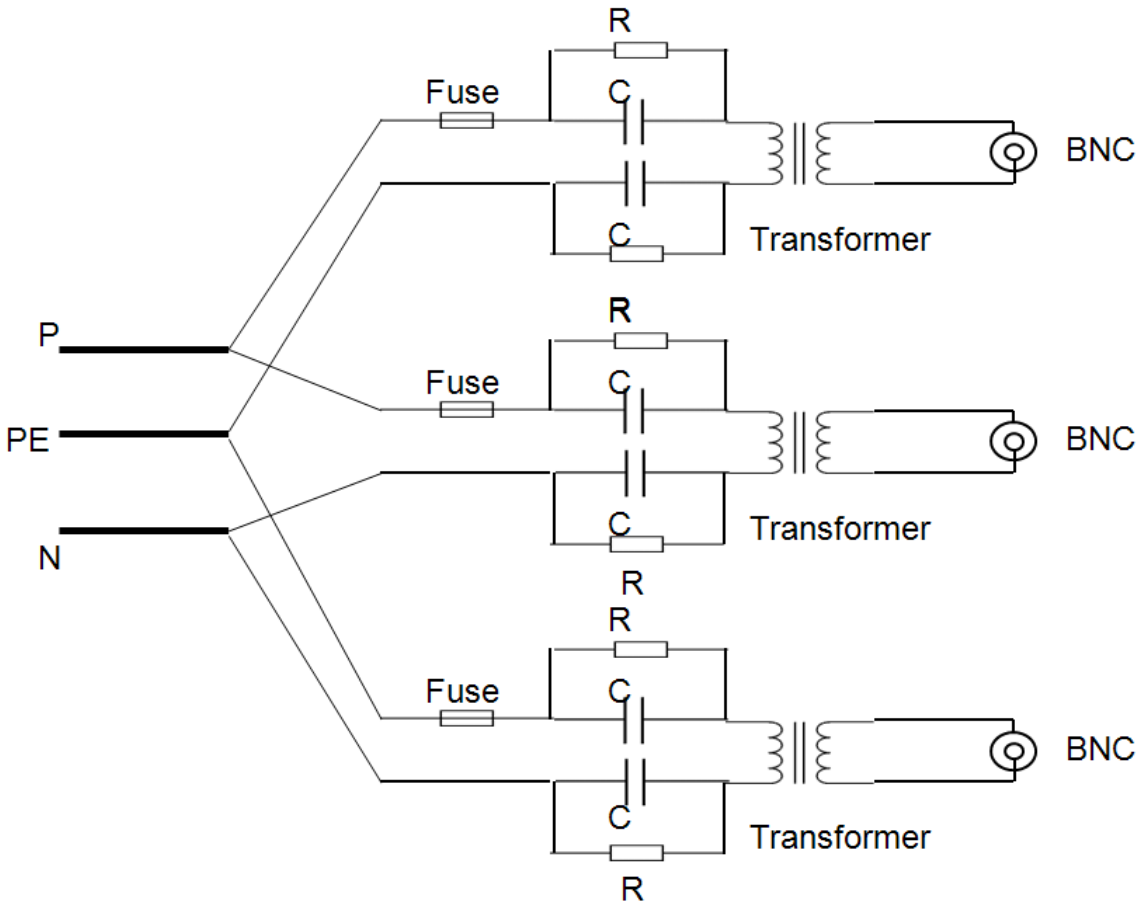

Figure 2.5. Schematic diagram of a compact MIMO PLC coupler

Transfer functions of a MIMO PLC coupler developed at Orange Labs Lannion are shown in Figure 2.6. It is evident that the MIMO PLC coupler exhibits more attenuation (10-15 dB) for cross-channels, in comparison to the co-channels (5-10 dB). Though isolation between various ports of the coupler is not perfect, it should be kept in mind that same will be the case for practical MIMO PLC modems. MIMO PLC couplers used in the measurements during this thesis have transfer functions similar to Figure 2.6. It should also be noted that during the measurements we considered the MIMO couplers as part of the PLC channel and the network analyzer was calibrated with the couplers, hence the measured channels need not to be normalized by the transfer functions of the coupler.

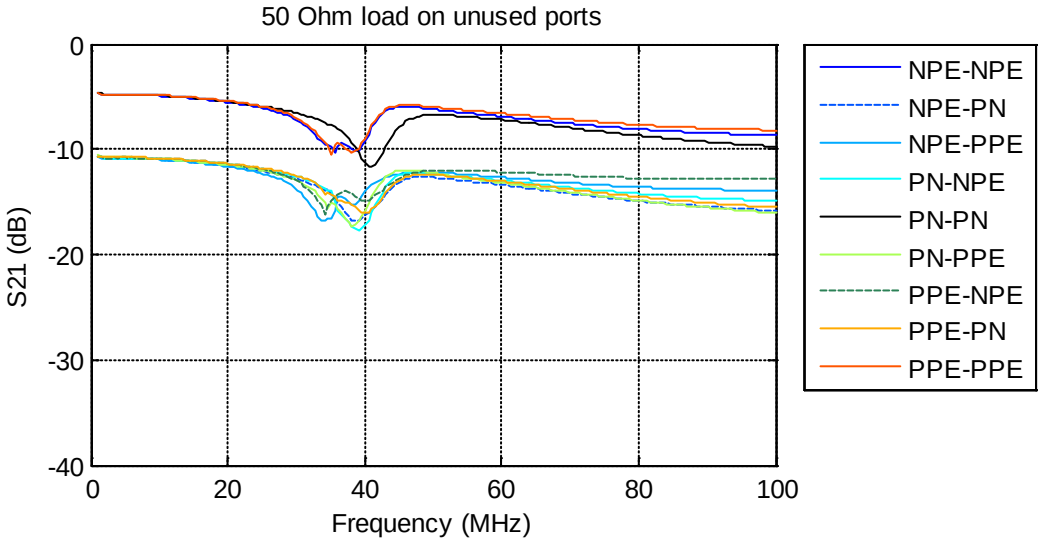

Figure 2.6. Transfer functions of a MIMO PLC coupler

3.2. Measuring instruments

3.2.1. **Vector network analyzer**

The Agilent E5071C vector network analyzer (VNA) is used for the channel transfer function measurement. A network analyzer provides the frequency domain picture of the channel in a single shot over the desired bandwidth. The VNA has the capability to store the measured data in several formats. For example, the scattering parameter S_{21} which serves as the channel transfer function can be stored in absolute magnitude, log-magnitude and complex formats. For a 2-port network, S_{21} stands for network gain (or loss). The complex format was selected for data storage. The advantage of the complex format is that the magnitude (which serves as the CTF) as well as the phase of S_{21} can be extracted from the stored data.

3.2.2. **Digital sampling oscilloscope**

The Tektronix DPO71254 is used for measuring the noise. This DSO is a high performance 4-channel instruments with a measurement bandwidth of 12.5 GHz. It can achieve a sampling rate as high as 50 GSample/s. The memory depth is in the range of 10M to 200M on all four channels. Generally, the performance of a DSO is a trade off between the number of channels, length of the measurement and the sampling rate. This means that a 4-channel DSO may be good enough to measure at 1 GSample/s for a duration of 5 ms on two simultaneous channels but to measure on four simultaneous channels one would be constrained to reduce either the measurement length or the sampling rate. We used the sampling rate of 1.25 GSample/s for a measurement length of 20 ms.

4. Measurement setup

4.1. Channel measurement setup

MIMO PLC channel measurements are performed on three different networks. For each network the measurement setup is different in order to adapt to the technical requirements.

4.1.1. **Experimental network**

The MIMO PLC channel measurements presented in this section were performed at Orange Labs on an experimental PLC network. The schematic diagram (not to the scale) of the network is shown in Figure 2.7. It can be observed that this is a very simple and stand alone network. It is nothing but a straightforward arrangement of copper wires used in household wiring.

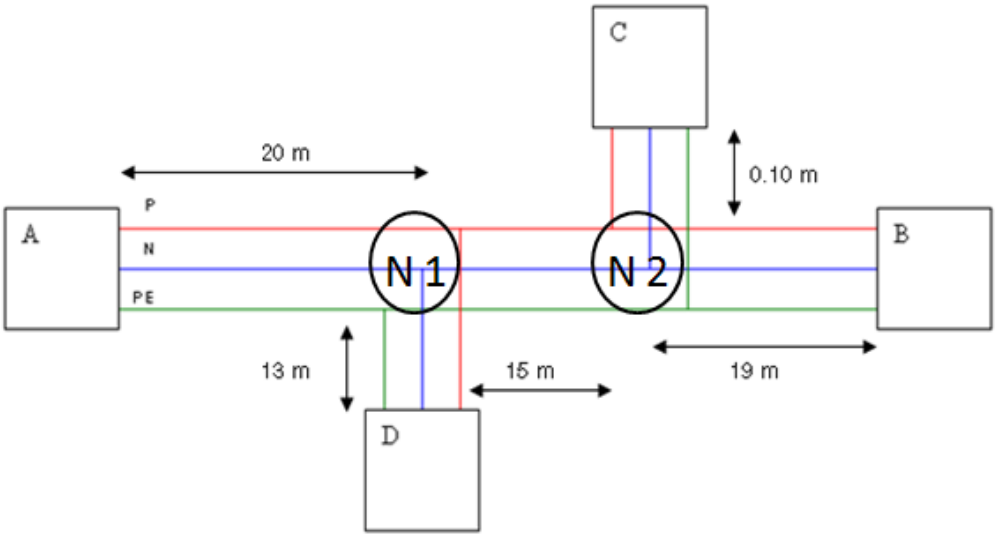

Figure 2.7. An experimental inhome PLC network

It should be noted that the network is not connected to AC mains of 230 volts. P, N and PE represent Phase, Neutral and Protective Earth wires respectively. The PE wire is not attached to any earth point. The absence of loads or appliances further simplifies the experimental setup. In a nutshell, this network offers a vey clean and almost a noise free environment. Absence of AC mains means no high voltage dependent channel variations and similarly absence of loads means no impulsive noise. However, the background noise and the narrow band noise do exist. The background noise comes from the physical nature of the medium. It depends on the

cable type used for wiring, length of the channel, quality of connections etc. The narrow band noise depends on the local radio stations and electromagnetic (EM) environment. In total, we measured 18 MIMO PLC 3x3 CTF matrices on the experimental network.

The circles represent two nodes N1 and N2 in the Figure 2.7. The boxes A, B, C and D represent the electrical sockets or PLC outlets. There are five branches in the network: N1-A, N1-D, N1-N2, N2-C and N2-B. The nodes and branches bring the signal scattering into consideration, which in turn leads to the multipath effect. Six distinct combinations of four sockets provide six PLC channels: A-B, A-C, A-D, B-C, B-D and C-D. Similar network structures, with enhanced complexity and practicality, are used in household wiring in the United States and Europe.

In order to measure the 3x3 MIMO channel matrix ***H(f)*** between two given sockets**,** nine SISO channels $h_{11}(f)$ through $h_{33}(f)$ need to be measured. The measurement set up is shown in Figure 2.8. A coupler is plugged in each socket to provide an interface between the PLC network and the measuring instrument, which in this case is a VNA. While measuring a given *h(f),* port 1 of VNA acts as a transmit port while port 2 acts as a receive port.

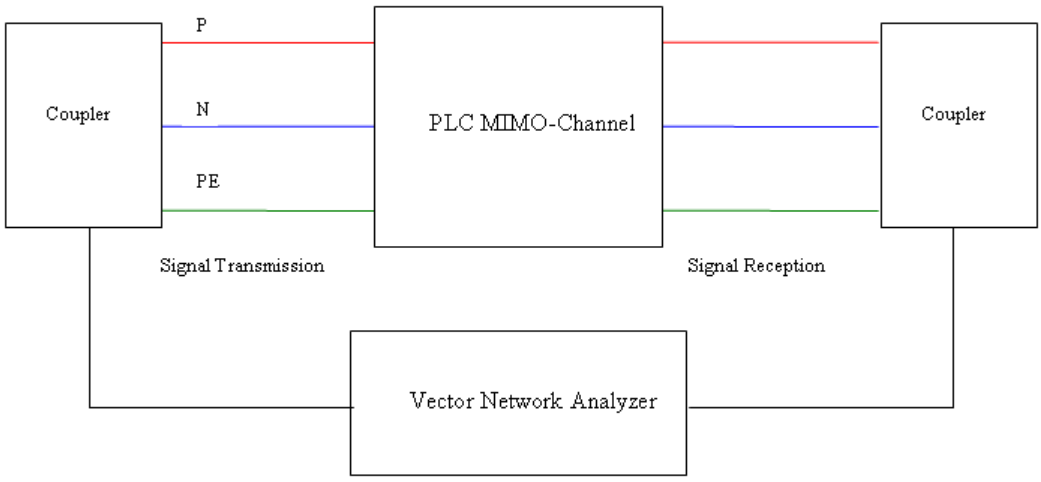

Figure 2.8. MIMO PLC channel measurement setup for the experimental network

The channel measurements were performed over a frequency band of 2-100 MHz. Although the existing PLC systems work in 2-30 MHz range only, the measurement band of 2-100 MHz is selected keeping in mind that the future PLC systems are expected to work beyond 30 MHz. The IEEE P1901 and HPAV2.0 standards already specify systems operating up to 50 MHz and 86 MHz respectively.

4.1.2. Live laboratory network

The MIMO PLC channel measurement set up mentioned above for the experimental network is repeated on a laboratory network as shown in Figure 2.9. The laboratory network in discussion is a real-life network which feeds the electricity to a laboratory used for tests and measurements on telecom equipment. It is a large network connected to 50 Hz single phase 230 volts AC mains and properly earthed. Various loads are connected to the laboratory network such as lights and measuring instruments. Therefore, practical aspects, for example, the impulsive noise generated by plugging and un-plugging events of the appliances are present in the network. Also, since the network is connected to AC mains, therefore, high voltage dependent impedance variations are also there. It should ne noted that the live laboratory network provides channel conditions which are not significantly different from a domestic network. In total, we measured 16 MIMO PLC 3x3 CTF matrices on the live laboratory network.

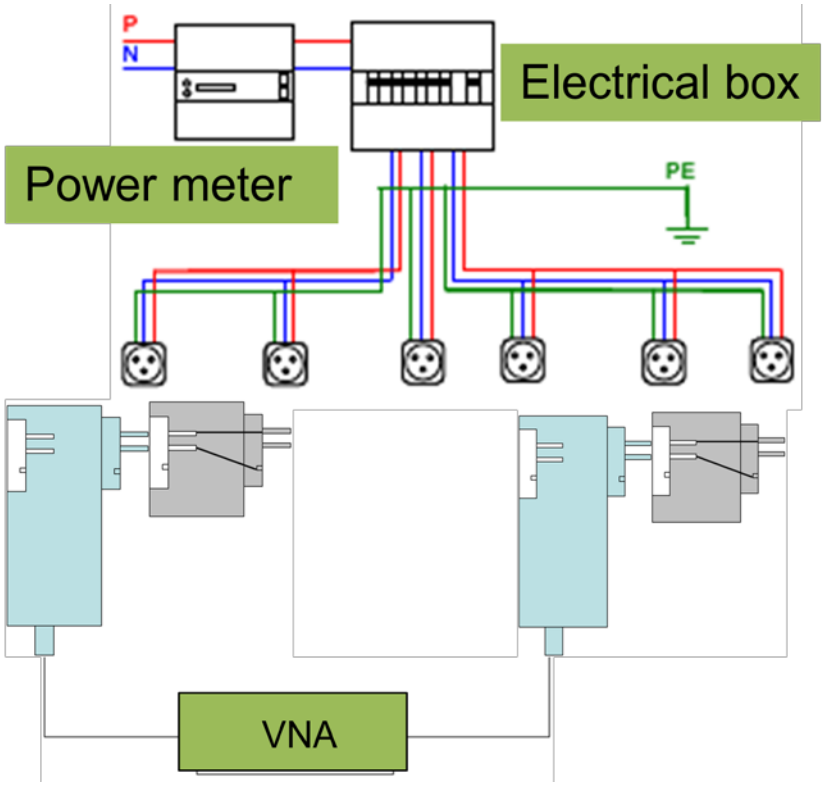

Figure 2.9. An illustration of MIMO PLC channel measurement setup for the laboratory network

4.1.3. In-home networks

Five houses were selected for measurements in a semi urban area at Lannion, France. The electrical wiring in new houses generally has the PE wire but in older houses PE

wire is often absent. Therefore, the measurements were performed only in those houses which are equipped with PE wire in electrical wiring circuits. The houses were selected to represent a good mix of characteristics like age, size and number of floors. The location of a house is also important. Different locations offer different electromagnetic noise environment, particularly the narrow band noise which is generated primarily by the local radio transmission services. The selected houses are good examples of real life scenario because they are equipped with all the appliances and electrical loads that one finds in common houses. In each house, 6 to 10 sockets were selected for measurements and 7 to 10 MIMO PLC channel (3x3 matrices) were measured. Figure 2.10 shows the MIMO PLC channel measurement set-up employed in a customer's houses.

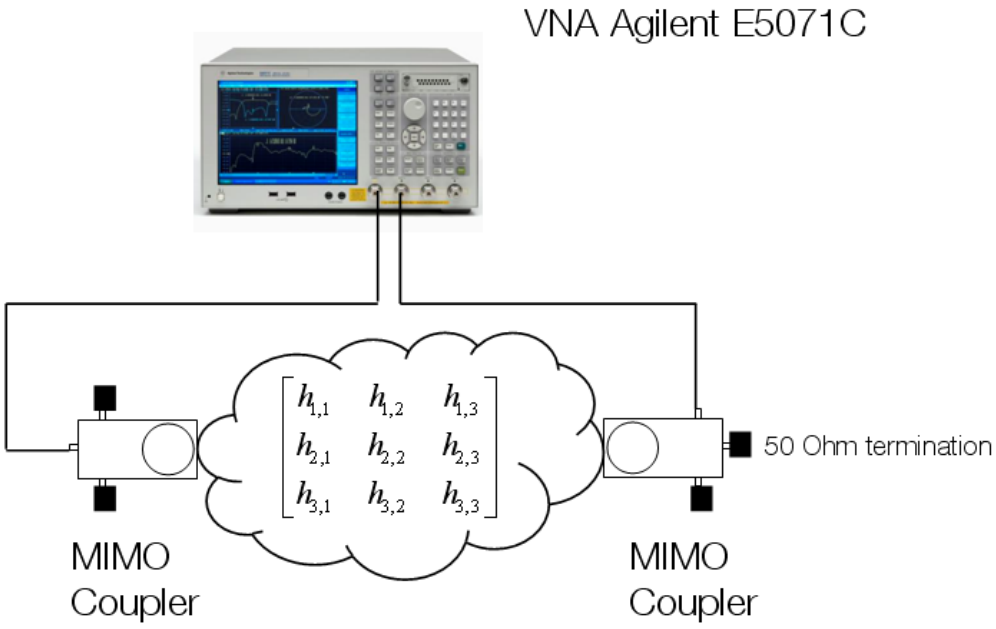

Figure 2.10. An illustration of MIMO PLC channel measurement setup used for inhome networks

Inhome PLC networks are fed by the single phase 50 Hz 230 volts AC mains, and duly earthed. The measurement set up and method is generally the same as described above for the experimental and live laboratory networks. However, there are some exceptions as well. For example, the channels are measured over a larger band i.e. 2-150 MHz. In addition, special precautions were employed to avoid contaminations in the measured data. The input impedance of a VNA port is typically 50 ohm. The unused ports at each coupler need to be terminated by a 50 ohm load. This helps to avoid unwanted reflections due to impedance mismatch at the coupler ports. It should

be noted that the power line impedance is not known *a priori*. Therefore, rather than matching the coupler ports to the power line impedance, the measurement setup assumes that the coupler ports are matched to a fixed impedance, as would be the case in a realistic system. Shielded cables are used for the connection between the MIMO coupler and the VNA. This precaution helps to avoid ingress of electromagnetic radiation on measurement set up which may pollute the measured data. The socket attached to port 1 of the VNA acts as a transmit socket, while the one attached to port 2 acts as a receive socket.

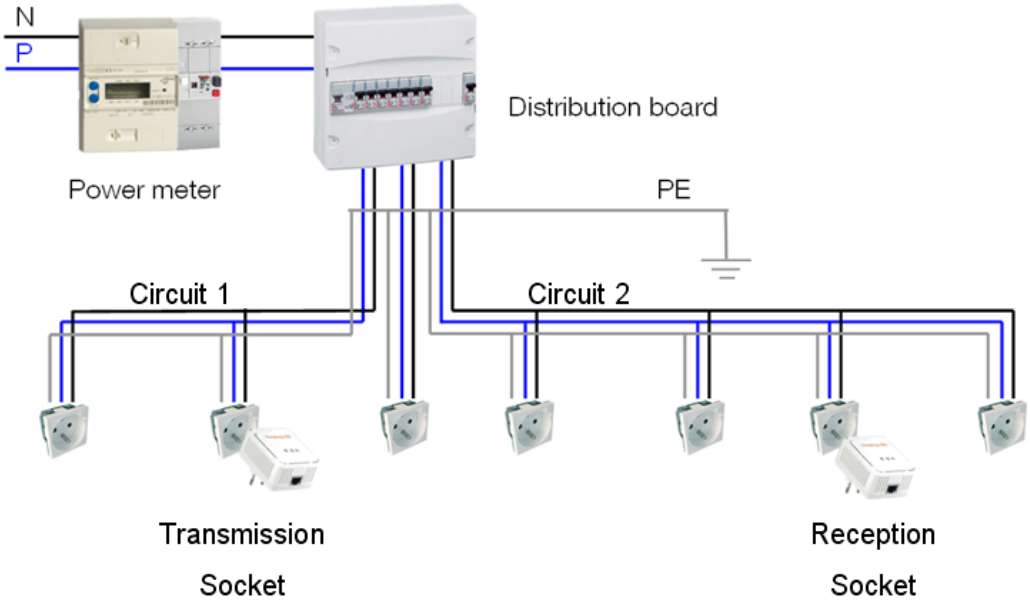

Figure 2.11. An illustration of signal communication over an inhome electrical network

The measurements campaigns described in the PLC literature generally ignore the topological aspects of the PLC network because the measurements are exploited to propose a top-down model. Consequently, the onus of the topological consideration is left to the bottom-up approach. However, between these two extreme positions there is a possibility to capture some, if not all, topological aspects of the PLC network during the measurements. For example, the identification of the physical circuits and the sockets connected to them can provide some topological information about the PLC network. During the measurement campaign under discussion this was done by physically switching the circuit breakers OFF and ON. The purpose of this test is to

identify which PLC socket is connected to which physical circuit. As a result the PLC sockets can be categorized as "same-circuit sockets" and "different-circuit sockets". For instance, Figure 2.11 shows a communication set up between two "different-circuit sockets" because the transmission socket is connected to the physical circuit 1 while the reception socket is connected to the physical circuit 2. The fundamental difference between the same-circuit sockets and different-circuit sockets is that the sockets found on the same circuit have nothing but copper wires between them, while the sockets situated on two different circuits are accessible to each other via the distribution box. Therefore, it is expected that the CTF measured between two same-circuit sockets would be stronger and cleaner than the one between two different-circuit sockets. Consequently, the same-circuit channels would offer more capacity than the different-circuit channels. In total, we measured 21 MIMO PLC 3x3 CTF matrices for the same-circuit channels and 21 MIMO PLC 3x3 CTF matrices for the different-circuit channels.

4.2. Noise measurement setup

The MIMO PLC channel noise consists of three noise sequences: P-N, N-PE and P-PE. The noise measurements are performed at the houses mentioned in the Section 4.1.3. Noise measurements are strictly related to the reception sockets. In total, there are 27 reception sockets and noise is measured at all of them. Figure 2.12 shows the schematic diagram of the MIMO noise measurement setup.

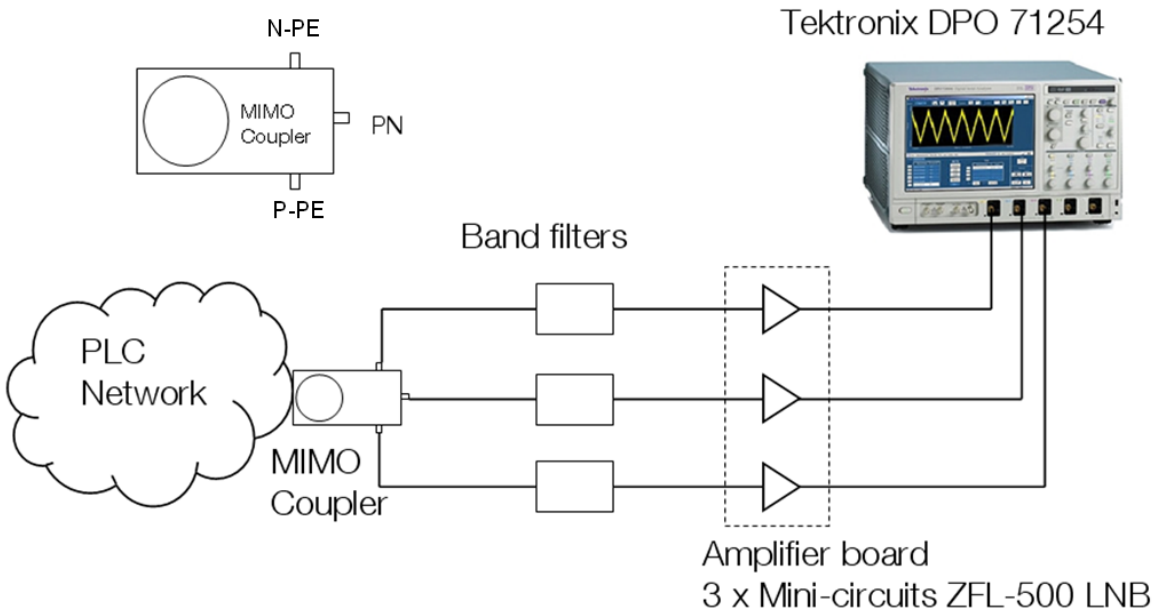

Figure 2.12. MIMO PLC channel noise measurement setup

The measurements discussed in this section were performed in time-domain at a sampling frequency of 1.25 Gsamples/second. Such a high sampling rate was selected in accordance with Nyquist-Shannon sampling theorem which states that if a function *f(t)* contains no frequency more than *B* Hertz, it is completely determined by giving its ordinates at a series of points spaced 1/(2B) seconds apart [Shan49]. In other words, for a signal of bandwidth *B* the sampling rate should be at least *2B*. So a sampling frequency of 1.25 Gsamples/second is good enough for a desired noise bandwidth of 500 MHz. The MIMO noise was measured over a period of 20 ms which corresponds to the period of one complete cycle of the 50 Hz 230 V AC mains. The impedance of many electrical appliances depends on the instantaneous level of the AC mains. It is desirable to measure the noise over one complete AC mains cycle to include this effect in the measured data. The band filters shown in Figure 2.12 consisted of three 2-500 MHz band pass filters and three FM notch filters. The lower cut-off value (2 MHz) of the band pass filters corresponds to the lower end of the current SISO PLC systems. The frequency band below 2 MHz is extremely noisy so it is not used for PLC signal transmission. The FM notch filters have a typical attenuation of 20-35 dB over the 88-108 MHz band. The measurements were performed with and without FM notch filters to capture the effect of the narrow band noise created by the FM broadcast stations. Moreover, the FM band generates a strong external ingress which leads to an overall increase in the level of the noise. Higher noise amplitude leads to a

higher quantization noise. Filtering out the FM noise allows the remaining noise to be measured with a better resolution. Although the three amplifiers are optional, they were used throughout the noise measurement campaign for better resolution of stored data. The amplifiers have typical gain of 28 dB over 2-500 MHz band and need +15 volts and 60 mA for biasing.

Some particular precautions were taken to ensure clean and uncontaminated capture of the noise samples. For example, for avoiding the radiated interference, short (1 meter length) shielded SMA cables were used to connect the MIMO coupler with the oscilloscope. The oscilloscope and amplifiers' biasing power supply were plugged into the 230 volts AC mains through a filtered power cable to prevent the conducted interference from the electrical wiring enter the measuring instrument. The instrument used for MIMO PLC channel noise measurement is a high performance multi channel digital oscilloscope. The choice of the oscilloscope was largely defined by the memory required to capture three simultaneous, high resolution noise sequences. In a single shot, with the settings mentioned above, MIMO PLC noises N-PE, P-N, and P-PE of a given reception socket are captured and stored.

5. Measurements and observations

This section presents the observations and findings based on the data obtained from the channel and noise measurements. We will discuss various aspects of the measured MIMO PLC channels and noise.

5.1. Channel measurements

5.1.1. **Experimental network**

A typical 3x3 MIMO PLC CTF matrix measured over the experimental network is shown in Figure 2.13. It can be noticed in Figure 2.13 that the channel strength decreases with the increasing frequency. This underlines the frequency dependent nature of the MIMO PLC channel. The other noticeable feature is the presence of notches or deep fades which signifies the multipath effect. The other important aspect which can be observed in Figure 2.13 is that the strength of NPE-NPE, PN-PN and PPE-PPE channels (co-channels or direct channels) is 3-5 dB higher than the remaining six channels (cross-channels or indirect channels). This is due to the fact that the strength of the cross-channels depends solely on the electromagnetic coupling

between wires while for the co-channels, in addition to the coupling, a direct conduction path is also available.

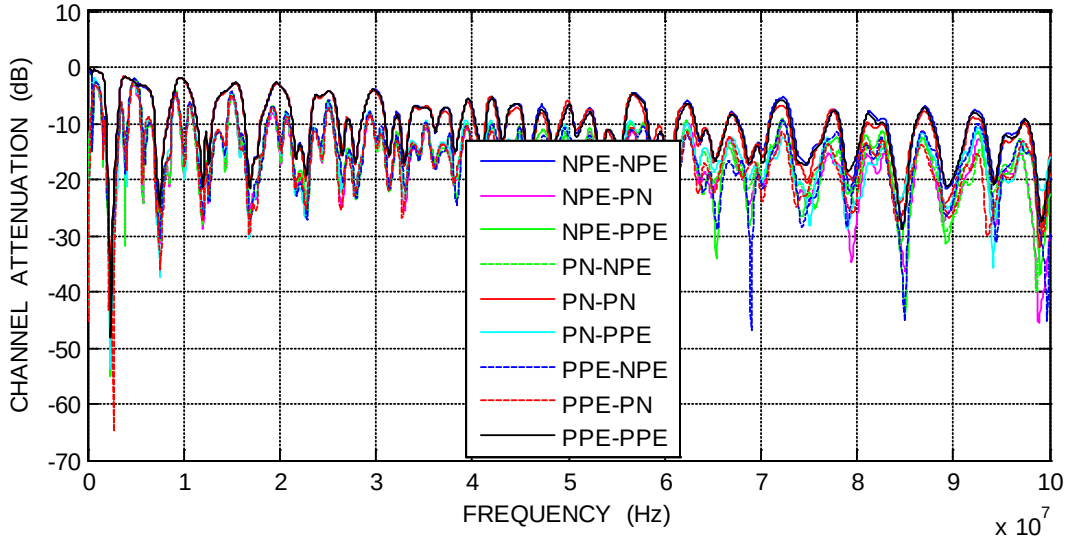

Figure 2.13. A typical 3x3 MIMO PLC channel magnitude matrix measured on the experimental network

5.1.2. **Live laboratory network**

A typical MIMO PLC CTF matrix measured on the live laboratory network is shown in Figure 2.14. The frequency dependent nature of the channel is quite evident. However, the laboratory network, which is real-life network feeding electricity to the laboratory, shows more channel attenuation than the experimental network. In addition, there are more frequent and deeper notches in the channel transfer function which signifies the complexity of the laboratory network. The other aspect that needs attention in Figure 2.14 is that there is no significant difference between the strength of co-channels and cross-channels which means that for a large, real-life network the effect of the direct conduction path is not significant. On the basis of this observation it can be argued that the increased complexity and size of the PLC network neutralizes the advantage the direct channels have in a simple and small PLC network.

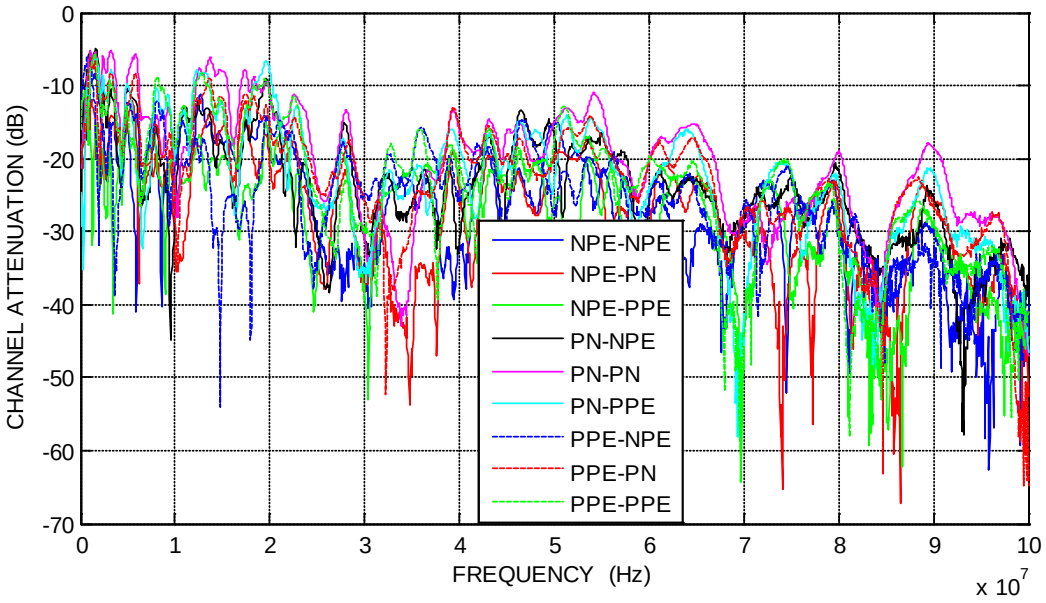

Figure 2.14. A typical 3x3 MIMO PLC CTF matrix measured on the live laboratory network.

5.1.3. **In-home PLC networks**

Measurements on the experimental and laboratory networks provided valuable introductory information about the MIMO PLC channels and offered an opportunity to learn and perfect the measurement skills. However, the measurement of MIMO PLC channels in houses is the final goal of this measurement campaign.

Figure 2.15 shows typical inhome MIMO PLC channel measured over the same-circuit sockets. It can be noticed that inhome MIMO PLC channels are frequency dependent, multipath channels. Moreover, the co-channels (or direct paths) are slightly stronger than cross-channels at lower frequencies.

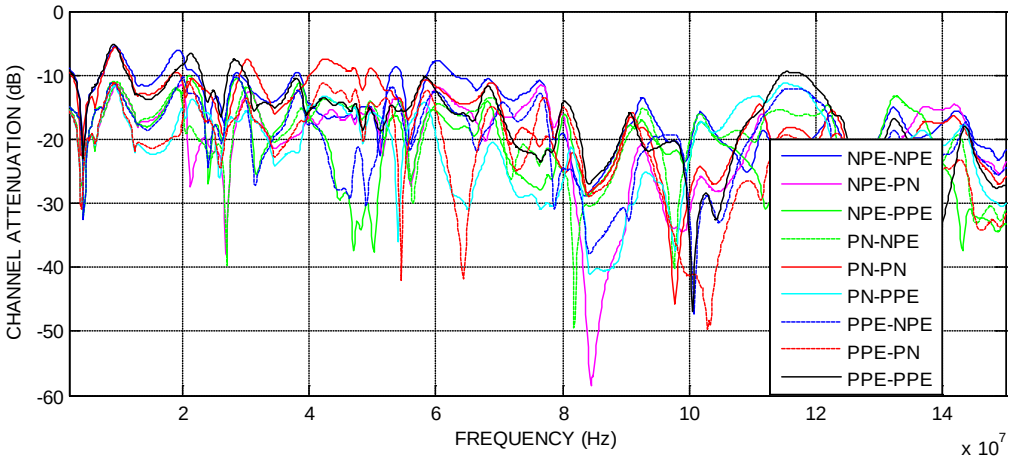

Figure 2.15. Typical inhome 3x3 MIMO PLC CTF matrix measured over the same-circuit sockets

Figure 2.16 shows typical inhome MIMO PLC channel measured over different-circuit sockets. The frequency dependent, multipath nature of the channel is quite evident. However, it should be noticed that the different-circuit channels are considerably weaker than the same-circuit channels. Moreover, the co-channels are not necessarily stronger than the cross-channels.

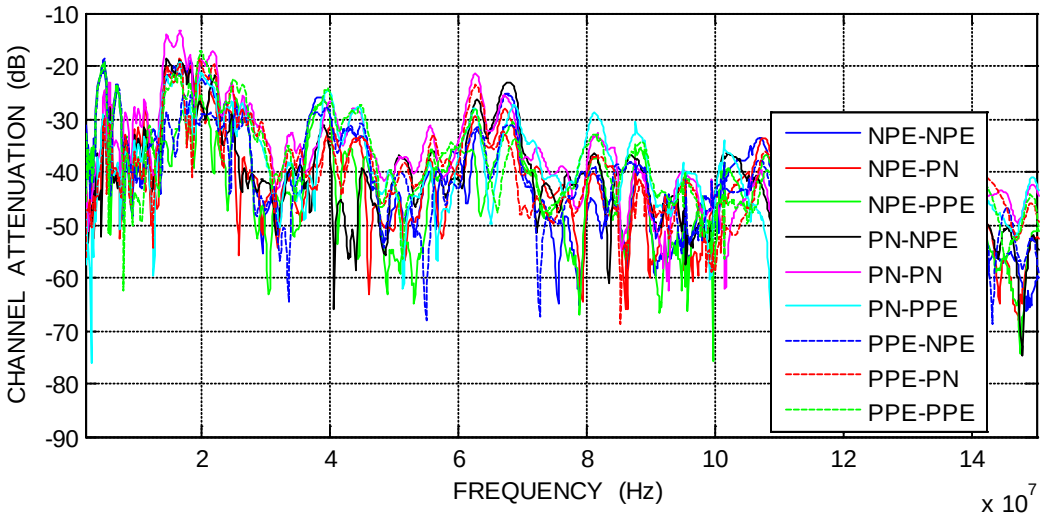

Figure 2.16. Typical inhome 3x3 MIMO PLC CTF matrix measured over the different-circuit sockets

5.2. Noise measurements

Figure 2.17 shows typical MIMO PLC channel noise sequences over a short interval of 0.33 ms. Some interesting observations can be made in Figure 2.17. The level of P-N noise is lower than N-PE and P-PE noises.

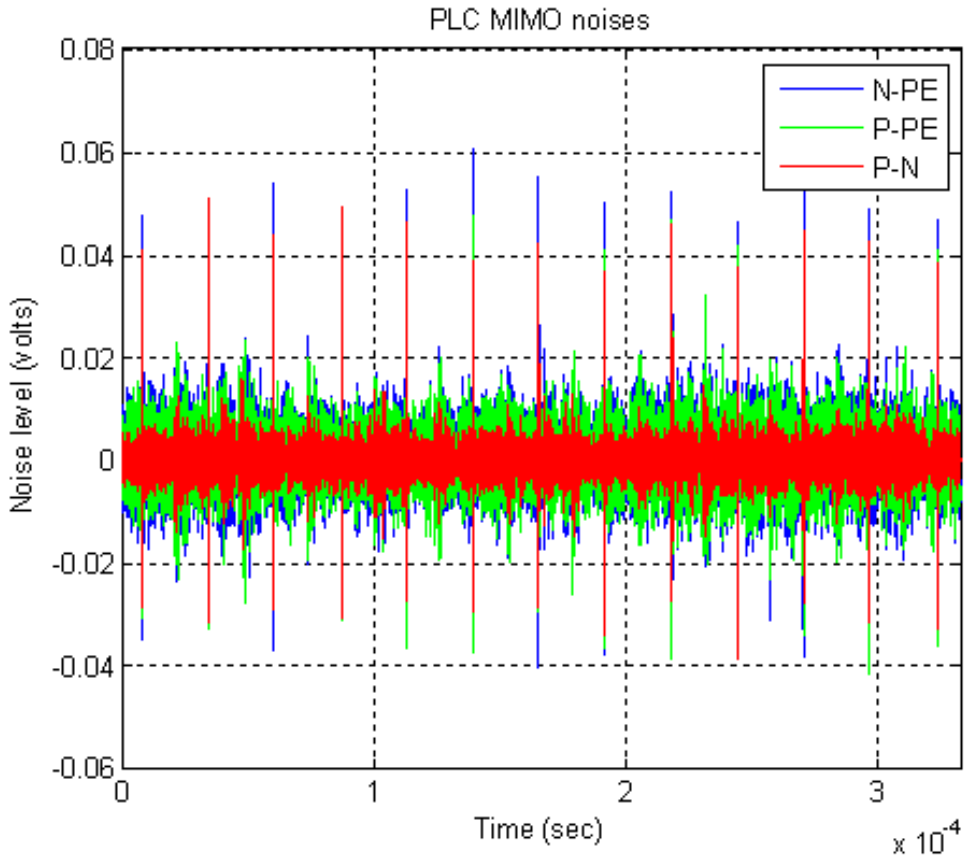

Figure 2.17. Noise measured on an in-home PLC network

Figure 2.18 shows the spectrum of N-PE, P-N and P-PE noises with FM band whereas Figure 2.19 shows the spectrum of N-PE, P-N and P-PE noises without FM band (FM band filtered out by the FM notch filters). The noise PSD is calculated by Eq. 2.1 where P_N stands for the PSD of a MIMO noise sequence in dBm/Hz and $N_{meas}(f)$ is the frequency domain noise obtained by the Fourier transformation of the measured time-domain noise in Volts. Z is the input port impedance of the oscilloscope in Ohm. The sampling frequency f_s is set equal to 1.25 Gsample/s. G is the gain of the amplifiers in linear scal and N_{FFT} is the length of noise sequence in time-domain.

$$P_N = 10Log_{10}\left[\frac{1000|N_{meas}(f)|^2}{Z\,N_{FFT}\,f_s G}\right] \text{ dBm/Hz} \qquad (2.1)$$

It is clear that the noise PSD below -160 dBm/Hz is clipped off for the frequencies above 150 MHz. The clipping effect was observed at all the sockets. Therefore, the MIMO noise analysis was restricted to the 2-150 MHz band. This clipping effect is

due to the sensitivity constraint of the oscilloscope we used. In fact all measuring instruments, however sophisticated, have a limit of level resolution below which they can not detect a signal.

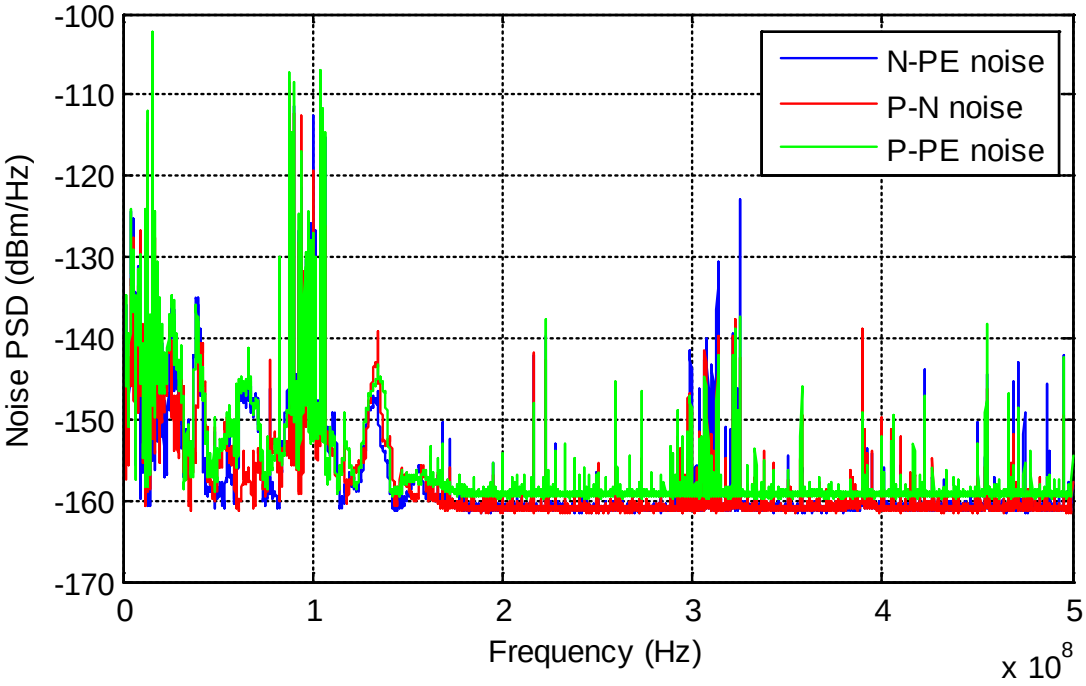

Figure 2.18. Spectrum of typical MIMO PLC channel noises (with FM band)

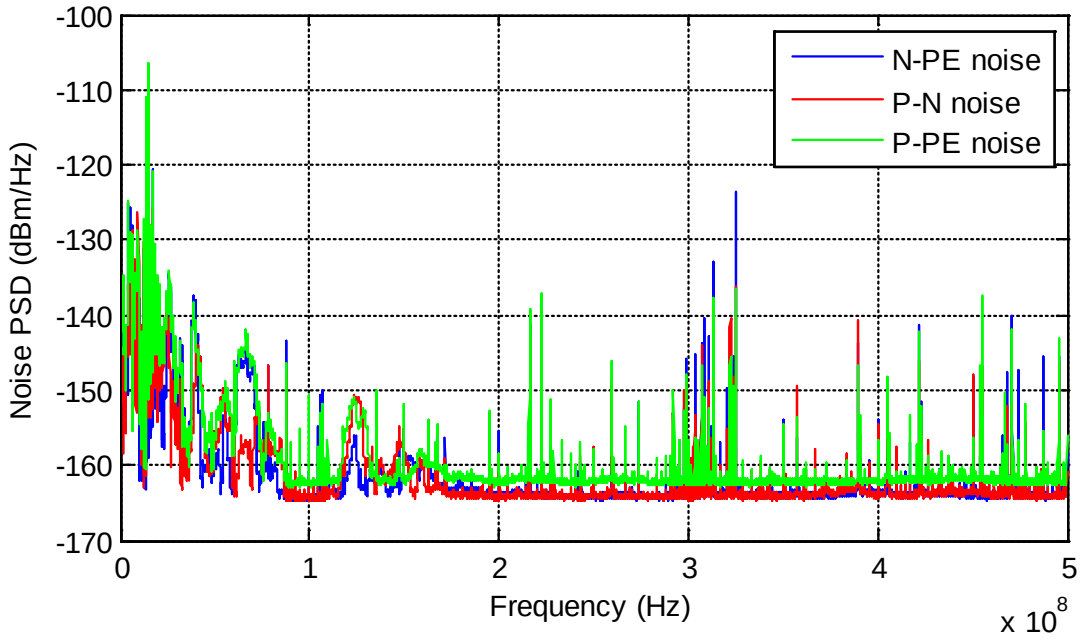

Figure 2.19. Spectrum of typical MIMO PLC channel noises (FM band filtered out)

From Figure 2.18 and Figure 2.19 it is evident that the noise has a frequency dependent nature. The noise level is higher at the lower frequencies and the level decreases as the frequency increases. In [Esma03] and [Omega08], SISO PLC channel background noise has been modeled as a decreasing exponential function of frequency and it seems true for MIMO PLC noise as well. Figure 2.18 and Figure 2.19 also shows that the PSDs of N-PE and P-PE noises are quite similar to each other and higher than that of the P-N noise. This difference is generally around 5 dB, however, for some frequencies it is of the order of 10 dB as well. In Figure 2.18, the strong narrow band FM noise is also visible in the 88-108 MHz range. It can be noticed in Figure 2.19 that due to the absence of the FM band the spectrum as low as -164 dBm/Hz is visible between 2-88 MHz while in Figure 2.18 it was limited to -160 dBm/Hz. Indeed, filtering out the FM band helps to improve the measurement resolution, since a narrower voltage observation window can be used.

6. Analysis and results

This section describes some preliminary results obtained from the channel and noise measurements. For example, MIMO channel capacity, MIMO capacity gain, mean noise PSD, noise correlation, etc.

6.1. MIMO channel capacity

6.1.1. **Experimental network**

The MIMO capacity C_{MIMO} for a multi-port channel is calculated by using the Eq. 2.2.

$$C_{MIMO} = \sum_{n=1}^{N_F} \Delta f \sum_{i=1}^{n_t} \log_2 \left(1 + \frac{P_{T_x}(f_n)\lambda_i(f_n)}{N_{R_x}(f_n) n_t}\right) \quad \text{bits/sec} \tag{2.2}$$

where $\lambda_i(f_n)$ denotes the eigenvalues of $\boldsymbol{HH}^{\dagger}$ at a given measurement frequency f_n and † stands for the Hermitian transpose. Similarly, $P_{T_x}(f_n)$ is the transmitted power, $N_{R_x}(f_n)$ is the noise at the receiver, n_t is the number of transmit ports, N_F is the number of carrier frequencies and Δf is the frequency step size. Here we have chosen Δf to be around 24 kHz which is the standard carrier spacing in commercial OFDM based PLC systems. The $P_{T_x}(f_n)$ mask recommended by the Omega Project [Omega08] has been selected in our calculations, according to which, a P_{T_x} of -50

dBm/Hz is transmitted from 0 to 30 MHz and -80 dBm/Hz for the frequencies onwards (Figure 2.20).

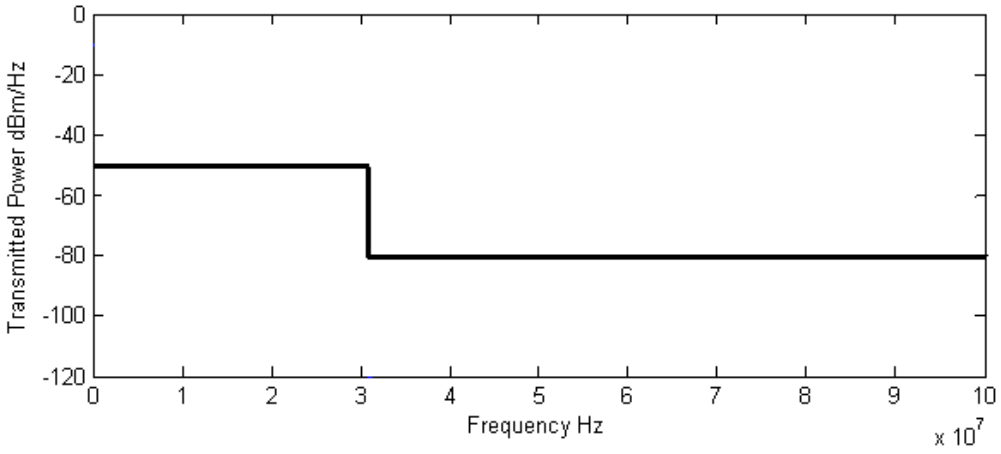

Figure 2.20. Transmit power (P_{Tx}) mask proposed for the PLC systems

For channel noise, a colored Gaussian noise model is considered. The Power Spectral Density (PSD) of $N_{R_x}(f_n)$ is a model described in ICT OMEGA project [Omega08]. This model, depicted in Figure 2.21 was extracted from practical measurements on SISO PLC networks. It closely resembles the noise model mentioned in [Beny03]. The channel noise $N_{R_x}(f_n)$ is represented by Eq. 2.3.

$$N_{R_x}(f_n) = \frac{1}{f^2} + 10^{-15.5} \quad \text{mW/Hz} \tag{2.3}$$

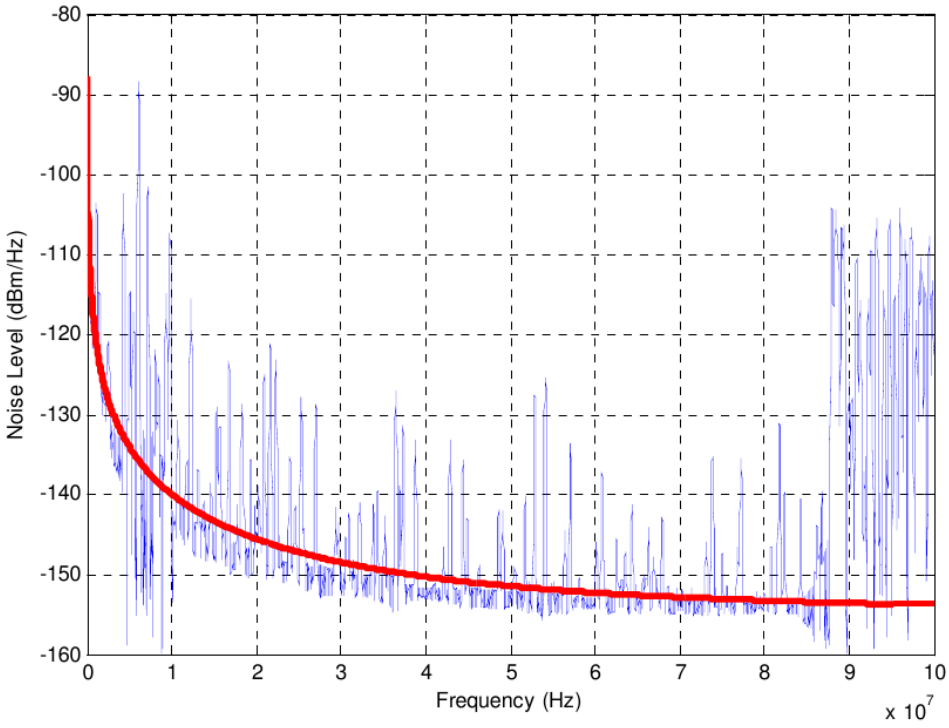

Figure 2.21. Noise model proposed in [Omega08]

The MIMO capacity gain of a system is obtained from the comparison between the MIMO capacity and the SISO capacity. For the calculation of the SISO capacity C_{SISO}, the channel transfer function measured between PN ports was selected. That is, the measurement for which the signal is transmitted and received between P and N wires. The selection of PN-PN transfer function for SISO capacity calculation is justified from the practical point of view as well because the existing SISO PLC systems use PN port for data transfer. The SISO capacity is determined by Eq. 2.4

$$C_{SISO} = \sum_{n=1}^{N_F} \Delta f \log_2 (1 + \frac{P_{T_x}(f_n)|h(f_n)|^2}{N_{R_x}(f_n)}) \quad \text{bits/sec} \tag{2.4}$$

where $h(f_n)$ denotes the PN port channel transfer function. It is important to notice at this point that in both SISO and MIMO capacity computations the same total transmit power is used. Finally, the MIMO capacity was divided by the SISO capacity to obtain the capacity gain as shown in Eq. 2.5.

$$Gain_{MIMO} = \frac{C_{MIMO}}{C_{SISO}} \tag{2.5}$$

The average MIMO capacity gain of eighteen (six NPE-PN, six PN-PPE and six NPE-PPE) 2x2 configurations is found out to be around 1.88, or in other words an almost 88% increase compared to the existing SISO PLC systems which utilize only two wires. Some important MIMO capacity results over the 2-100 MHz frequency band are summarized in Table 2.1.

	Max	Min	Mean
2x2 MIMO Capacity	4.50 Gbps	4.12 Gbps	4.32 Gbps
2x2 MIMO Capacity Gain	1.90	1.87	1.88

Table 2.1 Max, min and mean values of MIMO capacity and MIMO capacity gain over 18 measurements.

MIMO capacity, SISO capacity and capacity gain versus frequency are depicted in Figure 2.22. It can be observed that MIMO and SISO capacities are higher for the 2-30 MHz band. This effect simply corresponds to a higher transmit power in the 2-30 MHz range. Moreover, the capacities increase with frequency in 2-30 MHz band. It can be attributed to the decaying noise level $N_{R_x}(f_n)$. The sudden fall in the MIMO and SISO capacities at f = 30 MHz is due to the reduced level of transmit power as described in the transmit power mask (Figure 2.20). Interestingly, the capacity gain (which is around 1.88) is almost independent of the frequency throughout the 2-100 MHz band.

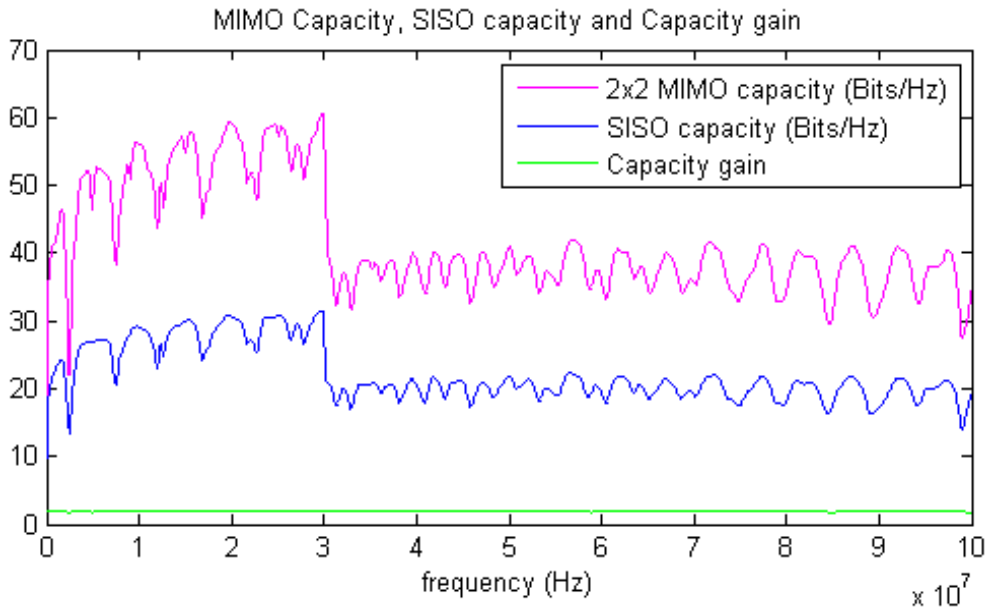

Figure 2.22. MIMO capacity, SISO capacity and capacity gain observed in the experimental PLC network

6.1.2. **Live laboratory network**

The algorithm and method of the channel capacity calculation for the live laboratory network are the same as presented in the Section 6.1.1. Table 2.2 shows some representative results.

	Max	Min	Mean
2x2 MIMO Capacity	4.58 Gbps	2.77 Gbps	3.65 Gbps
2x2 MIMO Capacity Gain	1.98	1.71	1.84

Table 2.2 Max, min and mean values of MIMO capacity and MIMO capacity gain.

Figure 2.23 shows MIMO capacity, SISO capacity and capacity gain as a function of frequency. It can be noticed that the level of MIMO and SISO capacities in Figure 2.23 is slightly lower than that in Figure 2.22. This is due to fact that the PLC channels in the live laboratory network are weaker and noisier than the experimental PLC network.

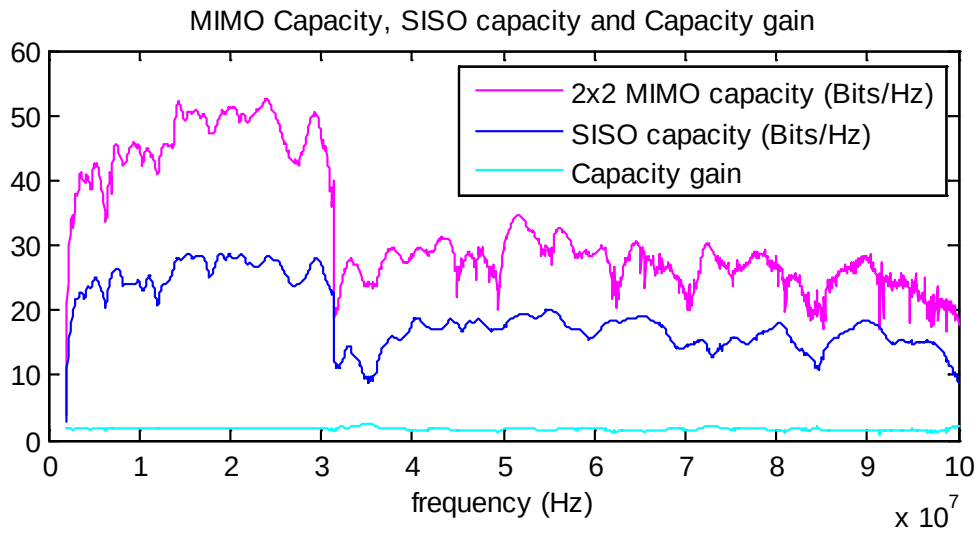

Figure 2.23. MIMO capacity, SISO capacity and capacity gain observed in the laboratory network

6.1.3. **In-home PLC networks**

For the calculation of MIMO and SISO capacities, again, Eq. 2.2 and Eq. 2.4 are used respectively. Similarly, for calculating the MIMO capacity gain Eq. 2.5 is used. However, there are some particularities as well. For example, the channel capacity results for the inhome networks are obtained over an extended frequency range i.e. 2-150 MHz. The other particularity is the type of the noise in Eq. 2.2 and Eq. 2.4. Instead of using a simple colored Gaussian noise model, the actual noise measured on the in-home PLC networks is used.

It is worth reminding here the topological consideration of the same-circuit and the different-circuit as described in the Section 4.1.3. While performing the capacity calculations this topological aspect is retained as well. Table 2.3 shows the results on MIMO capacity and capacity gain for the channels measured across two same-circuit sockets whereas Table 2.4 shows the results for different-circuit sockets.

	For same-circuit		
	Max	Min	Mean
2x2 MIMO Capacity	6.41 Gbps	3.2 Gbps	5.13 Gbps
2x2 MIMO Capacity Gain	1.90	1.70	1.81

Table 2.3 Max, min and mean values of MIMO capacity and MIMO capacity gain for inhome PLC networks (same-circuit channels)

	For different-circuit		
	Max	Min	Mean
2x2 MIMO Capacity	3.63 Gbps	1.32 Gbps	2.15 Gbps
2x2 MIMO Capacity Gain	1.92	1.39	1.70

Table 2.4 Max, min and mean values of MIMO capacity and MIMO capacity gain for inhome PLC networks (different-circuit channels)

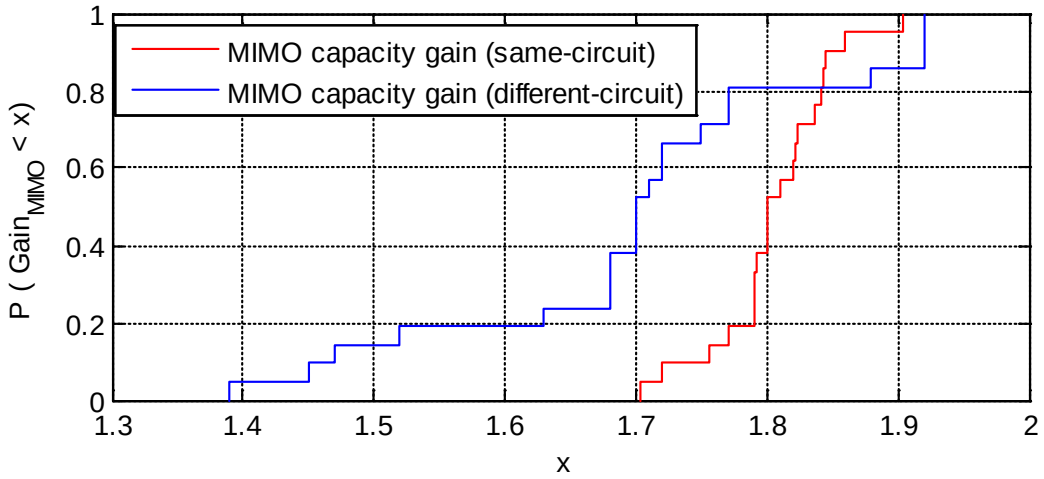

Figure 2.24. CDFs of $Gain_{MIMO}$ for same-circuit and different-circuit channels

The CDF of Figure 2.24 shows the statistical spread of 2x2 MIMO capacity gain for the same-circuit and the different-circuit channels. In Figure 2.24, it can be noticed that for the same-circuit case 80% of the channels exhibit a $Gain_{MIMO}$ between 1.7 and

1.84 and for the different-circuit case 80% of the channels show a $Gain_{MIMO}$ between 1.39 and 1.77.

6.1.4. Analysis of MIMO capacity results

The main results on MIMO capacity of various PLC networks have been shown in Table 2.1, Table 2.2, Table 2.3 and Table 2.4. It can be observed in Table 2.1 that for the experimental network the figures for MIMO capacity and MIMO capacity gain are quite monotonous, i.e. there is not a significant difference between the min, max and mean values. This effect is self evident because the experimental network represents a very simple network topology in an almost noiseless environment. The experimental network fails to offer appreciable diversity of real-life network conditions.

The results shown in Table 2.2, however, exhibit more fluctuation. Here, it can be viewed that the difference between maximum and minimum values of MIMO capacity is 1.8 Gb/s. Stated otherwise, the minimum value of MIMO capacity is 40% less than the maximum. The same effect is present, to some degree, for MIMO capacity gain. From the comparison of Table 2.1 and Table 2.2 it is evident that although the live laboratory network offers less MIMO capacity than experimental network, the MIMO capacity gain is nearly same for both the networks. This is because the SISO capacity of laboratory network decreases as well. The net decrease in MIMO capacity for the live laboratory network compared to the experimental network is not astonishing. This is due to the fact that the live laboratory network offers more practical environment for signal propagation such as noise, loads, network topology, network size etc.

Table 2.3 shows capacity results for the inhome networks, same-circuit case. The minimum value of MIMO capacity is 50% of its maximum value. However, the mean value tilts more towards the maximum value. The mean value of MIMO capacity is greater than Table 2.1 and Table 2.2 due the fact that a larger frequency band (2-150 MHz) has been explored for the inhome networks. The value of mean MIMO capacity gain is around the 1.8 mark which is not too far from the experimental and the live laboratory networks.

Finally, Table 2.4 presents the results for the inhome networks, different-circuit case.

The minimum value of MIMO capacity is 60% of its maximum value which is the largest deficit among all four Tables. Moreover, the mean MIMO capacity tilts towards the minimum value which is lowest (2.15 Gb/s) among all four Tables. For the MIMO capacity gain, the mean value is 1.70 which is not too far from other three Tables, however, there is a significant difference (27% of the maximum) between the maximum and minimum values. In fact, the overall low values of MIMO capacity and gain for the different-circuit case are understandable because these channels are the most attenuated.

The above mentioned results provided a consolidated evidence of the potential benefits offered by MIMO PLC systems. It has been consistently observed that a MIMO capacity gain of around 1.8 is realizable for a 2x2 MIMO system.

6.2. Noise analysis

MIMO PLC channel noise measurement campaign created a large database of noise sequences. Parameters like mean PSDs, difference between mean PSDs, time domain correlation etc. can be defined to analyze the data.

6.2.1. **Mean Noise PSD**

The mean PSDs of N-PE, P-N and P-PE noises for all measurements at 27 PLC sockets are calculated. The CDFs of mean noise PSDs are shown in Figure 2.25 where it can be observed that the mean PSD of PN noise is generally less than P-PE and N-PE noises by a factor of 3-5 dB. However, the mean PSDs of P-PE and N-PE noises are quite close to each other. This result is important as it presents a statistical analysis of noise levels in MIMO PLC channels.

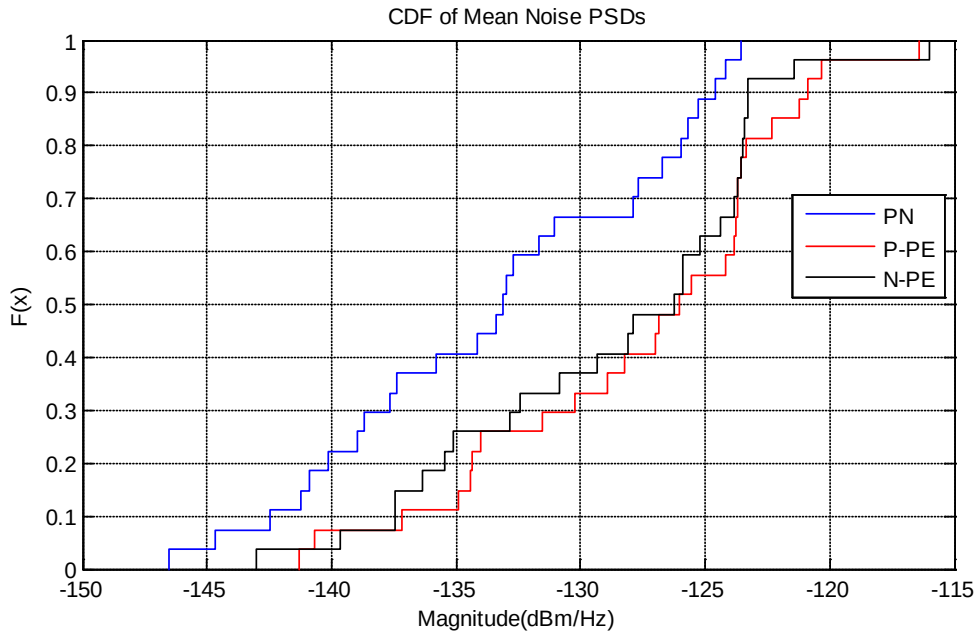

Figure 2.25. CDF of mean noise PSDs

A more illustrative and direct way to visualize the above statistics is the CDF of the difference between mean noise PSDs as depicted in Figure 2.26. It shows that for almost 80% of the sockets the P-PE noise is at least 3 dB stronger than P-N noise. Similar trend can be observed for N-PE noise. However, we find that P-PE and N-PE noises exhibit similar strength at majority of the PLC sockets. Such information about PLC MIMO noise statistics is useful for constructing a general MIMO PLC channel noise model. These results about the noise level, indicating the relative noisiness of the physical channels, are significant for PLC MIMO system's throughput calculation and capacity optimization.

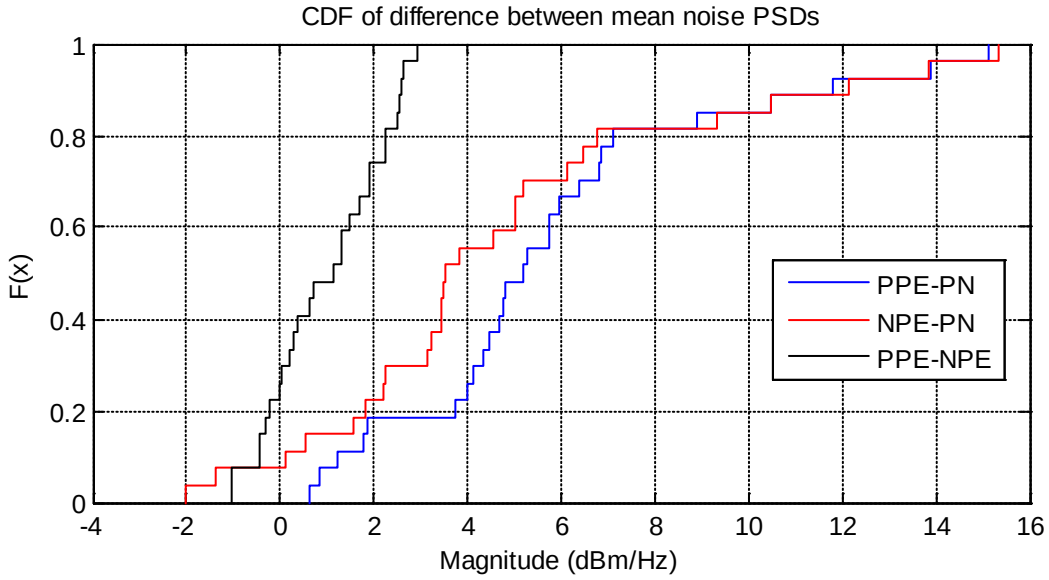

Figure 2.26. CDF of the difference between mean noise PSDs

6.2.2. **Cross Correlation between Noises**

Cross correlation between two data vectors or waveforms indicates their mutual dependency. For two vectors $X(n)$ and $Y(n)$ in discrete domain, the cross correlation coefficient $R_{x,y}$ is given by Eq. 2.6

$$R_{x,y} = \frac{E[(X-\mu_x)(Y-\mu_y)]}{\sigma_x \sigma_y} \tag{2.6}$$

where $E[.]$ stands for expectation or mean function, μ is the mean value and σ is the standard deviation. The value of $R_{x,y}$ varies between 0 and 1, where 0 shows a perfect mismatch or de-correlation between $X(n)$ and $Y(n)$ and 1 indicates a perfect correlation.

Cross correlation between noise sequences of the MIMO PLC channel are calculated and the results are shown in Figure 2.27. A low correlation between P-N and P-PE noises can be observed, and the same is true for P-N and N-PE noises also. However, a relatively higher value of correlation is found between N-PE and P-PE noises. The knowledge about correlation statistics of PLC MIMO noise is important, particularly for future PLC systems which will have MIMO functionality.

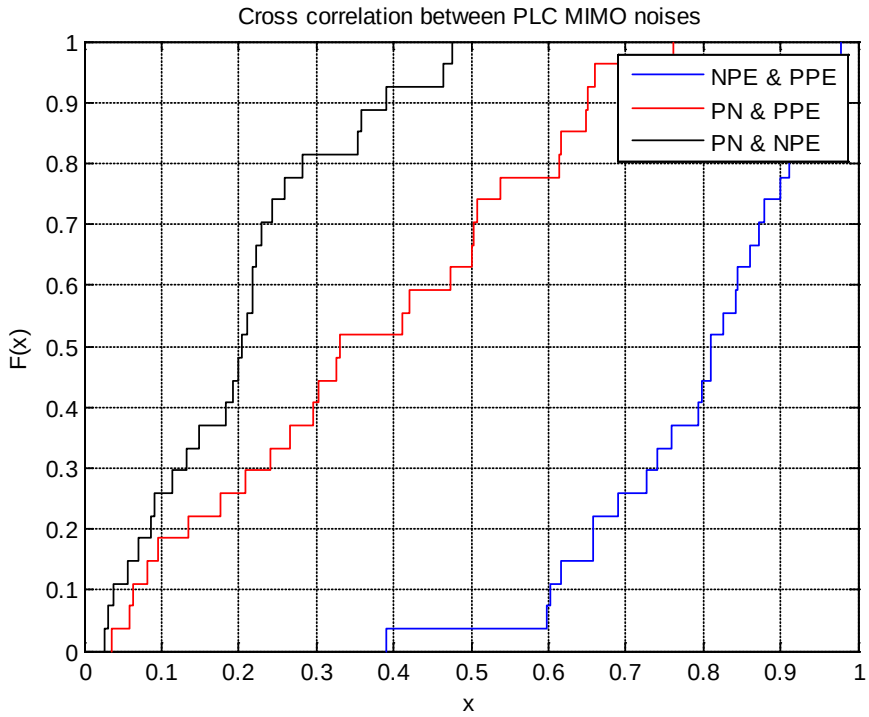

Figure 2.27. CDF of cross correlation between PLC MIMO noises

7. Conclusions

This chapter presents three MIMO channel measurement campaigns performed on three different PLC networks. Starting from a very simple network, the measurements are extended to real life, inhome PLC networks. This evolutionary methodology of channel measurement allows observing and analysing various fundamental characteristics such as the channel strength, MIMO capacity and MIMO capacity gain of various PLC networks in MIMO context. The principle inference drawn from the measurements is that although the absolute 2x2 MIMO capacities available at different networks do vary, however, the mean 2x2 MIMO capacity gain remains around 1.8. This figure is largely in line with the results reported in PLC literature [Stad08], [Vers11a]. From the original contribution's point of view it should be noticed that the results reported in this chapter cover the frequency range up to 150 MHz under the practical constraints of transmitted power and background noise.

Measurement and analysis of noise in MIMO PLC channels are also reported in this chapter. It is observed that the noise level at P-N port is lower than the P-PE and N-PE ports. The other important observation is that P-PE and N-PE noise sequences exhibit stronger cross-correlation compared to P-PE and P-N noises (and N-PE and P-N noises).

In chapter 3 and chapter 4, utilizing the channel and noise database generated by the in-home measurements described in this chapter, we will devise comprehensive models for the MIMO PLC CTF matrix and the MIMO PLC background noise.

Chapter .3
Characterization and modeling of the MIMO PLC channel transfer function

1. Introduction

In this chapter a MIMO PLC channel transfer function (CTF) model is presented. This channel model is based on the MIMO channel measurements discussed in chapter 2. For the purpose of modeling, a comprehensive statistical characterization of the channel parameters is provided. Channel modeling is an active research area in the PLC domain. At present, only a few SISO channel models exist in the PLC literature. However, a globally agreed upon channel model is still missing. The MIMO PLC channel model presented in this chapter is the first model of this kind. We have used the formalism of a SISO PLC multipath channel first proposed in [Zimm02a]. This formalism was later extended statistically in [Tone07] and [Omega08]. The MIMO PLC channel model proposed here is obtained through parameter estimation. For this purpose, the measured MIMO PLC channels are fitted to the model proposed in [Tone07] and [Omega08]. Once the parameters for all measured channels were estimated, we generalized the statistical properties of each parameter according to the experimentally observed statistical distributions.

This chapter also describes analysis and characterization of MIMO PLC channels. The characterization of SISO PLC channels has been presented in [Tlic08] where the channel characterization is achieved through a number of relevant metrics, for example, channel delay spread, coherence bandwidth. In our work, we have used similar metrics and introduced new parameters to characterize the MIMO PLC channels. For example, channel strength, delay spread, coherence bandwidth and channel correlation are typical SISO channel parameters, while the correlation between channels is typical of the MIMO

configuration. The advantage of channel characterization is quite obvious. It helps understand the nature of the measured MIMO PLC channels. The metrics used to characterize the measured channels serve as a benchmark for the validation of the channel model. Naturally, an efficient model should be able to generate the MIMO PLC channels which would produce similar statistical trends of the metrics as those of the measured channels. We find that the MIMO PLC channel model proposed here satisfactorily replicates the measured channels, and this validates the accuracy of this model.

2. PLC Channel modeling

In the PLC domain, there are two mainstream channel modeling strategies: the top-down approach, and the bottom-up approach. A brief description of the two methodologies has been given in the introduction section of chapter 2. In this chapter we will discuss them in more detail.

2.1. The top-down approach

The top-down approach is an empirical method employed for the modeling of the PLC channel which is based on measurements. The model parameters are extracted from the measured data. In most cases, the parameter extraction step relies on a number of assumptions regarding the mathematical description of the channel characteristics. As an output, a statistical description of the distribution of each channel parameter is obtained. The channel transfer function is then computed a posteriori by drawing one particular realization of each channel parameter, according to the underlying statistical distribution. The top-down approach is simple, fast and computationally efficient. The main drawback of this approach is that it is prone to measurement errors. In addition, this approach provides a global view of the channel as a filter, but the detailed information about the individual interactions within the channel is generally missing. A model based on the top-down approach is limited to the measured channel [Lagu08].

A most widely quoted SISO PLC channel model based on the top-down approach has been described in [Zimm02a] where the channel measurements are made in the time domain. The transmitted and received signals are recorded with a digital oscilloscope (DSO) and later the complex frequency response is computed using a Fourier Transform. In [Zimm02a], a multipath channel model has been presented for PLC channels which we will discuss in due detail in the next section. Generally, the top-down approach culminates into a multipath channel model, as has been presented for instance in [Liu08] and [Amir04].

The top-down approach has been used in [Maen06] where PLC channel characterization is discussed through signal attenuation up to 30 MHz. Attenuation characteristics of various in-building PLC channels is measured and it has been inferred that the number of branches in a PLC network plays a significant role in the determination of channel attenuation profile.

In [Tang03], the PLC channel is considered as a filter and the filter coefficients are extracted from a set of channel measurements. The underlying mathematical formalism is again the multipath channel. The proposed model is based on three parameters only. The modeled channels are compared to the measured channels and a close resemblance has been demonstrated. However, it has been stressed in [Tang03] that to make a top-down model computationally viable the number of parameters should be limited to some optimum number. Of course, a top-down model based on large number of parameters will be more exact but computationally more expensive.

2.2. The bottom-up approach

The bottom-up approach is analytical in its nature. Instead of relying on measurements, the bottom-up approach depends on a deterministic formalism to model the transfer function of the PLC channels. Therefore, the bottom-up approach is typically an *a priori* method which starts from the theoretical derivation of model parameters.

The bottom-up approach is commonly based on transmission line theory. In [Gall06], a two-conductor transmission line model has been discussed for power line channel. In [Meng04], a bottom-up model based on lumped-element circuit has been proposed. It has been argued in [Meng04] that for a complete bottom-up model, the two intrinsic line parameters i.e. the propagation constant γ and characteristic impedance Z_0 must be determined. These two parameters are defined in Eq. 3.1 and Eq. 3.2 respectively:

$$\gamma = \alpha + j\beta = \sqrt{(R + j\omega L)(G + j\omega C)} \tag{3.1}$$

$$Z_0 = \sqrt{\frac{R+j\omega L}{G+j\omega C}} \tag{3.2}$$

where ω is the angular frequency. The real part α and the imaginary part β of the propagation constant are the attenuation constant (in Np/m) and phase constant (in rad/m) respectively. R defines the resistance per unit length for both conductors (in Ω/m), L defines the inductance per unit length for both conductors (in H/m), G is the conductance per unit length (in S/m) and C is the capacitance per unit length (in F/m). [Meng04] continues to obtain the mathematical formulas for R, L, G and C. In both [Gall06] and

[Meng04] it is strongly recommended that the bottom-up approach should be employed in the frequency domain because it is much more computationally demanding to use the time domain modeling to account for all reflected and delayed paths.

Later, the two-conductor model has been extended to the multiconductor transmission line model [Gall06]. The basis of this model is the Multi-conductor Transmission Line theory (MTL). The key advantage of the MTL based channel model is that it can satisfactorily handle the inclusion of the third conductor i.e. the protective earth wire. Moreover, the effects of particular wiring and grounding practices can be easily incorporated. The estimation of Common Mode (CM) currents related to Electromagnetic Compatibility (EMC) is also facilitated by the MTL. The MTL based bottom-up modeling of PLC channel has also been discussed in details in [Banw05].

A deterministic model for PLC channels has been provided in [Chao08] where the *R, L, G* and *C* parameters are first measured for the cable used in a given PLC network. Then, with the help of a software named RESLINE and the knowledge of the network topology, various channel transfer functions have been simulated. It has been shown in [Chao08] that the modeled channels constitute a representative description of the measured channels.

A statistical channel simulator based on the bottom-up approach has been detailed in [Tone09]. The transfer function is modeled by the computation of the voltage ratio between the receiver and the transmitter ports, as shown in Eq.3.3.

$$H(f) = \frac{V_{Rx}(f)}{V_{Tx}(f)} \tag{3.3}$$

where $V_{Rx}(f)$ is the voltage measured at the receiver input port and $V_{Tx}(f)$ is the transmitter input port. The network topology is divided into units such as branches and sub-branches. The transfer function of each unit is computed. The overall transfer function of the network is obtained by computing the product of the transfer functions of all the units.

2.3. Comparison of the top-down approach and the bottom-up approach

It is obvious that both methodologies have their merits and de-merits. Both are equally popular. It is worthwhile to summarize the comparison between them.

2.3.1. Simplicity

The top-down approach is simpler than the bottom-up approach. The top-down approach requires a set of measurements from which the model parameters can be extracted. All practical aspects of the channel are already present in the measured data. Therefore, the model proposed on the basis of the top-down approach presents a very realistic picture of the given channel or network. On the other hand, the bottom-up approach is more complicated as it requires all the knowledge about the network to formulate a model.

2.3.2. Generality

A model based on the top-down approach is strictly related to the measured channel. Therefore, it is not straightforward to apply such a model to other networks. However, this constraint can be overcome by extracting the model from a measured database which is sufficiently large and covers as many practical scenarios as possible. On the other hand, the bottom-up approach yields a channel model by starting from proper theoretical basis. Therefore, a channel model based on bottom-up approach is more general and may represent a broader range of networks.

2.3.3. Correctness

The top-down approach is prone to measurement errors. These errors may arise from the limited accuracy of measuring instruments. Moreover, there are many other factors, such as unwanted electromagnetic interference, which can contaminate the measured data. The other source of errors is the data fitting algorithm used to estimate the model parameters. The measurement errors can be reduced by carefully configuring the measurement setup. The data fitting errors can be reduced by applying tight limits of Minimum Mean Square Error (MMSE) between the measured data and the estimated model. In comparison, the bottom-up approach is more accurate but to achieve a high accuracy all details of the channel such as cable type, network topology, network size, types of appliances etc should be provided.

2.4. Merger of the two approaches

Since the two approaches of channel modeling have some strong and some weak points, it would be interesting to formulate a channel modeling approach which merges the two approaches by picking the strong points of both. In [Lagu08], the idea of heuristic computing techniques, i.e. computational intelligence, has been proposed in order to develop an intelligent system which automatically determines the model and modeling parameters. Such an intelligent modeling approach would rely on deterministic channel model formulated on few easily measurable parameters. The tools such as evolutionary computing techniques and neural networks should be employed.

There are already some examples where a channel model has been proposed by utilizing the top-down and bottom-up approaches in tandem. In [Cane02], broadband modeling of indoor power line channels has been discussed, where the network topology information has been incorporated to the channel measurements.

In this chapter we will propose a MIMO PLC channel model based on measurements where some topological aspects of the network (the relative position of the transmitter and receiver socket on the electrical network) will be incorporated into the model as well.

2.5. Inhome MIMO PLC channel modeling: present scenario

In this section we will discuss and summarize various inhome MIMO PLC channel models. It is worth reminding that MIMO channel modeling for inhome PLC networks is still in early days and presently a very limited number of publications are available in this domain. The first comprehensive inhome MIMO PLC channel model has been developed in the framework of this thesis and was published in [Hash11]. In the next sections we will present a detailed description of this model. Two other proposals for MIMO PLC channel modeling were presented simultaneously in [Vero11] and [Vers11].

In [Vero11], the characterization of inhome MIMO power line channels is presented. The analysis is based on measurements performed in a frequency range from 0 to 100 MHz. Basically it is a statistical description of inhome MIMO PLC channels extracted from 96 channel measurements performed in North American houses. A time domain channel measurement method has been used. Two sounding signals are stored in an arbitrary waveform generator (AWG). The AWG injects the two signals into a MIMO coupler. These signals traverse through the power line network and are received at a data acquisition card. The channel transfer function is estimated by manipulating the transmit and receive signals. The main result provided in [Vero11] is that the power delay profile follows Weibull and Gaussian distributions. The MIMO PLC channel has been characterized through the average channel attenuation, the Root Mean Square (RMS) delay spread and the correlation among channels. It has been shown in [Vero11] that the average attenuation (dB) of the MIMO channels decreases linearly with frequency. The typical RMS delay

spread of 0.4 μsec is reported. As far as the channel correlation is concerned, a high correlation for almost 90% of the channels has been reported in [Vero11].
The MIMO PLC channel model proposed in [Vero11] relies on the accurate generation of a SISO channel. The full MIMO channel matrix is obtained from the SISO channel by introducing correlation matrices. It has also been reported that the modeled MIMO channels exhibit similar frequency response as those of the measured ones.

A bottom-up strategy for the simulations of MIMO PLC channels has been described in [Vers11]. This strategy is based on the MTL theory. The mutual interactions between the three conductors (wires) Phase, Neutral and Protective Earth have been considered. In [Vers11], a typical 2x2 MIMO PLC system is defined on the basis of the coupling effects. The model thus obtained has been validated through the comparison of the insertion loss for measured and modeled parameters.

3. Characterization of the MIMO PLC Channel Transfer Function

In this section we describe our method for MIMO PLC channel characterization and modeling. We will explain different parameters of channel characterization that we have utilized to identify various aspects of the nature of the MIMO PLC channel. On the basis of this channel characterization we will devise a complete MIMO PLC channel model in the 2-150 MHz frequency range in the next sections.

3.1. Multipath Channel Model

A SISO PLC deterministic channel model based on multiple path propagation was proposed in [Zimm02a]. The basic premise of multipath propagation is that signal does not travel only along a direct line of sight path between the transmitter and receiver. In fact, the receiver gets delayed and attenuated copies of the transmitted signal (along with a stronger direct path signal, only if the direct path is available). The net result of this phenomenon is a typical frequency selective, multipath scenario as described in Section 3.2.1 of Chapter 1.

In [Zimm02a] the final version of the transfer function or the frequency response has been derived. This formalism, as shown in Eq. 3.4, has been adopted in the ICT OMEGA Project as well [Omega08]. A statistical extension of the model was proposed in [Tone07].

$$H(f) = A\sum_{p=1}^{Np} g_p e^{-j\frac{2\pi d_p}{v}f} e^{-(a_0 + a_1 f^K)d_p} \tag{3.4}$$

where g_P, N_P and d_P stand for path gain, the number of paths and path length respectively. In addition, $v=2/3c$ is the speed of electromagnetic waves in the cable material. The attenuation parameters A, a_0, a_1, and K are discussed in the following paragraphs.

3.2. Median channel attenuation

The median attenuation of a channel, $A_{med} = median(|\boldsymbol{H}(f)|)$, is defined as the median value of the aplitude of the CTF over the measured frequency range. This parameter is a figure of merit for the global frequency domain attenuation of a given channel. It can be characterized for same-circuit and different-circuit sockets. We found that the channels measured between same-circuit sockets present median channel attenuation considerably lower than the ones between different-circuit sockets. The value of A_{med} for a channel also depends on its position in channel matrix. Indeed, a 3x3 channel matrix is measured between two PLC sockets. The diagonal entries of the channel matrix are called co-channels, and the off-diagonal entries are called cross-channels (see Section 5.1 of Chapter 1). In the same-circuit case, the co-channels are slightly stronger than the cross-channels (or off-diagonal) entries. This difference is because the cross-channels rely on coupling between differential ports, while for co-channels, the Tx and Rx ports are physically connected. Figure 3.1 shows the Cumulative Density Function (CDF) of the median channel attenuation for the same-circuit case. It can be observed in Figure 3.1 that the mean value of channel median attenuation is around -22 dBm. It can also be observed in Figure 3.1 that for about 15% of the channels the median channel attenuation varies from -47 dBm to -32 dBm. Such channels can be regarded as weak channels. For different-circuit case, the difference between the attenuation of co-channels and cross-channels remains smaller than 3 dB.

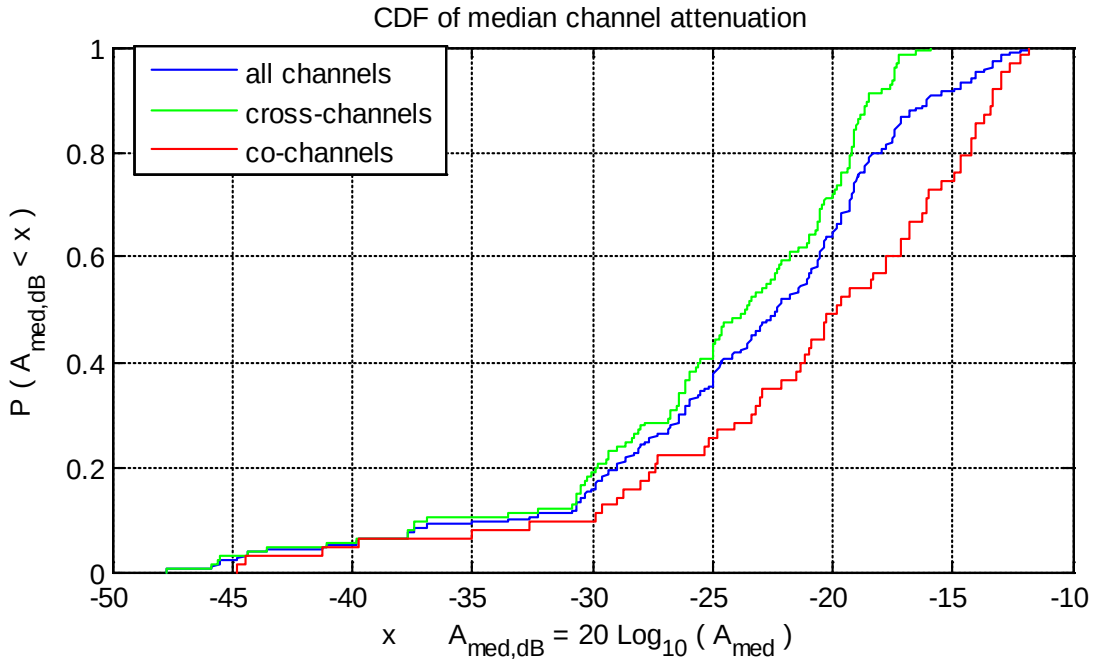

Figure 3.1. CDF of median channel attenuation for same-circuit case

3.3. Frequency dependent attenuation

Parameters A, a_0, a_1 and K are used to model the channel attenuation. It has been demonstrated in [Omega08] that according to the model given in Eq. 3.4, and assuming a uniform distribution of the path gains g_p in [-1, 1], the expected path loss (PL) of a PLC channel is given by Eq. 3.5.

$$PL_{a_0,a_1,K}(f) = A^2 \frac{\Lambda}{3} \frac{1-e^{-2L_{\max}(a_0+a_1 f^K)}}{(2a_0+2a_1 f^K)(1-e^{-\Lambda L_{\max}})} \tag{3.5}$$

where f is the frequency, $L_{\max}$ is the maximum path length, and Λ is the intensity of the Poisson arrival process which defines the distance among multipath reflections. A allows the addition of arbitrary attenuation, and we have selected it to be equal to the channel median to avoid outliers or extreme values. Let us define ΔA as Eq. 3.6.

$$\Delta A = A_{m,n} / A_{PN\text{-}PN} \tag{3.6}$$

for any off-diagonal channel in the MIMO matrix with input port m and output port n. ΔA gives a measure of the attenuation of the cross-channels compared to the PN-PN channel.

For a given $L_{\max}$, Λ and A, the parameters a_0, a_1, and K can be estimated by fitting a measured MIMO PLC channel to the OMEGA path loss model of Eq. 3.5 under the minimum mean square error (MMSE) constraint, as shown in Eq. 3.7. It should be noted that in Eq.3.7 $PL_{a0,\,a1,\,K}$, H_{meas}, f and BW stand for OMEGA path loss model (dB), measured channel transfer function (dB), frequency and measurement bandwidth respectively. We used a simulated annealing method for the curve fitting where the initial input values are the ones proposed within the ICT OMEGA project: a_0 = 0.003, a_1 = 4e-10 and K = 1. The other values have been fixed to L_{max} = 800 and Λ = 0.2, as proposed in the ICT OMEGA project. A typical MIMO PLC channel and the corresponding path loss calculated from the estimated parameters is shown in Figure 3.2. For the purpose of comparison, the path loss obtained from the parameter values stated in [Omega08] is also shown (red curve) in Figure 3.2. It can be observed in Figure 3.2 that the path loss PL calculated by using the estimated values satisfactorily represents the expected path loss of a measured channel.

$$min\,\frac{1}{BW}\int_{f_{min}}^{f_{max}}\left(PL_{(a_0,a_1,K)}(f)-H_{meas}(f)\right)^2 df \xrightarrow{yields} [a_0, a_1, K] \qquad (3.7)$$

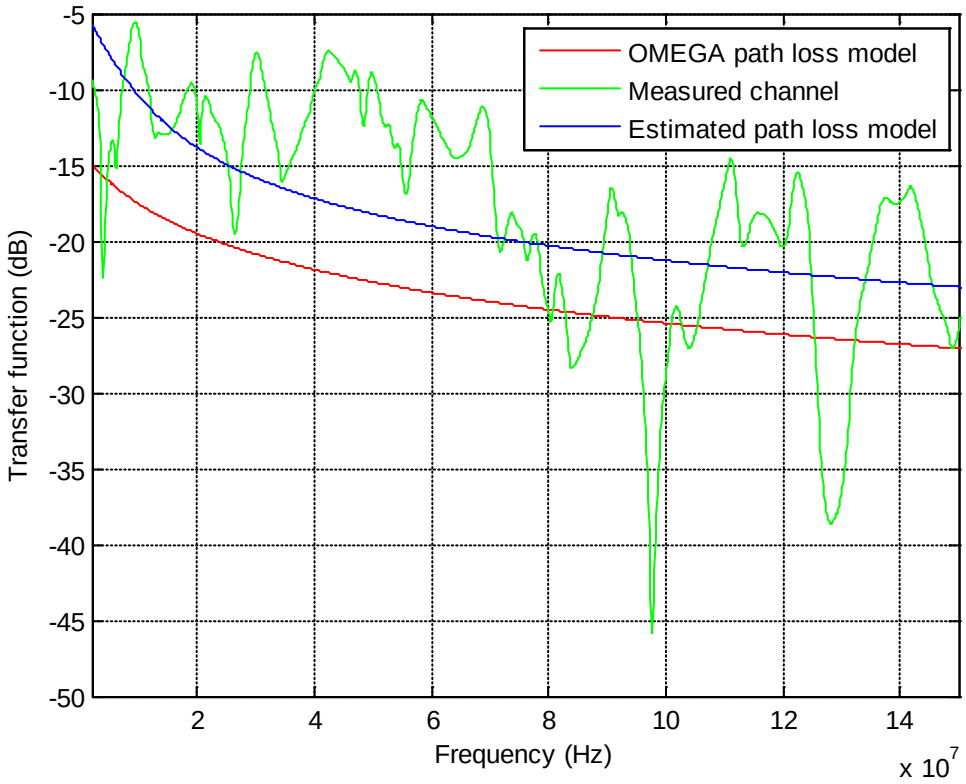

Figure 3.2. Estimation of MIMO path loss model by fitting the OMEGA path loss model to a measured MIMO channel

Once the parameters A, ΔA, a_0, a_1 and K were estimated for all measured channels, we modeled their statistics with appropriate statistical distributions. Table 3.1 summarizes the models obtained for different parameters. It can be observed in Table 3.1 that a_1 is a constant, K is normally distributed and a_0 follows a shifted exponential distribution. The channel median A is uniformly distributed for the channels measured between the same-circuit sockets, and exponentially distributed for different-circuit sockets. ΔA follows a shifted exponential distribution for the same-circuit case and almost constant and equal to one for different-circuit case.

	Same circuit		Different circuit	
	Co-channel	Cross-channel	Co-channel	Cross-channel
A	Uni (min=0.005, max=0.25)	Uni (min=0.005, max=0.15)	Exp(μ =0.00238)	
ΔA	Exp(μ =0.3659) + 0.45		≈ 1	
a_0	Exp(μ =0.00827) - 0.005			
a_1	4e-10			
K	$\mathcal{N}(\mu$ =1.01748, σ =0.01955)			

Table 3.1 Statistical models of channel parameters

The selection of a statistical distribution to model a given estimated channel parameter is primarily based on the visual appearance of the CDF of that parameter. Later on, the parameters of the distribution were determined by using the MMSE criterion between the estimated data and the modeled data, for instance, to evaluate the shift values of +0.45 and -0.005 for the model parameters of ΔA and a_0. As an example, a close resemblance between the Probability Density Functions (PDF) of the estimated values and the modeled values of parameter a_0 is shown in Figure 3.3. Similarly, Figure 3.4 shows a nice fit between the PDFs of the estimated values and the modeled values of parameter K. In case where the estimated values of a parameter do not follow a definite pattern we selected the uniform distribution for the model. For example, the histogram of Figure 3.5 shows that the data is too dispersed to draw any definitive conclusion; therefore, a uniform distribution was selected to model the parameter A for same-circuit, cross-channel case. Same procedure was adopted for other parameters modeled by uniform distributions in Table 3.1.

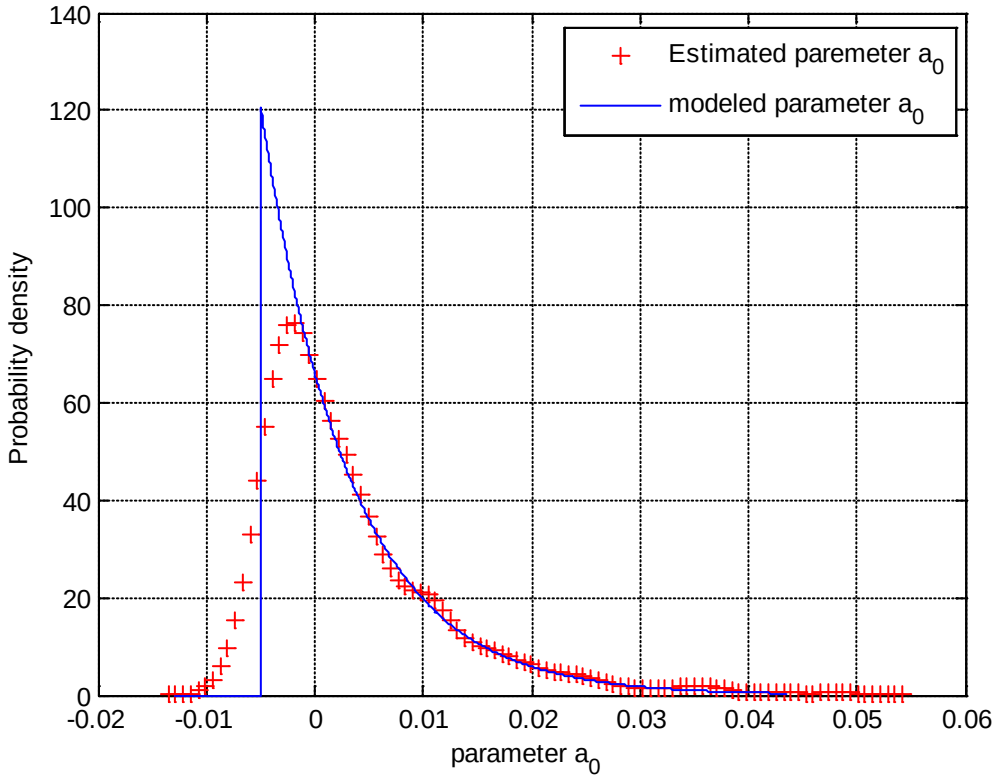

Figure 3.3. PDFs of the estimated values and the modeled values of parameter a_0

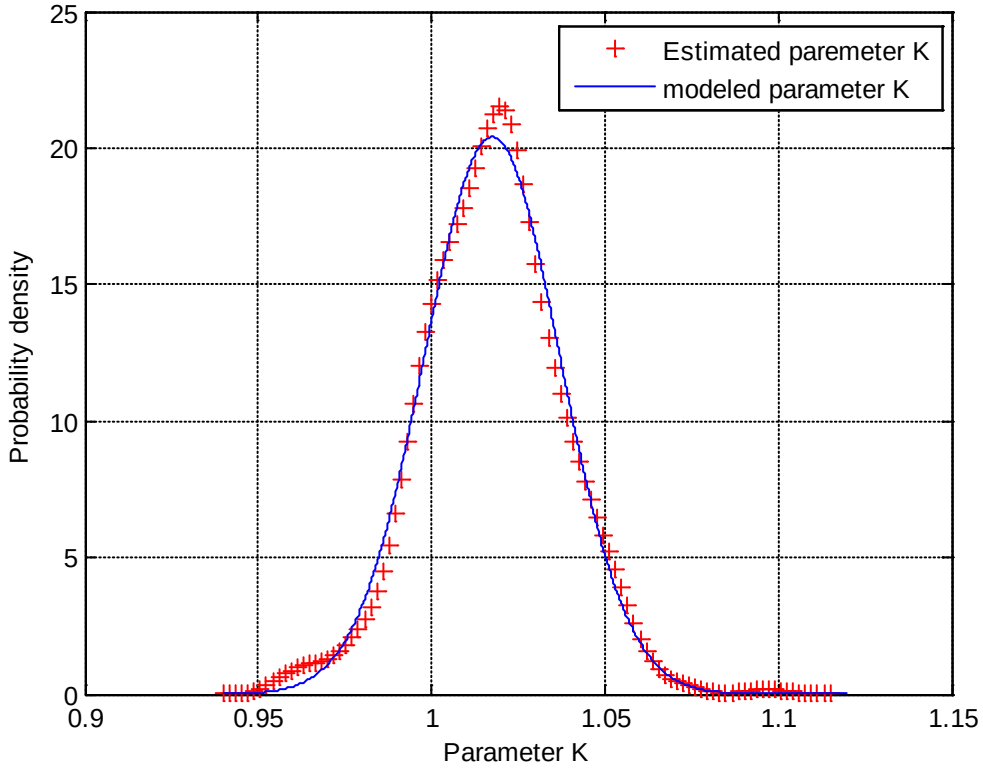

Figure 3.4. PDFs of the estimated values and the modeled values of parameter K

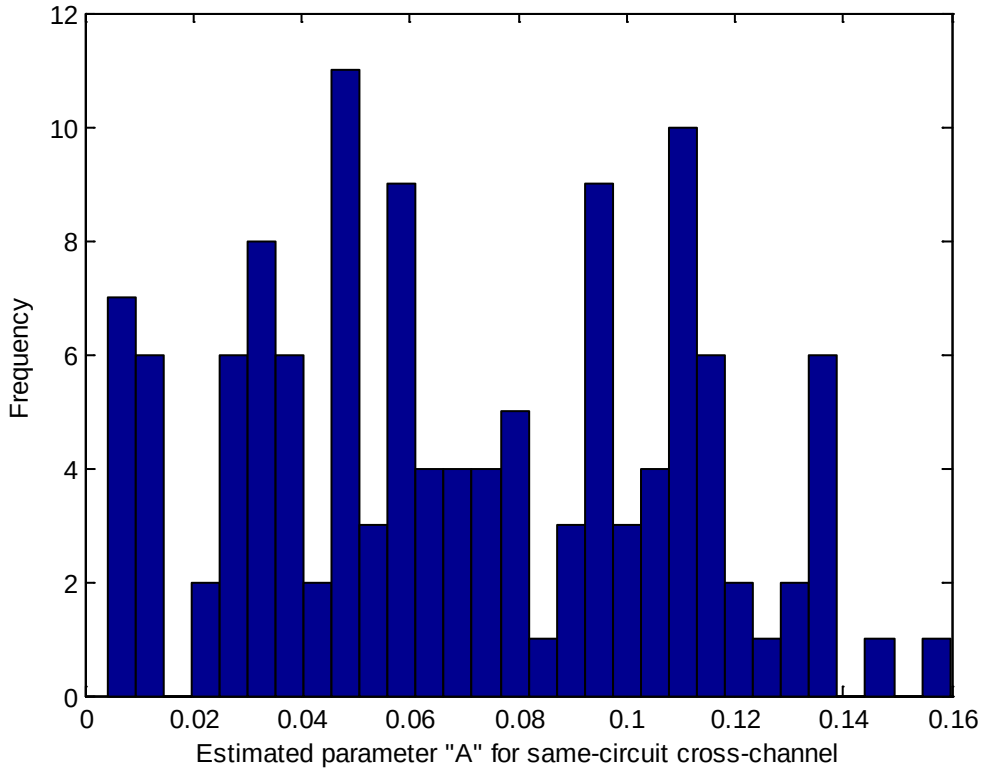

Figure 3.5. Histogram of the estimated values of parameter *A* for same-circuit, cross-channel case

3.4. Delay spread

The Root Mean Squared (RMS) delay spread is the square root of the second central moment of a power-delay profile $P(\tau)$ [Tlic08]. It is the standard deviation about the mean excess delay, and is expressed as shown in Eq. 3.8a.

$$\tau_{RMS} = \left[\int \left(\tau - \tau_e - \tau_A\right)^2 P(\tau) d\tau\right]^{1/2} \tag{3.8a}$$

where τ_A and τ_e stand for first arrival delay and expected delay respectively (Figure 3.6). The expected delay τ_e is defined in Eq. 3.8b.

$$\tau_e = \left[\int \left(\tau - \tau_A\right)\ P(\tau) d\tau\right] \tag{3.8b}$$

The power delay profile $P(\tau)$ is derived from the channel impulse response $h(t)$, as shown in Eq. 3.9.

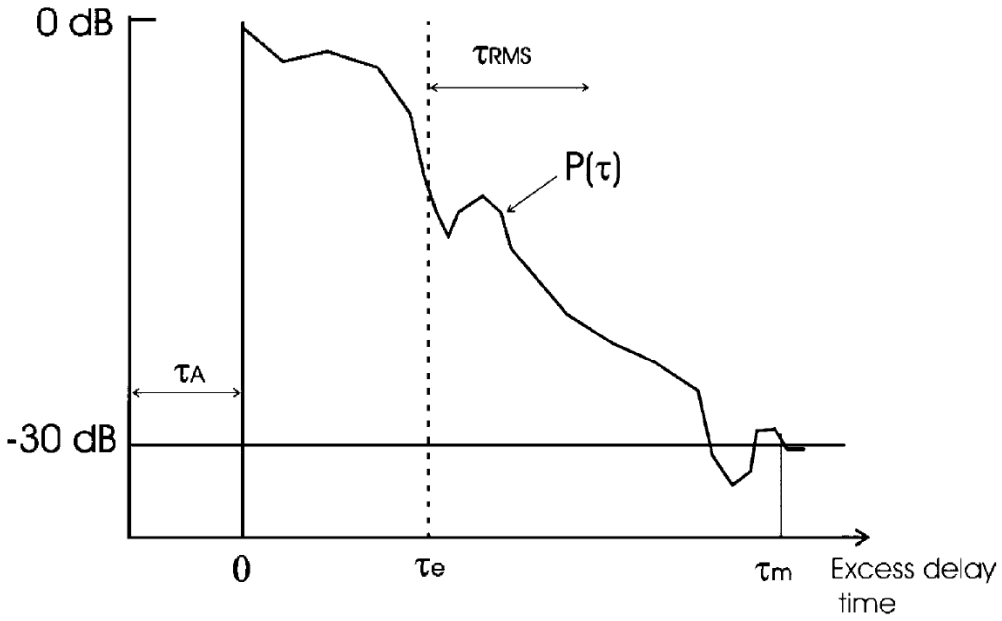

Figure 3.6. Illustration of various delay parameters

$$P(\tau) = \frac{|h(\tau)|^2}{\int_{-\infty}^{+\infty} |h(\tau)|^2 \, d\tau} \tag{3.9}$$

In a multipath propagation channel, the power-delay profile provides an index of transmitted power over various paths. Generally, for the strength of channel power-delay profile, a given threshold is used to prevent the noise enter the delay spread estimation, i.e. all values below this threshold are not considered in the computation. In our computations, we used thresholds of -20 dB and -30 dB.

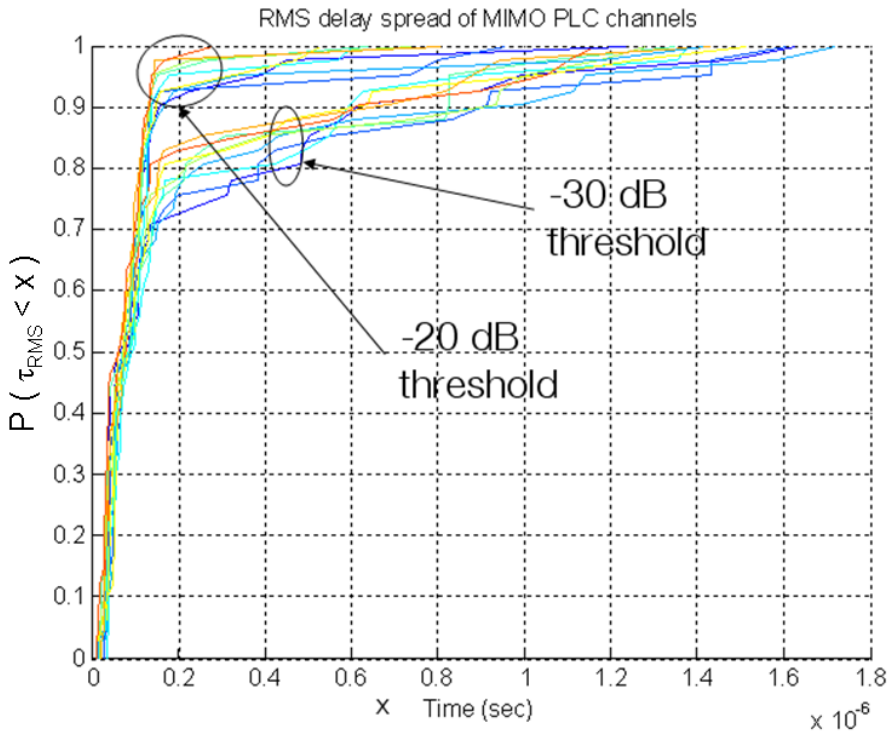

Figure 3.7. CDF of RMS delay spreads of measured 3x3 MIMO PLC channel

The RMS delay spread is a good measure of the multipath spread. It gives an indication of the sensitivity of the system against Inter-Symbol Interference (ISI). Strong echoes (relative to the shortest path) with long delays contribute significantly to RMS delay spread which may yield stronger ISI. Figure 3.7 presents the RMS delay spread of measured 3x3 MIMO PLC matrices for thresholds of -30 dB and -20 dB. It is evident from Figure 3.7 that setting the threshold to -30 dB brings more noise or echoes into consideration, and hence only 75% of the channels achieve an RMS delay spread equal to 0.15 µs or below. On the other hand, for a threshold of -20 dB, about 95% channels attain this performance.

For the comparison purpose, it should be noted that in [Tlic08] the mean value of τ_{RMS} = 0.309 for the SISO PLC channels has been reported, over a measurement frequency band of 2-100 MHz.

3.5. Coherence bandwidth

The coherence bandwidth is defined as the range of frequencies over which the Frequency Correlation Function FCF of a channel can be regarded as flat. Over this particular band one expects the channel to offer uniform gain and linear phase [Tlic08]. The FCF is defined by the Eq. 3.10.

$$R(\Delta f) = \int_{-\infty}^{+\infty} H(f)H^{*}(f+\Delta f)df \tag{3.10}$$

where ***H(f)*** is the complex transfer function of the channel, Δf is the frequency shift and * denotes the complex conjugate. The coherence bandwidth B_x is expressed in terms of FCF as shown in Eq. 3.11.

$$B_x = \min\left\{\Delta f : \frac{R(\Delta f)}{R(0)} = x\right\} \tag{3.11}$$

Generally the values of correlations coefficient equal to 0.5, 0.7, and 0.9 are quoted, and these are referred to as $B_{0.5}$, $B_{0.7}$ and $B_{0.9}$ respectively. Naturally, $B_{0.9}$ is smaller than $B_{0.5.}$ Figure 3.8 shows a typical FCF versus frequency shift curve, obtained from a measured CTF. We note that the shape of FCF in 2nd half of the frequency axis is merely the mirror image of its first half. Figure 3.9 is a magnified view of Figure 3.8. It shows that $B_{0.9}$ for this particular CTF is around 1.5 MHz.

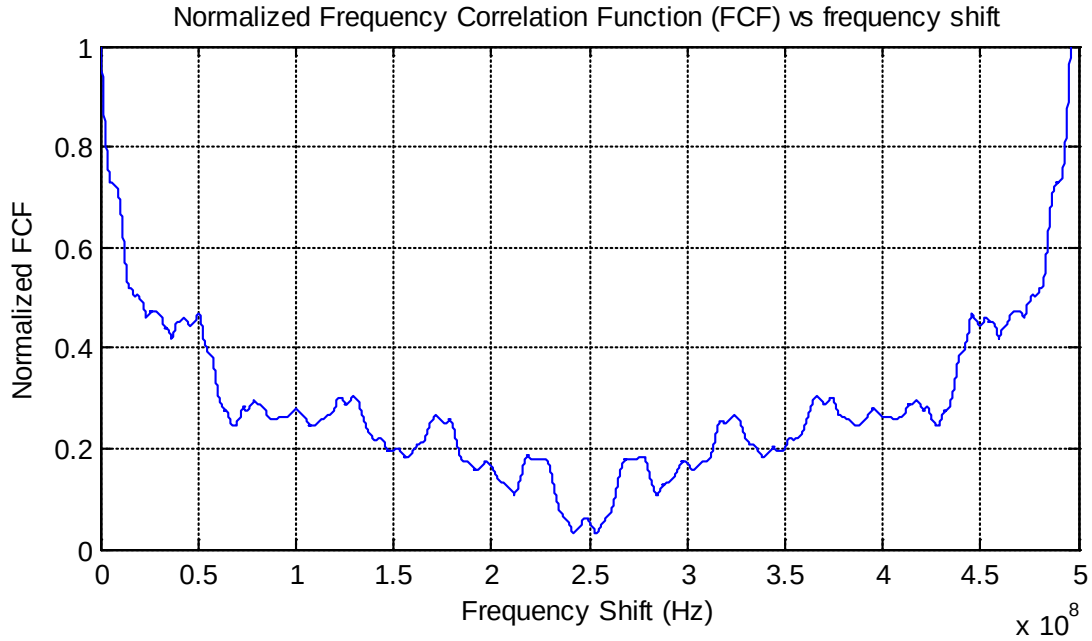

Figure 3.8. A typical Normalized FCF versus frequency shift curve for a CTF

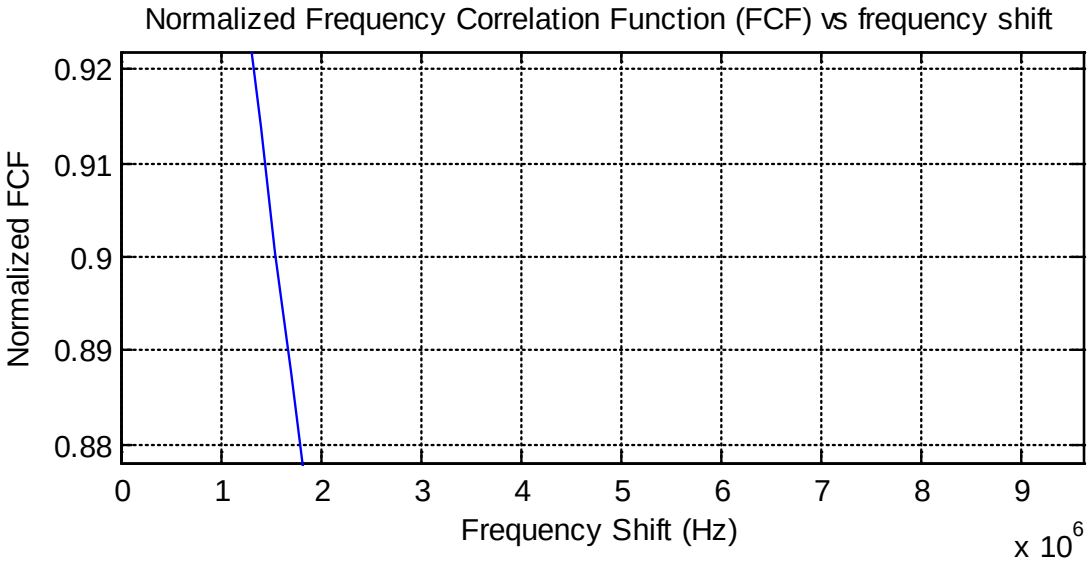

Figure 3.9. Magnified view of Figure 3.6 illustrating $B_{0.9}$

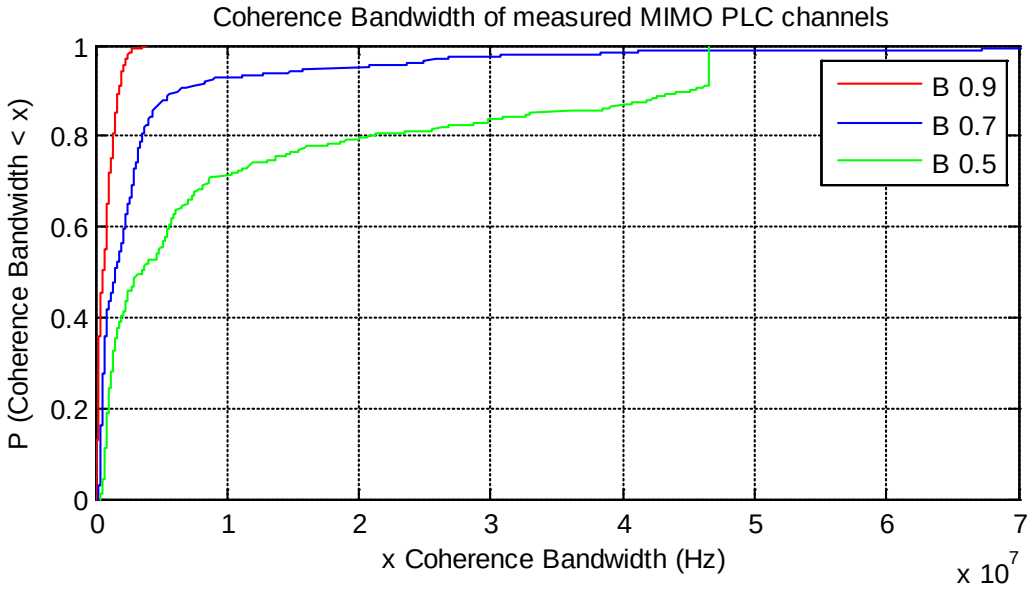

Figure 3.10. CDF of coherence bandwidths measured MIMO PLC channels

Figure 3.10 shows the CDF of the coherence bandwidth for all the measured MIMO PLC channels. It can be observed in Figure 3.10 that for about 80% of PLC channels the $B_{0.5}$ value is below 20 MHz. However, the coherent bandwidth $B_{0.7}$ shrinks quite remarkably. For about 80% of PLC channels, the $B_{0.7}$ value is below 4 MHz. $B_{0.9}$ is, as expected, the narrowest. For about 80% of the PLC channels the $B_{0.9}$ is below 1.5 MHz.

For the comparison purpose, it should be noted that in [Tlic08] the mean values of $B_{0.5}$=4.8 MHz, $B_{0.7}$=0.867 MHz and $B_{0.9}$=0.33 MHz for the SISO PLC channels have been reported, over a measurement frequency band of 2-100 MHz.

3.6. MIMO Channels Correlation

One of the key features in a MIMO communication system is the degree of correlation between the different available channels. Theoretically, the capacity of uncorrelated MIMO channels increases linearly with the number of sensors [Fosc98]. As the correlation between channels increases, the MIMO systems underachieves this maximum capacity [Shiu00]. It is thus of prime interest to reflect the correlation observed in experimental measurements when modeling the MIMO PLC channel.

Several definitions of the correlation between channels are available in the literature. We will use the complex correlation coefficient defined for two complex random variables *u* and *v* as follows [Kyri03]:

$$\rho_{i,j} = \frac{E[uv^*] - E[u]E[v^*]}{\sqrt{\left(E\left[|u|^2\right] - |E[u]|^2\right)\left(E\left[|v|^2\right] - |E[v]|^2\right)}} \tag{3.12}$$

where $E[\ ]$ represents the statistical expectation and * denotes the complex conjugate operation. Since, today's PLC systems generally operate in the frequency domain [Home07] (using OFDM waveforms or similar variants), we will consider the correlation between complex frequency domain channels. We note $\boldsymbol{H}_i(f)$ and $\boldsymbol{H}_j(f)$ the CTF of channels *i* and *j* in the MIMO frequency response matrix. Wide Sense Stationary (WSS) statistical processes are ergodic and hence the expectations in Eq. 3.12 can be replaced by frequency domain averages. However, in general, $\boldsymbol{H}_i(f)$ and $\boldsymbol{H}_j(f)$ are not WSS, since their expectation varies over frequency. This is characterized by the frequency dependent expected path loss $PL(f)$. It is thus necessary to first isolate the average fading component of the CTF, by computing the normalized CTF as defined in Eq. 3.13.

$$\tilde{H}_i(f) = \frac{H_i(f)}{\sqrt{PL_i(f)}} \tag{3.13}$$

where $PL(f)$ is computed through Eq. 3.5. Finally, the complex correlation coefficient between channels *i* and *j* in the MIMO matrix is computed as

$$\rho_{i,j} = \frac{\overline{\tilde{H}_i(f)\tilde{H}_j^*(f)} - \overline{\tilde{H}_i(f)}\,\overline{\tilde{H}_j^*(f)}}{\sqrt{\left(\overline{\left|\tilde{H}_i(f)\right|^2} - \left|\overline{\tilde{H}_i(f)}\right|^2\right)\left(\overline{\left|\tilde{H}_j(f)\right|^2} - \left|\overline{\tilde{H}_j(f)}\right|^2\right)}} \tag{3.14}$$

where $\overline{(.)}$ denotes the frequency domain average.

For a MIMO system with three inputs and three outputs, represented by the differential ports PN, PPE and NPE, there are 9 different channels, and thus 36 different pairs of distinct channels. Each channel pair will exhibit a given correlation coefficient for a given experimental channel measurement. It is thus possible to characterize the statistics of the correlation coefficient for each of the 36 channel pairs over the measurement ensemble.
Figure 3.11 represents the statistics of the magnitude of the correlation coefficient $|\rho_{i,j}|$ for the 36 channel pairs, for the case of a channel measured over the same electrical circuit. Figure 3.12 shows the CDF of channel correlations for the different-circuit case.

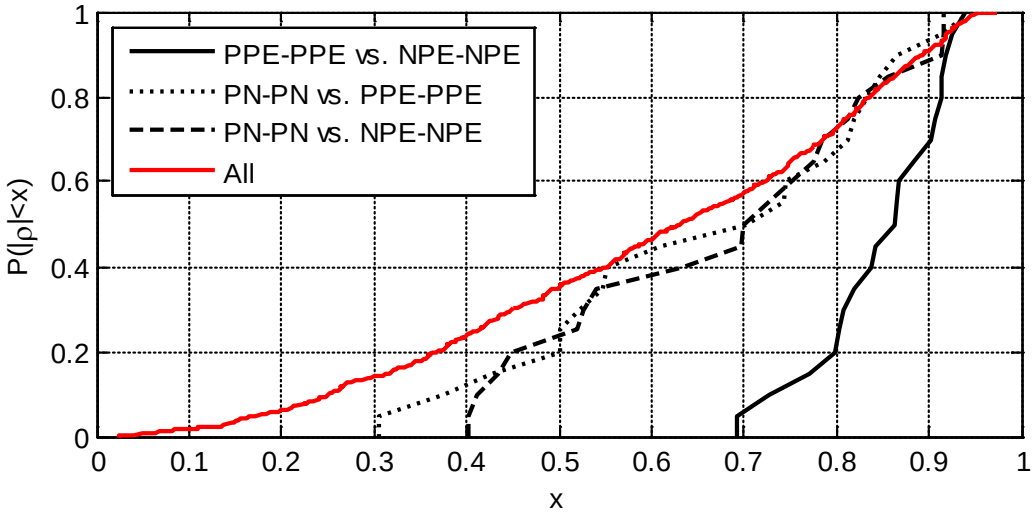

Figure 3.11. CDF of the correlation coefficient for measurement over the same circuit

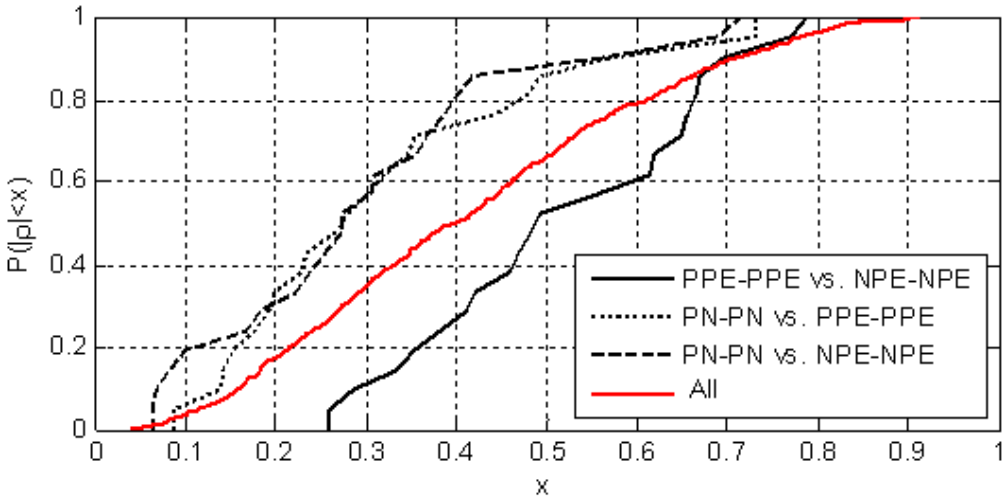

Figure 3.12. CDF of the correlation coefficient for measurement over different circuits

When considering all channels (red curves), parameter $|\rho_{i,j}|$ is nearly uniformly distributed over the range of possible values in both cases. This means it is difficult to predict the

correlation between any two channels because strongly correlated channels ($|\rho_{i,j}|>0.9$) and weakly correlated channels ($|\rho_{i,j}|<0.1$) are almost equally likely. However, some specific cases are still worth studying, as represented by the black curves in Figure 3.11 and Figure 3.12. Firstly, the PPE-PPE channel and the NPE-NPE channel are in general highly correlated ($|\rho_{i,j}| > 0.7$) for all channels recorded over the same circuit, and this trend persists for channels recorded over different circuits as well. Secondly, the correlation between the PN-PN channel and the NPE-NPE channel is of the same order as between the PN-PN channel and the PPE-PPE channel with observed correlation coefficients ranging between 0.3 and 0.9 for channels recorded over the same circuit, and between 0.1 and 0.7 for channels recorded over different circuits. These results are very important for MIMO PLC system design. Strong correlation between channels leads to reduced diversity and is detrimental to MIMO system's performance. Therefore, for a 2x2 MIMO PLC system, it would be better to use PN and PPE (or NPE) ports. Stated otherwise, a 2x2 MIMO PLC system realized by using NPE and PPE ports will offer sub-optimal performance.
For the comparison purpose, it is worth mentioning that in [Vero11] a high channel correlation (correlation value of 0.9 for 80% of the channels) has been reported for the measured MIMO PLC channels in 0-100 MHz range.

4. Generating the statistical SISO PLC channel

In the following, we present the MIMO channel model based on the statistics shown in Table 3.1.

4.1. SISO Channel Model for the PN-PN Path

The first step in the proposed MIMO channel model is to generate a random realization of a SISO link for the PN-PN path (to be consistent with traditional SISO PLC literature). This SISO channel model builds on the model proposed by [Zimm02a] and [Tone07] in the sense that it uses a similar path loss and multipath fading framework.

4.2. Attenuation Model

The frequency dependent attenuation of the randomly realized SISO link can be modeled with the help of the expected path loss defined in Eq. 3.5. More specifically, parameters A, a_0, a_1 and K are drawn randomly according to the statistical distributions given in Table 3.1. It should be noted that the path loss statistically derived in Eq. 3.5 is only valid for a fixed value of A, a_0, a_1 and K. Hence, we consider in this work that Eq. 3.5 is valid conditioned on these parameters. Following the proposal in the ICT OMEGA Project [Omega08], we fix $L_{max} = 800$ and $\Lambda = 0.2$.

4.3. Multipath Model

The multipath model is given in Eq. 3.4. As suggested in the ICT OMEGA Project, the path lengths d_p are randomly selected as a Poisson arrival process with intensity Λ. The maximum path length is given by L_{max}. The paths gains g_p are drawn according to a uniform distribution between -1 and 1.

5. Generating the MIMO PLC Channels

5.1. Different-Circuit Channels

Once the PN-PN path is modeled, the 8 other channels in the 3x3 MIMO need to be defined. The method proposed in this thesis allows creating diversity which in turn can capture the main correlation features observed in Figure 3.12. The proposed approach is to keep the same multipath structure for the PN-PN channel and all the other channels in the MIMO matrix. This is consistent with the physical observation that the electrical network topology is constant, regardless of the actual ports (PN, NPE or PPE) that are used for signal transmission. However, it has been experimentally observed that different channels in a given MIMO matrix exhibit different frequency fading patterns, which is characterized by the correlation factor between channels. To reproduce this, the idea is to assign a random phase φ_p to each defined path. The CTF expression is thus modified from Eq. 3.4 to Eq. 3.15:

$$H(f) = A\sum_{p=1}^{Np} g_p e^{-i\varphi_p} e^{-j\frac{2\pi d_p}{v}f} e^{-(a_0+a_1 f^K)d_p} \tag{3.15}$$

The values of φ_p are drawn randomly according to a zero-centered, uniform distribution between $-\Delta\varphi/2$ and $\Delta\varphi/2$. $\Delta\varphi$ is a figure of merit of the maximum phase shift between two transmission channels is the MIMO matrix for any given propagation path. As $\Delta\varphi$ decreases from 2π to 0, channels given by Eq. 3.15 present a larger channel correlation with the PN-PN channel. The adequate values of $\Delta\varphi$ were selected empirically by running Monte Carlo simulations. Our recommendations (as a rule of thumb) are as follows:

- The PPE-PPE channel is obtained from the PN-PN channel by choosing $\Delta\varphi = 2\pi$;
- The NPE-NPE channel is obtained from the PPE-PPE channel by choosing $\Delta\varphi = \pi$;
- All other channels are obtained from the PN-PN channel by choosing $\Delta\varphi = \pi$.

5.2. Same-Circuit Channels

The procedure to generate same-circuit channels is similar to the one for different-circuit channels. One difference is that it has been observed in this case that the median channel attenuation of cross-channels is generally larger than for co-channels. Therefore, the parameter A drawn for the PN-PN channel is also used for the PPE-PPE and NPE-NPE channels, while it is replaced by $A \times \Delta A$ for all other channels in the MIMO matrix. Parameter ΔA is drawn from the statistical distribution shown in Table 3.1.

In addition, our recommended values of $\Delta\varphi$ for same-circuit channels are the following:

- The PPE-PPE channel is obtained from the PN-PN channel by choosing $\Delta\varphi = \pi$;
- The NPE-NPE channel is obtained from the PPE-PPE channel by choosing $\Delta\varphi = \pi/2$;
- All other channels are obtained from the PN-PN channel by choosing $\Delta\varphi = \pi$.

6. Simulations and Model Validation

An arbitrary number of 3x3 MIMO PLC channel matrices is generated with the help of the statistics described in Table 3.1.

6.1. The modeled MIMO CTF matrix

Figure 3.13 gives an example of simulated channel according to the proposed model. The CTF for the full 3x3 MIMO matrix is represented in the same-circuit case. We can note the similarity with the measurement example of Figure 2.15.

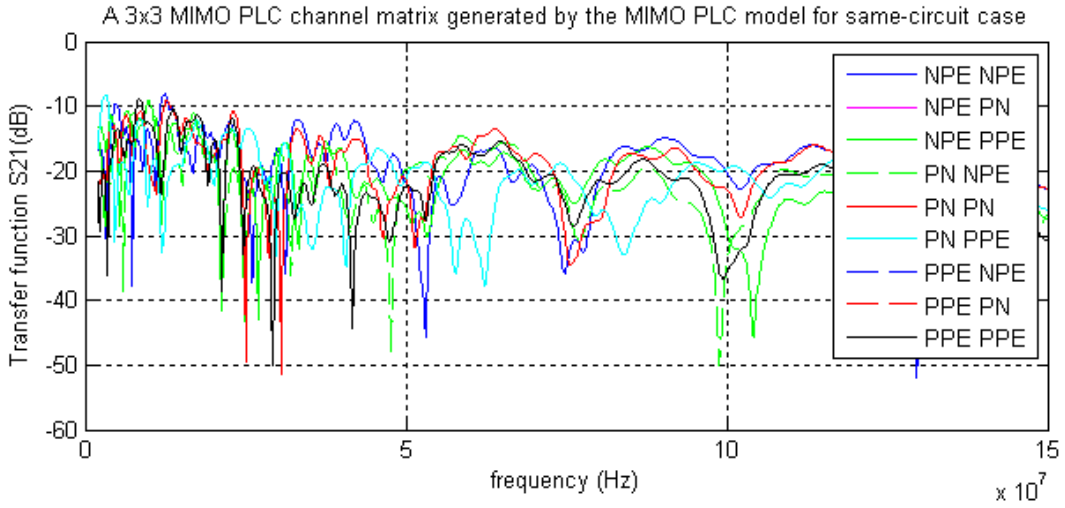

Figure 3.13. Example of simulated CTF for the same-circuit case

6.2. Coherence Bandwidth and Delay Spread

The channel matrices generated by 100 simulations were used to find channel correlation, coherence bandwidth and RMS delay. We observed a close resemblance between the results obtained from measurement and the ones supplied by the simulations. The CDF of coherence bandwidth of the channels generated by our PLC MIMO channel model is shown in Figure 3.14. It can be observed that it closely matches Figure 3.10 particularly for $B_{0.7}$ and $B_{0.9}$. Figure 3.15 shows the CDF of RMS delay spreads calculated from the channels generated by the model. We note that Figure 3.15 closely resembles Figure 3.7. However, there is not much clearance between the curves for two threshold levels since we have not taken any noise into consideration in the channel simulation. In the next chapter we will demonstrate a global MIMO PLC channel model obtained by incorporating the modeled MIMO noise into the modeled MIMO CTFs.

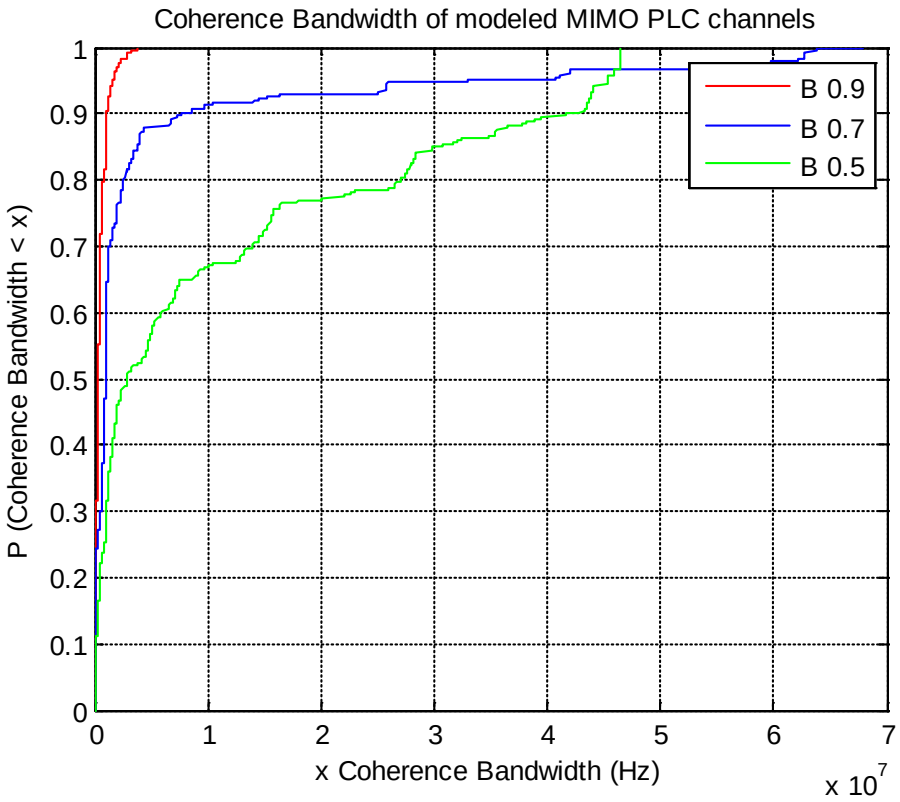

Figure 3.14. CDF of coherence bandwidths of the channels generated by the MIMO PLC channel model

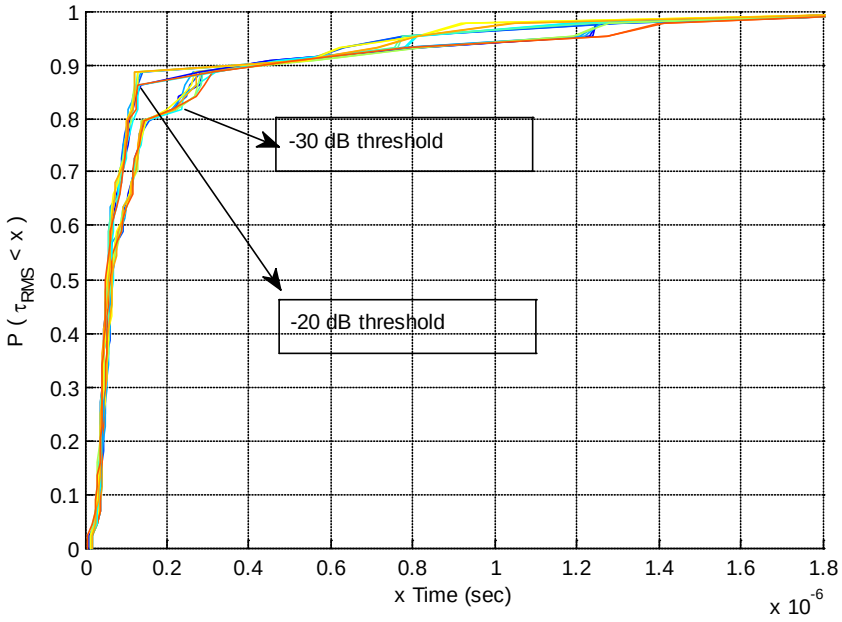

Figure 3.15. CDF of RMS delay spread of the channels generated by the MIMO PLC channel model

6.3. MIMO Channels Correlation

Channel correlation is an important metric for the validity of a channel model. In Figure 3.16 we have shown the channel correlation statistics obtained from the channels generated from the proposed model (same-circuit case). It can be observed that the results shown in Figure 3.16 closely match those in Figure 3.11. It can be observed from the comparison of Figure 3.11 and Figure 3.16 (and Figure 3.12 and Figure 3.17) that the proposed channel model is well capable of producing the similar overall channel correlation (red curves). Moreover, the statistics of three important correlations i.e. the mutual correlations between PN-PN, NPE-NPE and PPE-PPE are also replicated by the model with good fidelity.

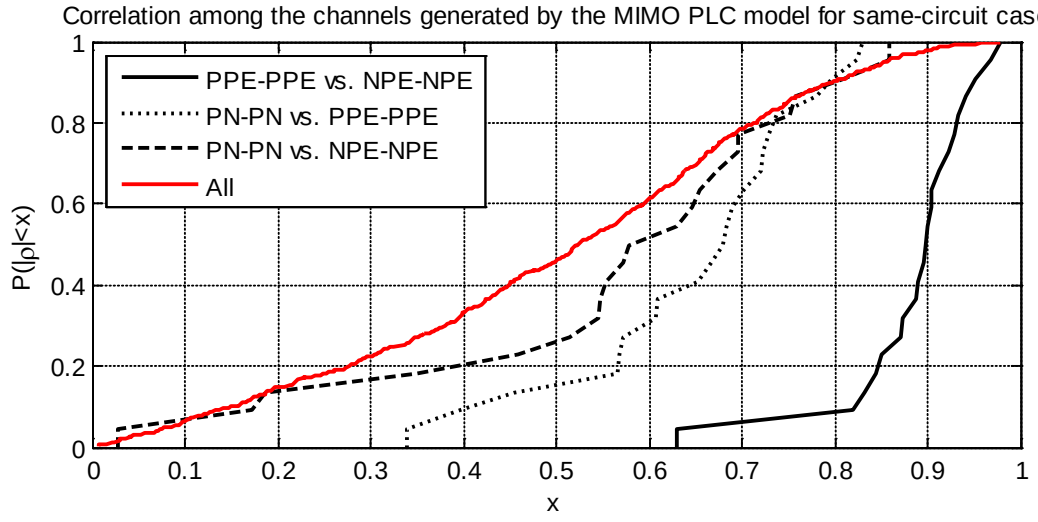

Figure 3.16. CDF of the correlation coefficient for measurement over the same-circuit

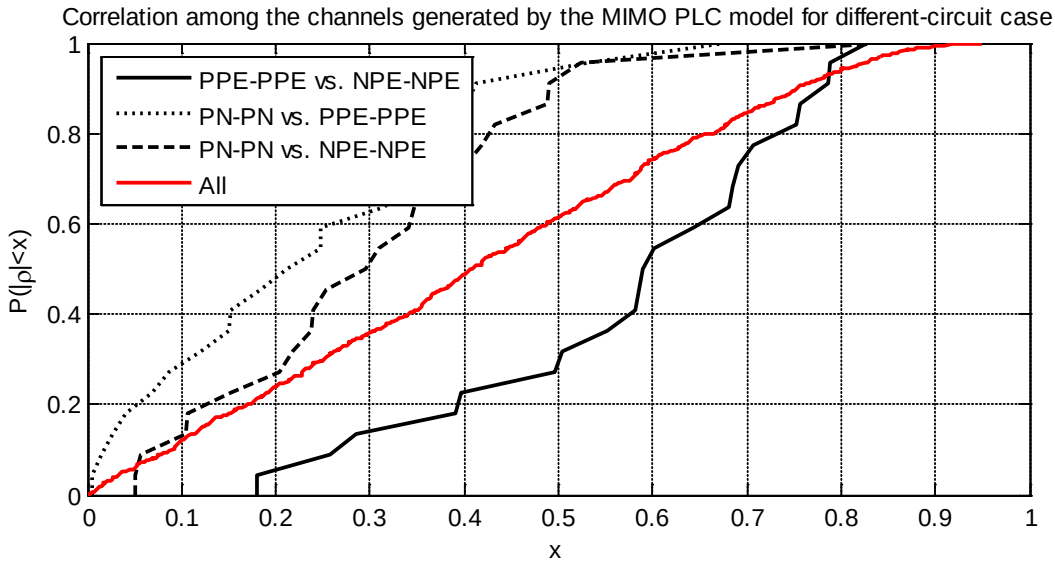

Figure 3.17. CDF of the correlation coefficient for measurement over the different-circuits

7. Conclusions

In this chapter we have we have discussed various channel modeling approaches available in the PLC literature. For this purpose, the top-down approach and the bottom-up approach are included in the discussion along with their strong and weak points. We have summarized some of the present MIMO PLC channel modeling publications.

As a major step with respect to the state-of-the-art in the field, we have presented the development of a complete MIMO in-home PLC channel transfer function model, based on measurements performed in real-life domestic environment. The proposed MIMO PLC channel transfer function model is based on multipath formalism for SISO channels which was first unveiled by Zimmerman and later extended in statistical terms by Tonello. We have extracted a set of channel transfer function parameters by fitting the measured MIMO channels to the average path loss of the multipath SISO PLC channel. A full MIMO 3x3 channel transfer function matrix has been generated statistically, by introducing and selecting path phases in given offset ranges. The channel transfer function characteristics such as RMS delay spread, coherence bandwidth and channel correlation exhibited by the proposed MIMO channel model closely match the experimental values obtained from the measured channels.

The interest of PLC community in MIMO is increasing. It is expected that more research activity will be visible in this field in order to reap the potential benefits of MIMO. We expect that the MIMO PLC channel model presented in this chapter will serve as a basis for

the realistic simulation of MIMO PLC systems and favor their implementation in future PLC products.

Chapter .4
MIMO PLC background noise model

1. Introduction

This chapter presents the analysis, characterization and modeling of background noise in MIMO power line channels. Two types of noise models are proposed: a frequency domain noise model and a time domain noise model. The study and analysis of noise and interference present in a communication channel is important and the power line channel is no exception. However, in contrast to the well analyzed and formulated radio communication channel, power lines are not affected by a simple additive white Gaussian noise (AWGN). The interference scenario is rather complicated, as the signal encounters not only the colored background noise but also narrowband interferences. In addition, to aggravate the scenario, there are different types of impulsive noise in PLC channel. It is worthwhile to recall a typical measured MIMO PLC channel noise (Figure 4.1). We observe in Figure 4.1 the three simultaneous noise sequences measured at an inhome PLC socket: P-N, N-PE and P-PE. It can be noted that the MIMO PLC noises consist of low level part as well as the impulses. It should be noted in Figure 4.1 that the level of P-N noise is lower than the N-PE and P-PE noise.

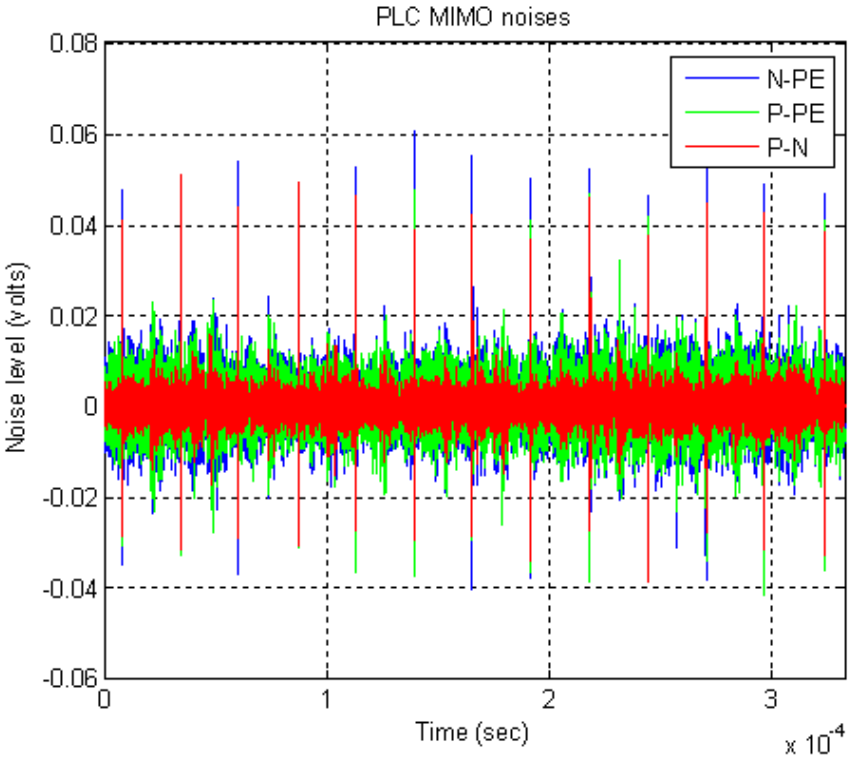

Figure 4.1. Measured MIMO power line noise

Figure 4.2 presents an overview of the noise exhibited by the PLC channel [Götz04]. After passing through a channel with the impulse response $h(t)$ the transmitted signal $s(t)$ reaches a summing node, where a variety of interference $n(t)$ is added, before the signal $r(t)$ arrives at the receiver. According to [Zimm02b], the noise found in power line channel can be roughly separated into five classes: colored background noise, narrowband noise, periodic impulsive noise synchronous or asynchronous to the mains frequency (usually 50 or 60 Hz), and asynchronous aperiodic impulsive noise. A similar classification into background, narrowband, and impulsive noise can be found in [Meng07].

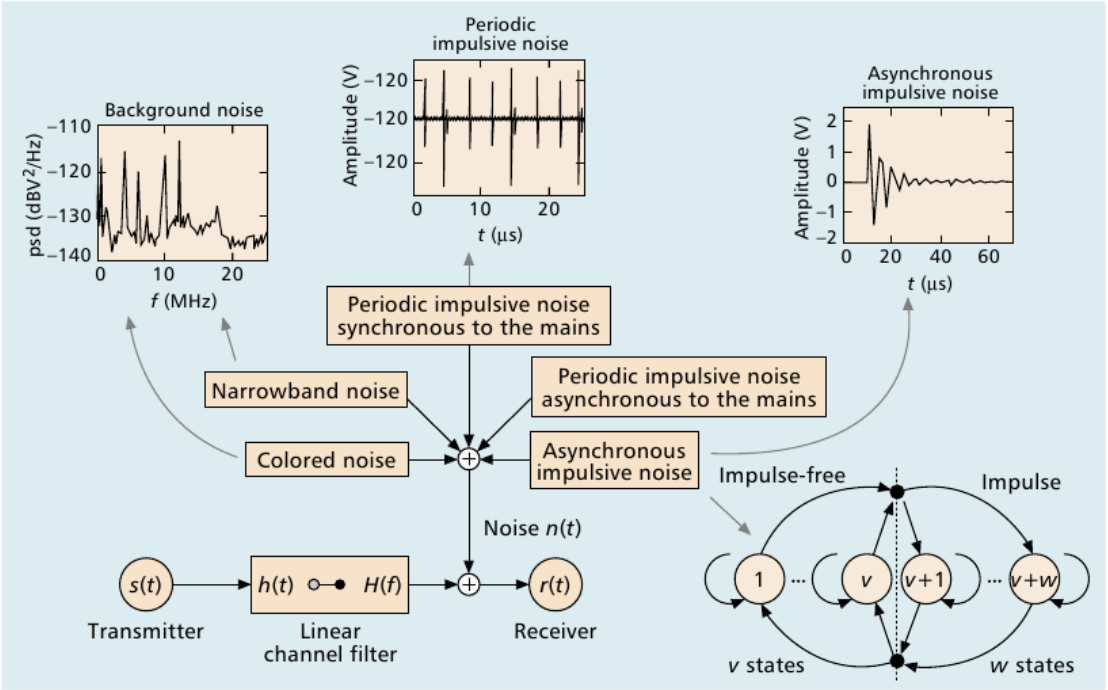

Figure 4.2. Noise types in PLC channel [Götz04]

1.1. Background noise

Background noise is directly associated to the intrinsic physical properties of the medium or channel. The background noise of radio channels is generally considered to exhibit a flat or white PSD. This means that the power density of the noise over all frequencies is the same. In contrast, for PLC channels, the background noise is colored. This means that the noise PSD is dependent on the frequency. Generally, the noise PSD is higher at lower frequencies and decreases exponentially as the frequency increases. This kind of noise can be approximated by several sources of white noise in non overlapping frequency bands with different noise amplitudes [Zimm02b]. This kind of noise is generally modeled in the frequency domain by fitting a decreasing function with its voltage profile or its power spectral density. The OPERA consortium suggests a model (Eq. 4.1) for the background noise [Lagu08]:

$$A(f) = A_{\infty} + A_0 e^{\frac{-f}{f_0}} \tag{4.1}$$

where A_∞ is the limit of the noise power density as f approaches $+\infty$, and A_0 is the difference between A_∞ and $A(0)$. Some appliances may also contribute to the background noise and can cause disturbances in the frequency range of up to several MHz. In [Meng07], the background noise has been found to have a power spectral density (PSD) well approximated as Eq. 4.2.

$$S_n(f) = -140 + 75e^{\frac{-f}{5\times10^5}} \quad \text{dBm/Hz} \tag{4.2}$$

1.2. Narrow-band noise

The main sources of narrow-band noise are the broadcasters in long, medium and short wave range, as well as the amateur radio. At higher frequencies, narrow-band noise due to Frequency Modulation (FM) radio is also perceived by PLC modems. The narrowband noise can be modeled as a sum of sinusoids (Eq. 4.3) [Lagu08]:

$$n_{narrow}(t) = \sum_{i=1}^{N} A_i(t)\sin(2\pi f t + \varphi_i) \tag{4.3}$$

where N is the number of carriers considered in the model, each with different amplitude $A_i(t)$ and different phase φ_i. It has been mentioned in [Meng07] that narrow band noise may reach power levels of 30 dB greater than the background noise at frequencies greater than 1 MHz. The narrow band noise level may fluctuate remarkably depending upon the geographical location of the receiver and hour of the day. In urban centres the level of narrow band noise is higher than in rural localities. Similarly, various amateur and local broadcasters may be more active at day time compared to the night hours.

1.3. Impulsive noise

Impulsive noise is caused by components in Switch Mode Power Supply (SMPS) such as the rectifier diodes, switching transistors, etc. Duration of impulsive noise is quite short, i.e. around 1 msec, and its power spectral density (PSD) is about 50 dB higher than that of the background noise [Yoon08]. Although the impulse noise appears during short time intervals, it is considered the main source of errors in data transmission over PLC channels, due its high power spectral density (PSD) [Baig03]. This noise has been studied both in time and frequency domains, but the time domain

models are the most common in PLC literature. In the time domain, the impulse noise is characterized by the impulse amplitude *A*, the impulse width t_w, and interarrival time (IAT), t_{arr}. All of these parameters are random variables whose statistical properties may be derived from measurements. In [Zimm02b] an impulse noise model n_{imp}, based on a generalized impulse function *imp(t)*=1 if *t*=[0,1] and 0 elsewhere, has been proposed (Eq. 4.4).

$$n_{imp} = \sum_i A_i imp(\frac{t-t_{arr,i}}{t_{w,i}}) \tag{4.4}$$

2. Frequency domain MIMO PLC noise model

In this section, we propose a model for the MIMO PLC noise on the basis of a series of experimental data. The measurement campaign that we conducted to collect realistic noise samples is fully described in Chapter 2. Our frequency domain modeling of MIMO PLC background noise is based on two well accepted SISO PLC noise models: the OMEGA model [Omega08] and the Esmailian model [Esma03].

2.1. The OMEGA model

The OMEGA model is a frequency domain model for SISO PL background noise, developed within the framework of the ICT Project OMEGA [Omega08]. This model, based on measured SISO PL noise, captures the typical frequency dependent character of the background noise.

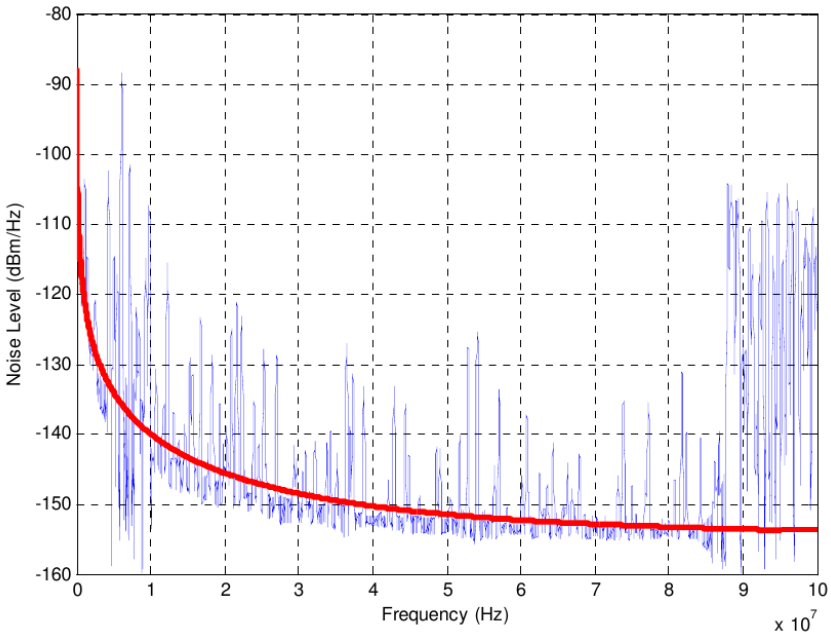

Figure 4.3. The OMEGA model of background noise for SISO PL channel

The general mathematical form of the OMEGA model is shown as in Eq. 4.5

$$N_{OM} = 10\log_{10}\left(\frac{1}{f^{x}} + 10^{y}\right) \tag{4.5}$$

where N_{OM} stands for the OMEGA noise PSD in dBm/Hz, f denotes the frequency in Hz and x and y are the noise model parameters. The parameter x controls the form of frequency dependent decay while the parameter y controls the noise floor. In [Omega08], the values of x and y are set equal to 2 and -15.5 respectively, which correspond to a quadratic decay and a noise floor of -155 dBm/Hz. In addition to the general decreasing shape of the PLC background noise described by Eq. 4.5, the reference [Omega08] provides a procedure to add a number of background noise sources, leading to realistic realizations of the noise perceived by a PLC modem. Figure 4.3 shows the OMEGA noise model (red) in a 0-100 MHz range.

2.2. The Esmailian model

The Esmailian model [Esma03] is also a frequency domain model for SISO PL background noise. This model is also based on measurements and depicts the PL background noise as a decaying frequency dependent function as given by Eq. 4.6.

$$N_{ES} = a + b.\left|\frac{f}{10^6}\right|^c \tag{4.6}$$

where N_{ES} stands for the noise PSD in dBm/Hz, f denotes the frequency in Hz and a, b and c are the model parameters. The parameter a controls the noise floor, b controls the value of noise PSD at starting frequency and c controls the form of the frequency dependent decay.

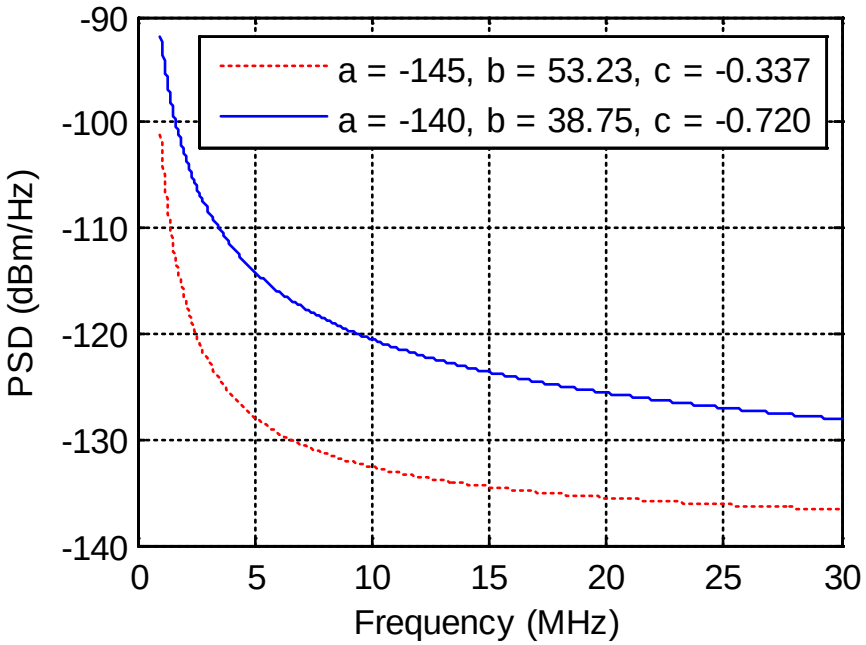

Figure 4.4. The Esmailian model of background noise for SISO PL channel

In [Esma03], two sets of parameter values have been provided. For stronger noise, the values are: a = -140, b = 38.75 and c = -0.720. For weaker noise, the values are: a = -145, b = 53.23 and c = -0.337. Figure 4.4 shows the Esmailian models for the two parameter sets in the 0-30 MHz range.

2.3. Simulations for parameter estimation

We estimated the parameters of the OMEGA and Esmailian models by fitting the models to the measured noise sequences, collected during the measurement campaign described in Chapter 2. The Simulated Annealing (SA) algorithm is used for this purpose. The criterion for the best fit is the minimum mean square error (MMSE) between the measured and modeled PSD in dBm/Hz. MMSEs for the extraction of OMEGA and Esmailian models are defined in Eq. 4.7 and Eq. 4.8

$$min \frac{1}{BW} \int_{f_{min}}^{f_{max}} \left(N_{OM,(x,y)}(f) - N_{meas}(f) \right)^2 df \xrightarrow{yields} [x, y] \tag{4.7}$$

$$min \frac{1}{BW} \int_{f_{min}}^{f_{max}} \left(N_{ES,(a,b,c)}(f) - N_{meas}(f) \right)^2 df \xrightarrow{yields} [a, b, c] \tag{4.8}$$

where *min* stands for the minimum value, f_{min} and f_{max} denote the start and end frequency, *BW* stands for the bandwidth and N_{meas} is the measured noise PSD in dBm/Hz. The seed values for the estimation of OMEGA model's parameters are set equal to $x = 2$ and $y = -15.5$. Similarly, the seed values for the estimation of Esmailian model's parameters are set equal to $a = -145$, $b = 53.23$ and $c = -0.337$.

Figure 4.5 shows a measured N-PE noise, the original OMEGA model and the estimated model in the 2-150 MHz range. It can be observed in Figure 4.5 that the estimated values of *x* and *y* provide a better fit to the measured noise than the original OMEGA model.

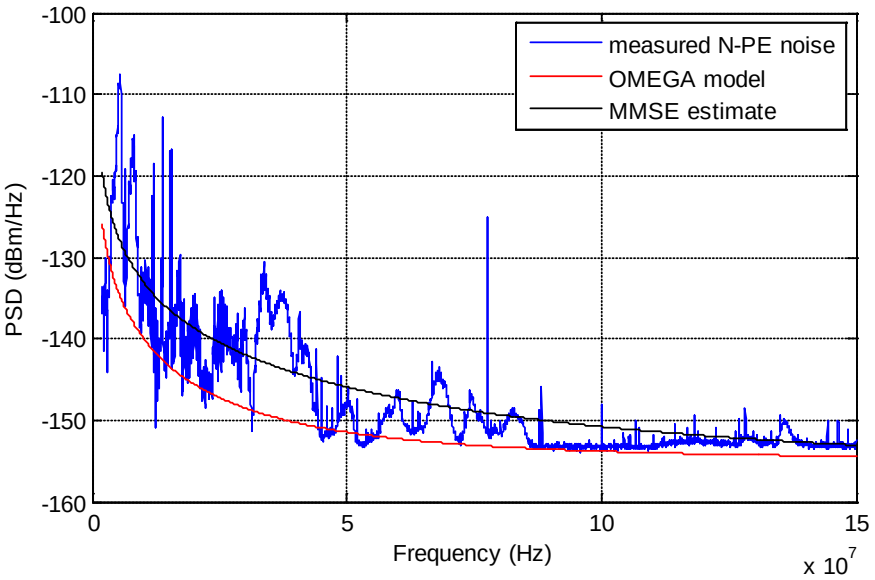

Figure 4.5. A measured N-PE noise, the original OMEGA model and the estimated model

Similar trend (goodness of fit), as shown in Figure 4.5, is noticed for the Esmailian model in Figure 4.6. However, there is a larger distance between the measured noise and the original Esmailian model. This is due to the fact that the original Esmailian model was defined for the 0-30 MHz range only.

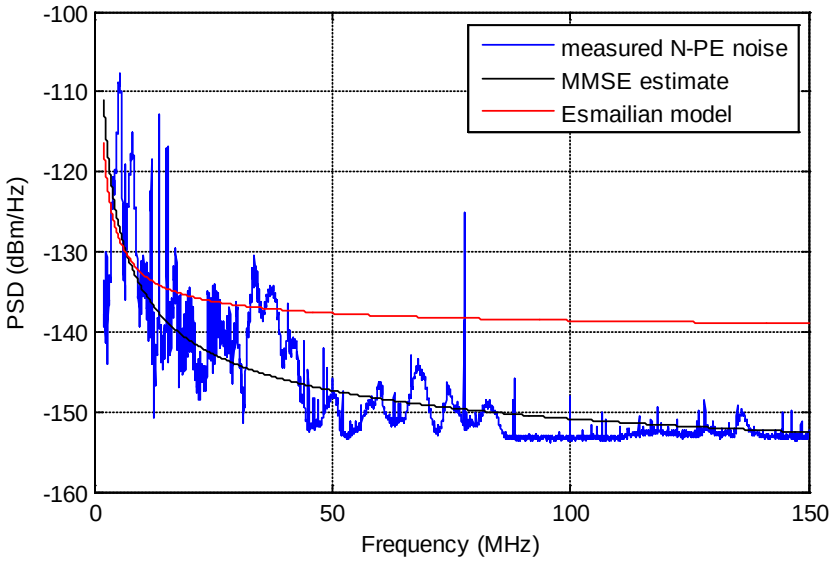

Figure 4.6. A measured N-PE noise, the original Esmailian model and the estimated model

3. Statistical Frequency Domain Models for MIMO PL Noise

As mentioned in Section 1 of this chapter, the MIMO PL noise consists of three noise sequences: N-PE, P-N and P-PE. Therefore, a MIMO PL noise model should contain the statistical properties of model parameters for the three sequences.

3.1. MIMO PL noise model based on the OMEGA model

In the case of the OMEGA model, we propose a model for the MIMO PL noise providing the statistics of the parameters x and y for the N-PE, P-N and P-PE sequences. Table 4.1 summarizes the statistics of the MIMO PL noise model based on the OMEGA model fitting.

		Noise Sequence		
		N-PE	**P-N**	**P-PE**
MIMO PL noise model parameter	x	**Uniform (1.75 , 2.1)**	**Uniform (1.86 , 2.2)**	**Uniform (1.75 , 2.1)**
	y	**Uniform (-16.1 , -15)**		

Table 4.1 MIMO PL noise model based on OMEGA model

It can be noted in Table 4.1 that parameters *x* and *y* for N-PE, P-N and P-PE noises are described by various uniform distributions. The parameter *x*, in case of N-PE and P-PE noises, is represented by a uniform distribution with min=1.75 and max=2.1 whereas for the P-N noise, *x* ranges from 1.86 to 2.2. The statistical trends of the parameter *x* reiterate the fact that the N-PE and P-PE noises closely resemble each other. Since *x* controls the frequency dependent decay in noise PSD, the slightly higher values of *x* for the P-N noise suggest that the P-N noise generally has lower PSD than the N-PE and P-PE noises. The parameter *y* for all three noises is represented by a uniform distribution with min= -16.1 and max= -15. This statistical trend of the parameter *y* suggests that the three noise sequences in the modeled MIMO PL background noise eventually attain the same floor level.

Here, it is appropriate to briefly describe why the uniform distribution is selected to model the estimated parameters. As mentioned in Section 4.2 of Chapter 2, we measured the noise on 27 sockets. However, 27 values of do not provide sufficient sample size. Therefore, we selected the uniform distribution to model the parameters. For example, Figure 4.7 shows the histogram of parameter *x* for the N-PE noise, and it is evident that no definitive conclusion about the distribution of the data can be made. Same principle was applied for other parameters as well.

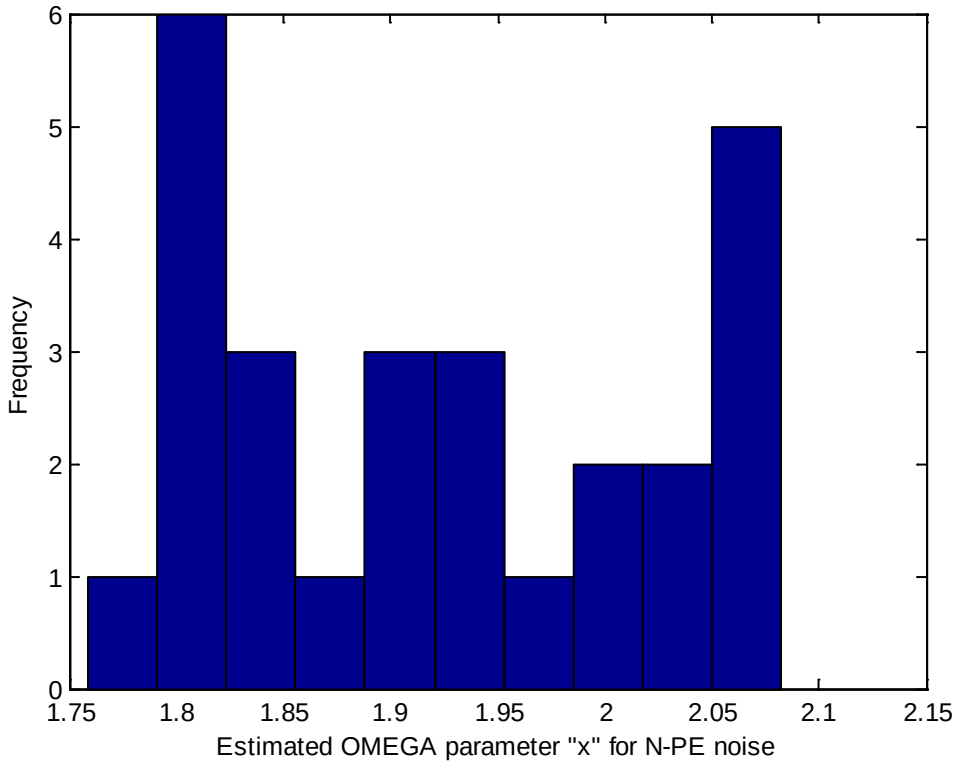

Figure 4.7. Histogram of parameter *x* for N-PE noise

3.2. MIMO PL noise model based on the Esmailian model

We propose another model for MIMO PL noise, based on the Esmailian model, and providing the statistics of the parameters *a*, *b* and *c* for N-PE, P-N and P-PE sequences. Table 4.2 summarizes the MIMO PL noise model based on the Esmailian model.

		Noise Sequence		
		N-PE	**P-N**	**P-PE**
MIMO PL noise model parameter	***a***	**Uniform (-174,-150)**	**Uniform (-174,-165)**	**Uniform (-174,-150)**
	b	**Uniform (54,70)**	**Uniform (47,67)**	**Uniform (54,70)**
	c	**Uniform (-0.410,-0.275)**	**Normal (μ = -0.29, σ =0.03)**	**Uniform (-0.410,-0.275)**

Table 4.2 MIMO PL noise model based on Esmailian model

It can be noted in Table 4.2 that parameters *a*, *b* and *c* for N-PE, P-N and P-PE noises are modeled by various uniform distributions, except for the parameter *c* in the case of P-N noise where it is modeled by a normal distribution. We again notice that MIMO PL noise model parameters follow similar statistical trends for the N-PE and P-PE noises. In Table 4.2 we observe that the parameter *b* for N-PE and P-PE noises tends to be slightly higher than that for the P-N noise. This demonstrates the fact that at the start frequencies the PSD of the modeled N-PE and P-PE noises is likely to be higher than that of the P-N noise, as observed in the measured data. Another interesting observation is that the parameter *a*, which controls the noise floor, has lower mean value for the P-N noise compared to the N-PE and P-PE noises. This is a better representation of the measured data compared to the parameter *y* of OMEGA based model which is unable to capture this effect.

Again, the insufficient data size as shown in Figure 4.8, prompted us to select the uniform distribution to model all the estimated parameters except for the *c* parameter for P-PE noise where it is modeled as a normal distribution.

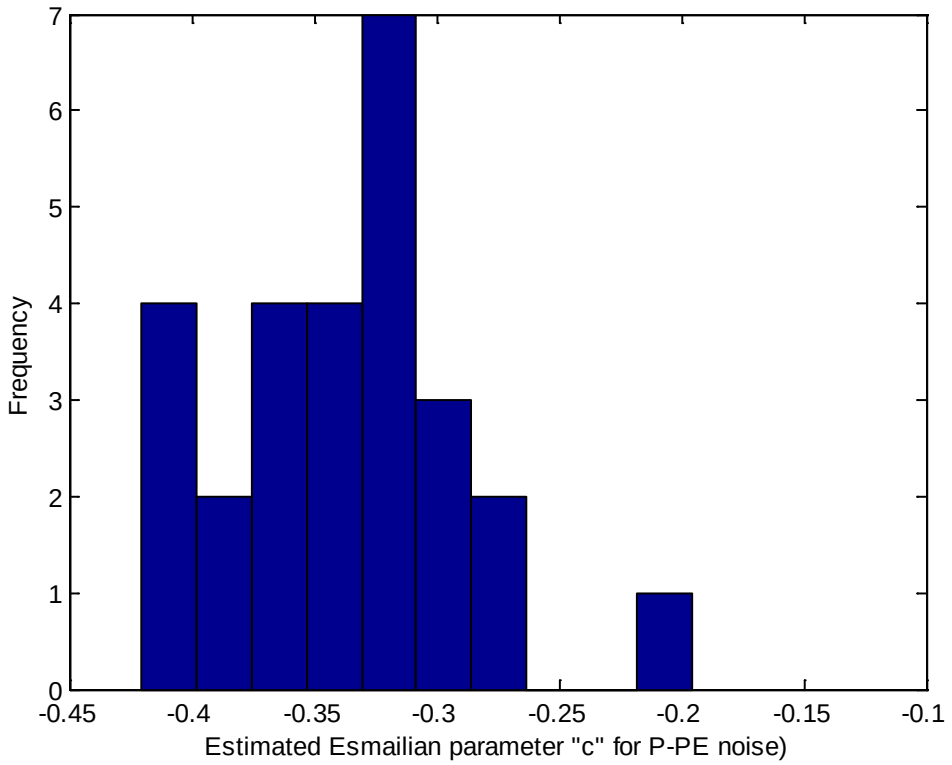

Figure 4.8. Histogram of parameter *c* for P-PE noise

3.3. Comparison of MIMO PL Noise Models

It will be interesting to know which model is more efficient between the OMEGA based model and the Esmailian based model. For this purpose, we calculate the root mean square error (RMSE) between a given measured noise and its estimated OMEGA (resp. Esmailian) based model as shown in Eq. 4.9 and Eq. 4.10.

$$RMSE_{est,OM} = \sqrt{\frac{1}{BW}\int_{f_{min}}^{f_{max}} \left(N_{est,OM}(f) - N_{meas}(f)\right)^2 df} \tag{4.9}$$

$$RMSE_{est,ES} = \sqrt{\frac{1}{BW}\int_{f_{min}}^{f_{max}} \left(N_{est,ES}(f) - N_{meas}(f)\right)^2 df} \tag{4.10}$$

where $N_{est,OM}$ and $N_{est,ES}$ are OMEGA and Esmailian noises in dBm/Hz obtained with estimated parameters.

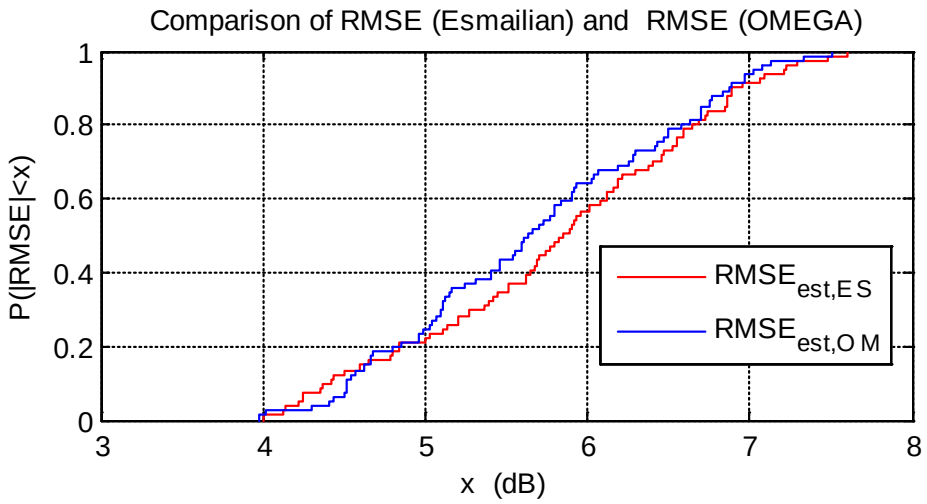

Figure 4.9. CDFs of $RMSE_{est,OM}$ and $RMSE_{est,ES}$

Figure 4.9 compares the CDF of the RMSE obtained for the OMEGA model fitting and the Esmailian model fitting. From this comparison it is evident that both models offer similar RMSE statistics, though OMEGA based model has a slight edge (about 0.25 dB at P=0.5) over the Esmailian based model. This may be due to the fact that the OMEGA model was itself defined in the 0-100 MHz range while the Esmailian model covers only the 0-30 MHz band.

It is worth mentioning that by definition the two models are quite similar to each other. However, the OMEGA model is simpler: it has only two parameters compared to three parameters of the Esmailian model. Therefore, we conclude that the OMEGA model is a better choice for the modeling of MIMO PL noises.

4. Time domain model for MIMO PL noise

The frequency domain models of the background noise provide a very simple and brief picture of the noise present in the power line channel. However, a complete and detailed noise model can be achieved only through time domain modeling techniques. Multivariate time series analysis is a powerful mathematical technique used for the modeling and forecasting of the future values of time sequences. The suitability and utility of multivariate time series modeling in the context of MIMO PLC noise is described in the following sections.

4.1. Multivariate Time Series

Let us visualize the MIMO PLC channel noise as a tri-variate time series (TTS), which is a special case of a multivariate time series (MTS). A time series $\{\boldsymbol{x}_t\}$ is a sequence of data values measured at equally spaced time intervals Δt. A MTS consists of simultaneous observations of several variables. Consider a MTS $\{N_t\}$ with n variables such that $N_t = (\boldsymbol{x}_{1t},\ldots, \boldsymbol{x}_{nt})^T$ where ^{T} stands for transpose.

MIMO PLC channel noise as shown in Figure 4.1 when limited to 150 MHz bandwidth can be characterized as a MTS $\{N_{MIMO,t}\}$ with n=3, sampling period Δt=0.0033 μs, and where $\{\boldsymbol{x}_{1t}\}$, $\{\boldsymbol{x}_{2t}\}$ and $\{\boldsymbol{x}_{3t}\}$ represent N-PE, P-N and P-PE noises respectively. In the sequel, the $\{N_{MIMO,t}\}$ is taken as vectors of duration 46.52 μs which corresponds to OFDM symbol duration in HomePlug AV standard for commercial PLC devices [Home07].

4.2. Frequency Domain Cross-Correlation

Since MIMO PLC noise consists of three noises, therefore their spectrums need to be observed individually. We find that general spectral form of MIMO PLC noise is a decreasing exponential as shown in Figure 4.10.

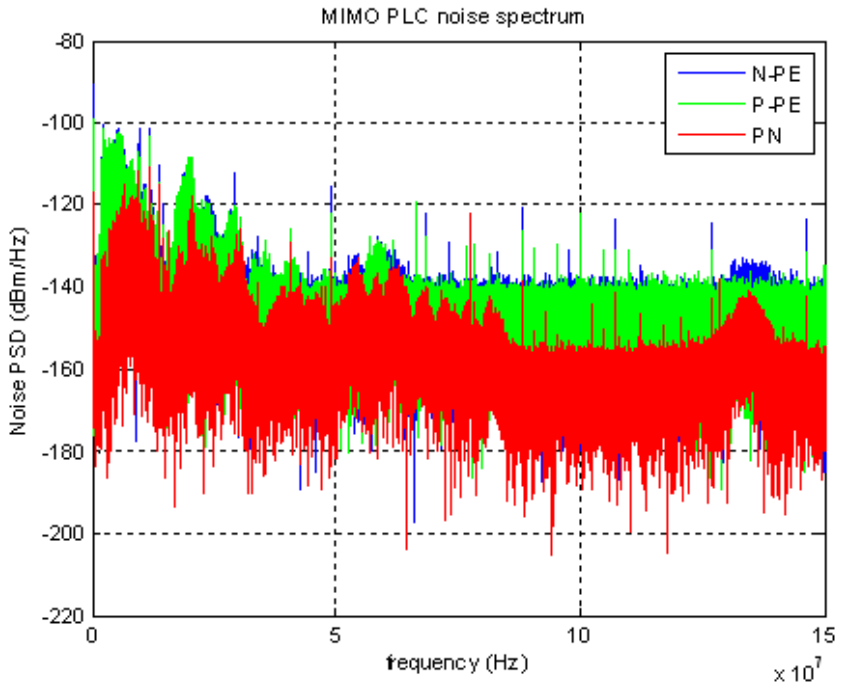

Figure 4.10. Typical spectra of measured MIMO PLC channel noises

Let us consider that the parameter $\Psi_{i,j}$, defined in Eq. 4.11, denotes frequency domain cross-correlation between measured P-N noise PSD and modeled P-N noise PSD

(same applies to N-PE and P-PE noises as well). $\Psi_{i,j}$ serves as a metric of spectral resemblance between measured and modeled noise.

$$\psi_{i,j} = \frac{\overline{N_i(f)N_j^*(f)} - \overline{N_i(f)}\,\overline{N_j^*(f)}}{\sqrt{\left(\overline{N_i(f)^2} - \overline{N_i(f)}^2\right)\left(\overline{N_j(f)^2} - \overline{N_j(f)}^2\right)}} \tag{4.11}$$

where N represents the envelope of noise PSD in dBm/Hz, subscripts i and j stand for measured and modeled noise respectively and $\overline{(.)}$ denotes frequency domain average. High values of $\Psi_{i,j}$ are desirable as it suggests that the PSD of modeled noise has a close resemblance to the PSD of measured noise and vice versa.

4.3. Time-domain Cross-correlation

The time-domain cross correlation $\rho_{ti,j}$ between N-PE, P-N and P-PE noises is very important because it designates the dependence of a noise sequence upon the other two. $\rho_{ti,j}$ is defined as Eq. 4.12:

$$\rho_{t\,i,j} = \frac{\overline{n_i(t)n_j^*(t)} - \overline{n_i(t)}\,\overline{n_j^*(t)}}{\sqrt{\left(\overline{|n_i(t)|^2} - |\overline{n_i(t)}|^2\right)\left(\overline{|n_j(t)|^2} - |\overline{n_j(t)}|^2\right)}} \tag{4.12}$$

where n denotes a noise sequence in time domain and $\overline{(.)}$ represents the time domain average. The indices i, j and k stand for N-PE, P-N and P-PE noises respectively. It should be noted that Eq. 4.12 defines $\rho_{ti,j}$, whereas $\rho_{ti,k}$ and $\rho_{tj,k}$ can be defined as well using similar formalism.

A variant of $\rho_{ti,j}$ is $\rho_{meas,i,j}$ which stands for measured noise. In the next sub-section, we will discuss another variant of $\rho_{ti,j}$ denoted by $\rho_{VAR,i,j}$ which signifies time-domain cross-correlation for noise generated by Vector Autoregressive (VAR) model. After analyzing the measurements we observe that there is a stronger correlation $\rho_{meas,i,j}$ between N-PE and P-PE noises, as shown in Figure 4.11. To some extent the N-PE and P-N noises are also correlated to each other, and the same applies to the P-PE and P-N noises. The correlation behavior of MIMO PLC channel noise is quite different from MIMO wireless noise, as the noise in MIMO wireless channels is generally treated as uncorrelated unless for closely spaced antennas [Kruz07].

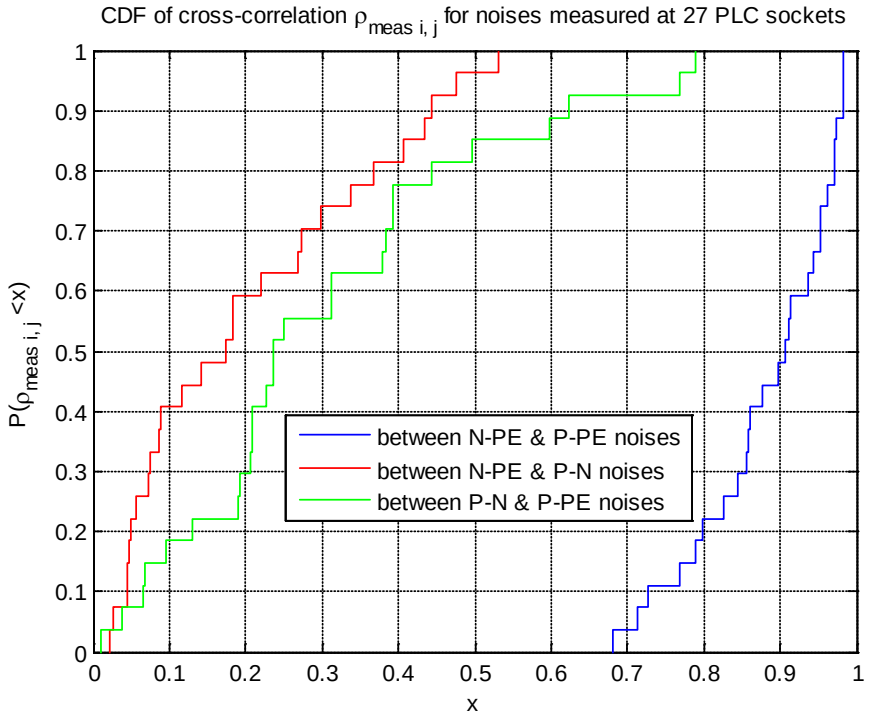

Figure 4.11. CDF of the time-domain correlation for the measured MIMO PLC noises

4.4. Frequency-domain root mean square error

The frequency domain root mean square error (RMSE), denoted by $\varepsilon_{rms,f}$, is defined as Eq. 4.13:

$$\varepsilon_{rms,f} = \sqrt{\frac{1}{k}\sum_{i=1}^{k}(N_i - N_j)^2} \tag{4.13}$$

where N_i and N_j represent the spectrum in dBm/Hz of a given MIMO PLC noise measurement and its VAR realization respectively, and k is the length of noise sequences. The frequency-domain RMSE, like $\rho_{ti,j}$ and $\Psi_{i,j}$, is a parameter used to estimate the accuracy of VAR model. Lower values of RMSE indicate a more accurate model and vice versa.

4.5. Description of the proposed noise model

In this section we present a novel model for MIMO PLC channel noise. The goal is to generate a MTS which imitates the properties of the measured noise. The challenge is

how to model this MTS so that the modeled $\{x_{1t}\}$, $\{x_{2t}\}$ and $\{x_{3t}\}$ not only have similar spectral characteristics but also the mutual correlation as the measured MIMO PLC channel noise. As we are going to see, one method that can efficiently model the MIMO PLC channel noise is the Vector Autoregressive (VAR) model.

4.5.1. Vector Autoregressive (VAR) Model

A Vector Autoregressive (VAR) model is basically an autoregressive (AR) model in multivariate context. Autoregressive models are often used to model and predict a time series. The notation *VAR(p)* stands for a VAR model of order *p*. A *VAR(p)* model of a *m*-variate time series is defined as Eq. 4.14

$$x_t = w + \sum_{l=1}^{p} A_l x_{t-l} + \varepsilon_t \quad , \ \mathrm{cov}(\varepsilon_t) = \boldsymbol{C} \tag{4.14}$$

where $\boldsymbol{x}_t \in \Re^m$ are the vectors representing the MTS at a given time instant *t*. ε_t are zero-mean, uncorrelated random noise vectors. $\boldsymbol{C} \in \Re^{mxm}$ is the noise covariance matrix and $\boldsymbol{A_1}$, ….., $\boldsymbol{A_p} \in \Re^{mxm}$ are model coefficient matrices. The vector $\boldsymbol{w} \in \Re^m$ serves to introduce the mean value if the MTS has non-zero mean [Neum01].

Equation 4.14 serves a two-fold purpose. This equation is used to extract a VAR(p) model from noise measured at a given socket. Such a VAR model consists of $\boldsymbol{A_1}$, ….., $\boldsymbol{A_p}$, $\boldsymbol{C}$ and $\boldsymbol{w}$. We denote it by $\mathrm{VAR}(p)_{socket}$ as this model is associated to a given socket for a given order *p*. Once $\mathrm{VAR}(p)_{socket}$ is obtained, MIMO PLC noise can be generated for that particular socket and order by using Eq. 4.14.

4.5.2. Order Selection of the VAR Model

As mentioned in Section 4.2 and Section 4.3 of this chapter, frequency domain cross-correlation $\Psi_{i,j}$ and time-domain cross-correlation $\rho_{ti,j}$ are used for noise characterization. Therefore, we look for a $\mathrm{VAR}(p)_{socket}$ model which can satisfactorily achieve cross correlation $\rho_{VAR,i,j}$, so that $\rho_{VAR,i,j}$ is close to $\rho_{meas,i,j}$. For this purpose we study the variation of $\rho_{VAR,i,j}$ w.r.t. *p*. This procedure was applied to 27 measured MIMO PLC noises. It can be observed in Figure 4.12 that as *p* varies, $\rho_{VAR,i,j}$ remains almost constant. Although this result does not help much for order selection of VAR model, it demonstrates that VAR modeling approach is capable of achieving similar values of $\rho_{ti,j}$ as the measured data.

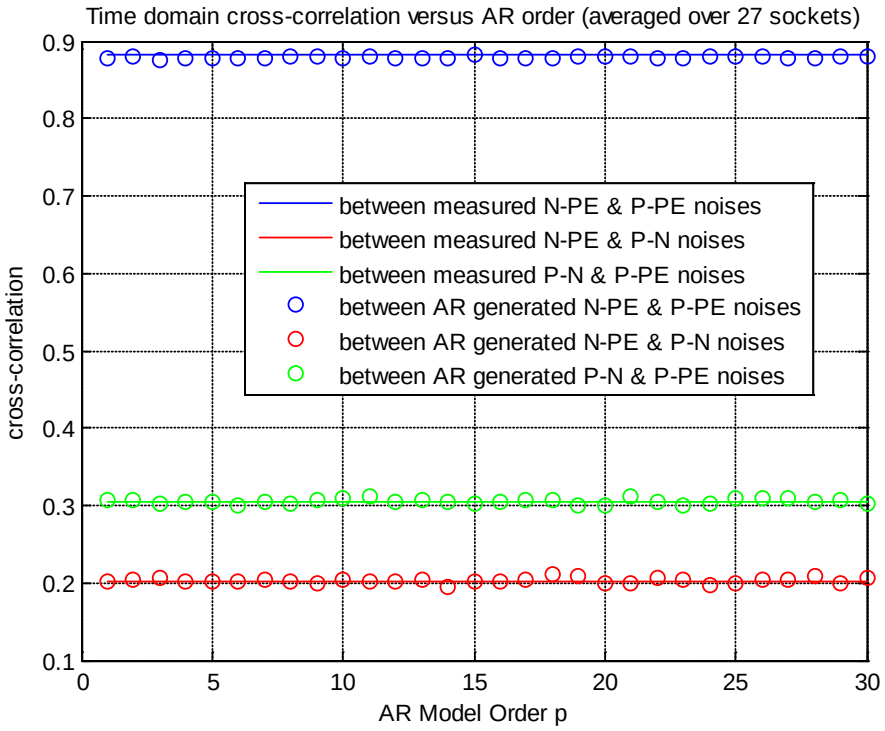

Figure 4.12. Time-domain cross-correlation versus VAR model order

Next the spectral resemblance between the measured MIMO PLC channel noise and its VAR realization VAR(p)$_{socket}$ is studied. We calculate the root mean square error (RMSE) and cross-correlation $\Psi_{i,j}$ between the spectra of a measured noise and the realization VAR(p)$_{socket}$ for different p. It can be seen in Figure 4.13 that RMSE initially decreases sharply as the VAR order increase, but later the rate of fall reduces. The dependence of $\Psi_{i,j}$ on VAR order is even more evident as we see in Figure 4.14. Parameter $\Psi_{i,j}$ initially increase sharply as p increases but then tapers off. As a conclusion of this parametric analysis, we select an order p = 15 to model MIMO PLC noise as a compromise between accuracy and complexity.

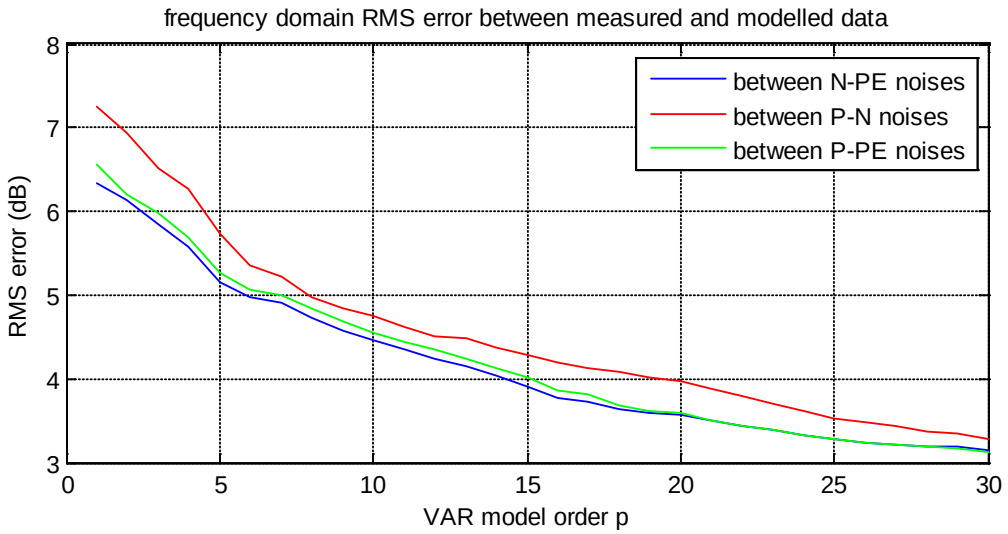

Figure 4.13. Relationship between frequency domain RMS error and VAR order

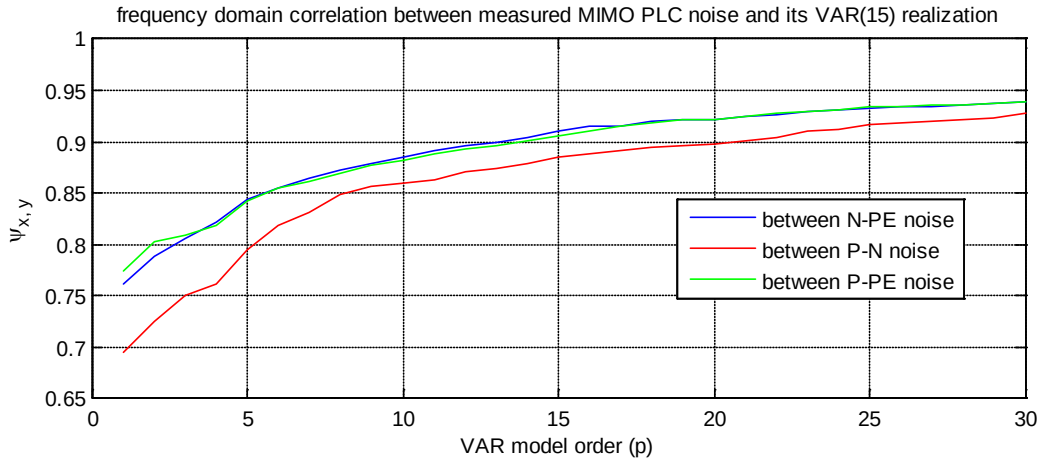

Figure 4.14. Relationship between frequency domain cross-correlation and VAR model order

The resemblance between the spectra of measured MIMO noise sequences and the modeled noise may serve as an indicator to select the order of the VAR model. In the Figure 4.15, Figure 4.16, Figure 4.17 and Figure 4.18, it is obvious that the said spectral resemblance increases as the order of the VAR model increase. In fact, VAR (1) model roughly captures the frequency dependent decay of the measured noise spectrum. As the order of the VAR model increases, the spectrum of the modeled noise resembles more to that of the measured noise. It can be observed in Figure 4.18 that the spectrum of the VAR (30) modeled noise is almost an exact replica of that of the measured noise. It can be shown that for sufficiently high values of the model order *p*, a perfect spectral match can be achieved. However, as described above, keeping the computational effort and time in mind, a compromise value of the model order should be selected.

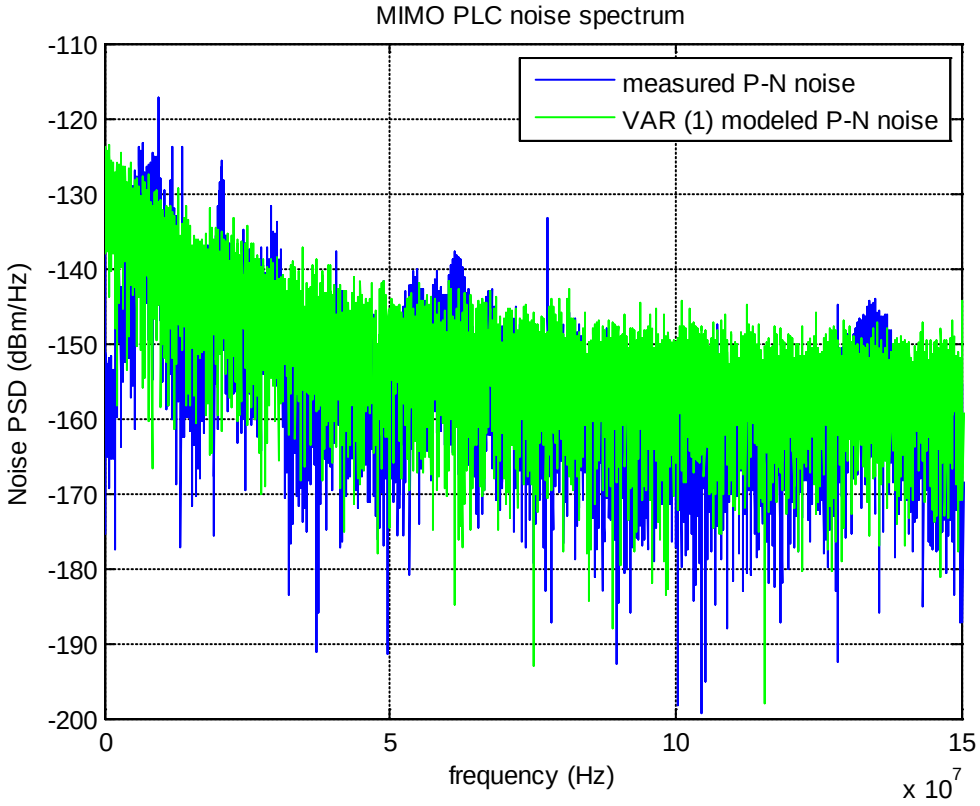

Figure 4.15. Resemblance between the spectra of a measured noise and its VAR(1) model

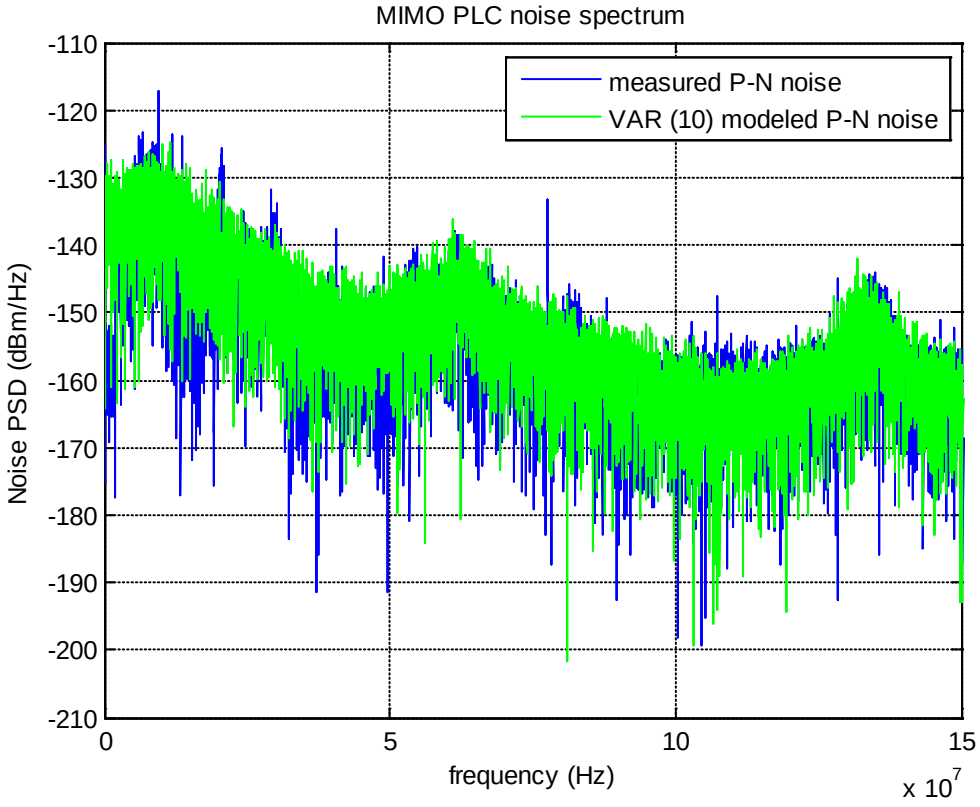

Figure 4.16. Resemblance between the spectra of a measured noise and its VAR(10) model

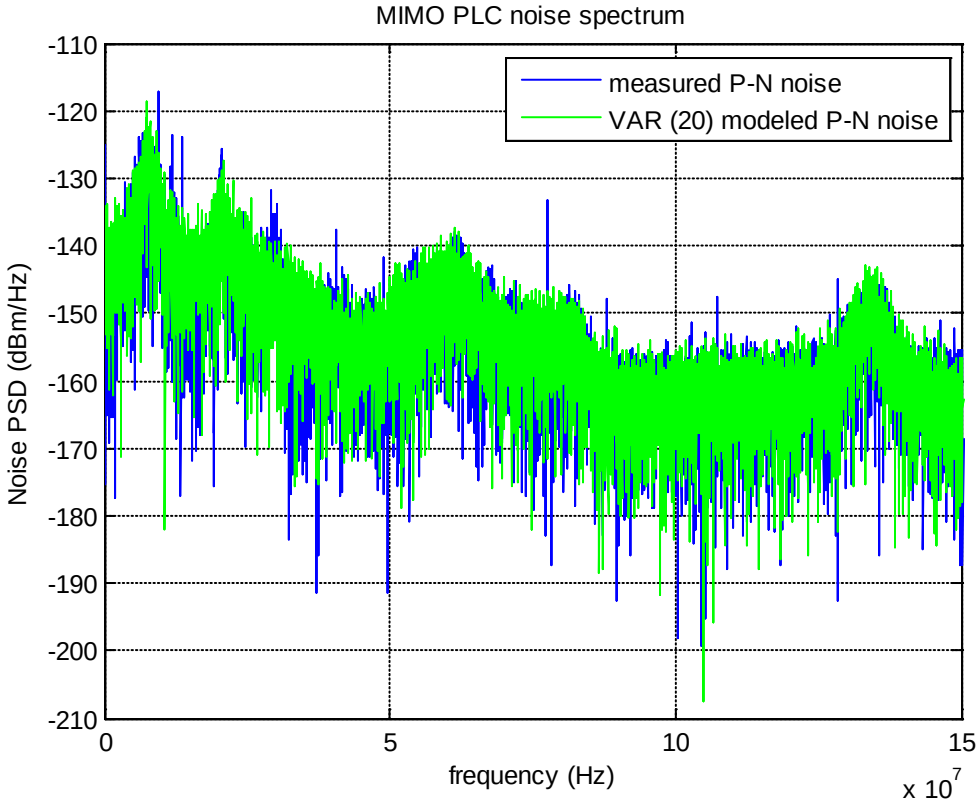

Figure 4.17. Resemblance between the spectra of a measured noise and its VAR(20) model

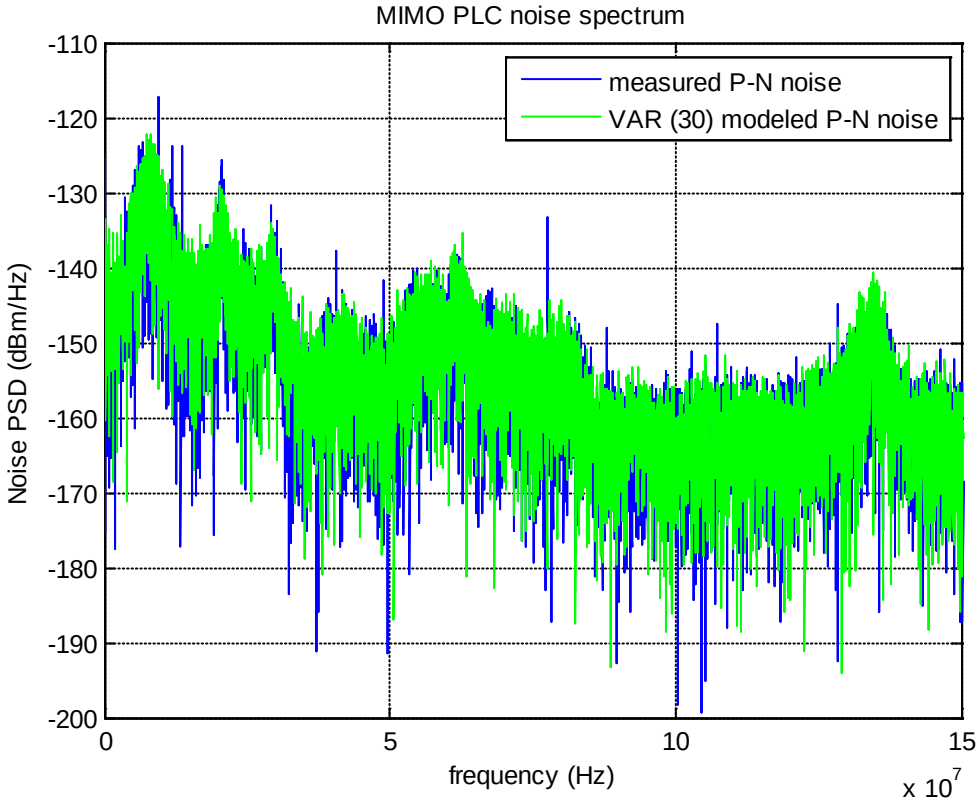

Figure 4.18. Resemblance between the spectra of a measured noise and its VAR(30) model

4.5.3. Extraction of VAR(15) Model

Once the order of the VAR model is selected as p=15, the next step is the extraction of the model parameters from the measured data. We observe in Figure 4.1 that the measured data has zero mean. Therefore, $\boldsymbol{w}$ can be taken as a null vector. Now, according to Eq. 4.14, the problem of model extraction reduces to the estimation of matrices $\boldsymbol{A}$ and $\boldsymbol{C}$ which are 3x45 and 3x3 matrices respectively. Estimation methodology of $\boldsymbol{A}$ and $\boldsymbol{C}$ has been elaborated in [Neum01]. It should be noted here that matrices $\boldsymbol{A}$ and $\boldsymbol{C}$ are real valued. Since we measured data at 27 PLC sockets, the estimation procedure produced 27 $\boldsymbol{A}$ and 27 $\boldsymbol{C}$ matrices. From here onward one may try some method to find a generalized form of $\boldsymbol{A}$ and $\boldsymbol{C}$. However, the pool of 27 samples is not rich enough to provide a reliable statistical trend. Keeping this in view an average model may be a good choice. Eventually we propose a model with one $\boldsymbol{A}$ matrix and one $\boldsymbol{C}$ matrix which are arithmetic means of 27 $\boldsymbol{A}$ and 27 $\boldsymbol{C}$ matrices respectively. This can be termed as the VAR(15)$_{avg}$ model. The average $\boldsymbol{A}$ and $\boldsymbol{C}$ matrices can be denoted with $\boldsymbol{A}_{avg}$ and $\boldsymbol{C}_{avg}$. For instance, an element $c_{row,col}$ of $\boldsymbol{C}_{avg}$ is arithmetic mean of $c_{row,col}$ elements of 27 $\boldsymbol{C}$ matrices. The same procedure applies to matrix $\boldsymbol{A}$.

4.5.4. Generating the MIMO PLC channel noise

MIMO PLC channel noise can be generated with the help of the above mentioned VAR(15)$_{avg}$ model. Figure 4.19 shows a typical noise sequence measured at a given socket. The record length is approximately equal to one OFDM symbol's duration. Figure 4.20 depicts the noise generated by the VAR(15)$_{avg}$ model. Clearly, the two figures do not resemble each other. We can observe distinct peaks in the measured noise while they are absent in modelled noise. This suggests that the VAR model is unable to realize the distinct peaks which, in fact, represent the periodic impulsive noise. However, it can be noted that the overall envelope of the modelled noise is larger than the off-impulse parts of measured noise. Figure 4.21 shows a good resemblance between the spectral envelopes of the measured noise and the modeled noise, which suggests that the dissimilarity between Figure 4.19 and Figure 4.20 does not affect much in the frequency domain.

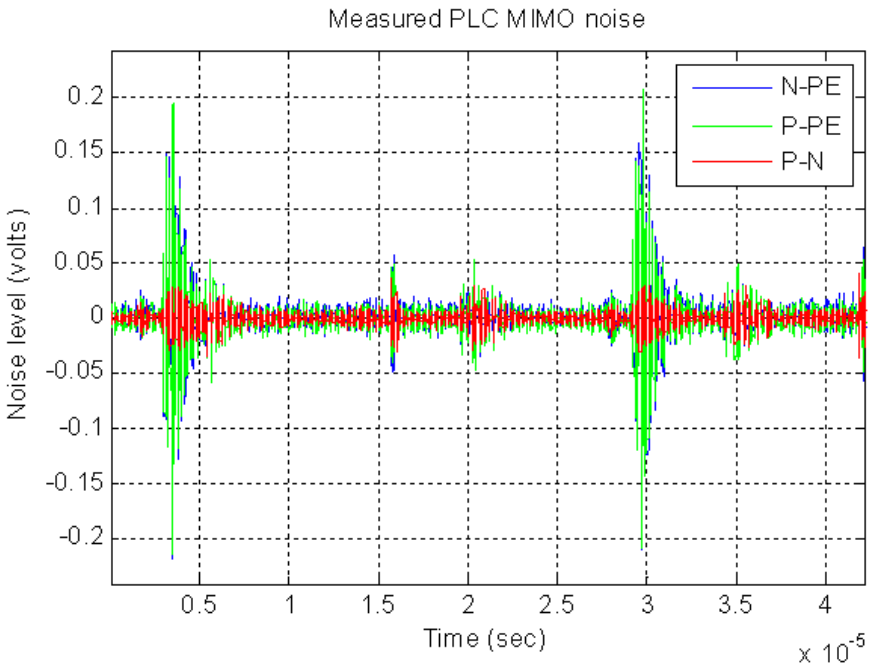

Figure 4.19. Typical measured MIMO PLC channel noise (duration ≈ one OFDM symbol)

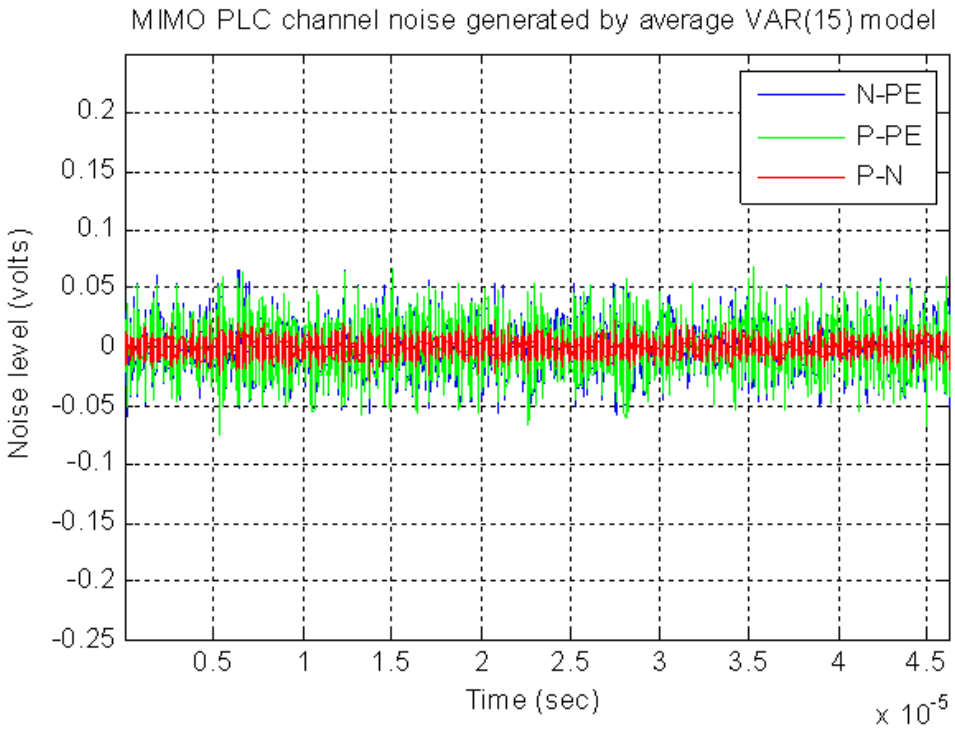

Figure 4.20. MIMO PLC noise generated by average VAR(15)$_{avg}$ model (duration ≈ one OFDM symbol)

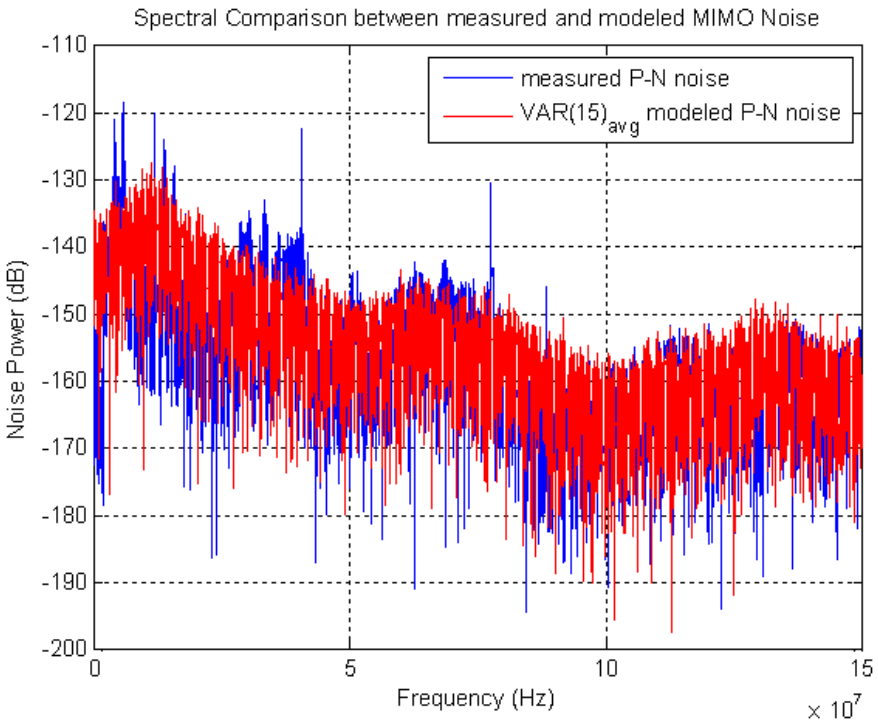

Figure 4.21. Spectral resemblance between the measured and the modeled MIMO PLC P-N noise

It should be noted that for the multicarrier communication, such as the OFDM, the absence of the impulses in the modelled noise may not be a serious problem but for the single carrier communication, generation of the impulses in the modelled noise is necessary.

The impulses can be generated in the modeled noise by modifying the form of the uncorrelated white noise ε_t at the input of the VAR(15)$_{avg}$ filter. We denote this noise as N_{in}, and it can be easily generated by multiplying ε_t with a mask illustrated in Figure 4.22. The statistics of the mask parameters i.e. the impulse height h_{imp}, the inter-impulse distance d_{imp} and the impulse width w_{imp} can be extracted from the measured MIMO PLC noises. It is worth mentioning that we propose a right triangular shape for the impulse in N_{in}.

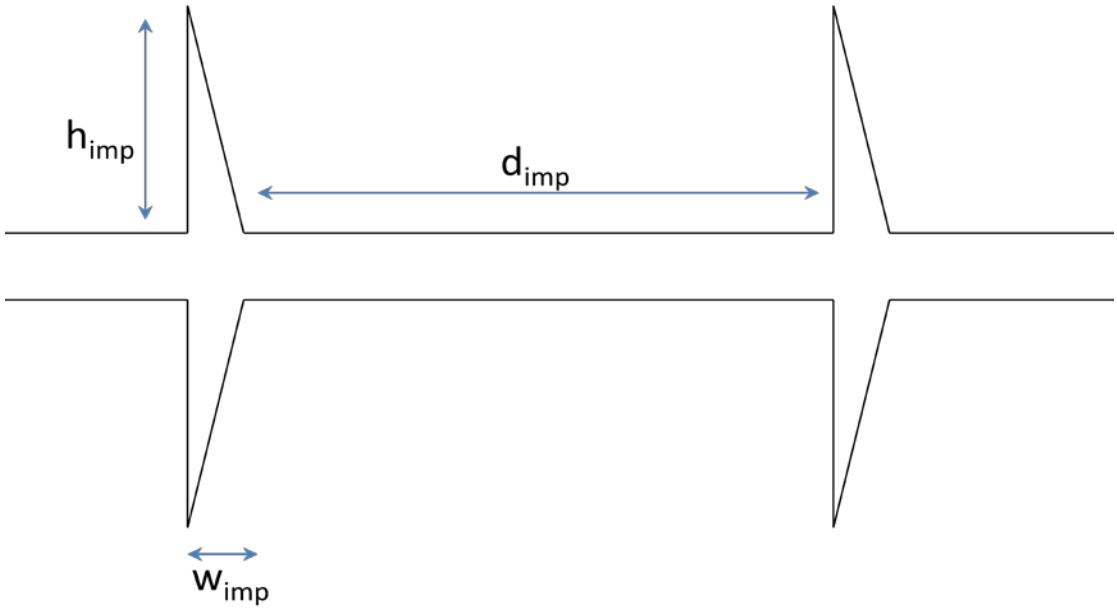

Figure 4.22. Illustration of the mask to generate N_{in}

A typical MIMO PLC noise obtained with N_{in} at the input of the VAR(15)$_{avg}$ filter is shown in Figure 4.23. It can be noted in Figure 4.23 that the impulses are successfully generated by the VAR(15)$_{avg}$ model.

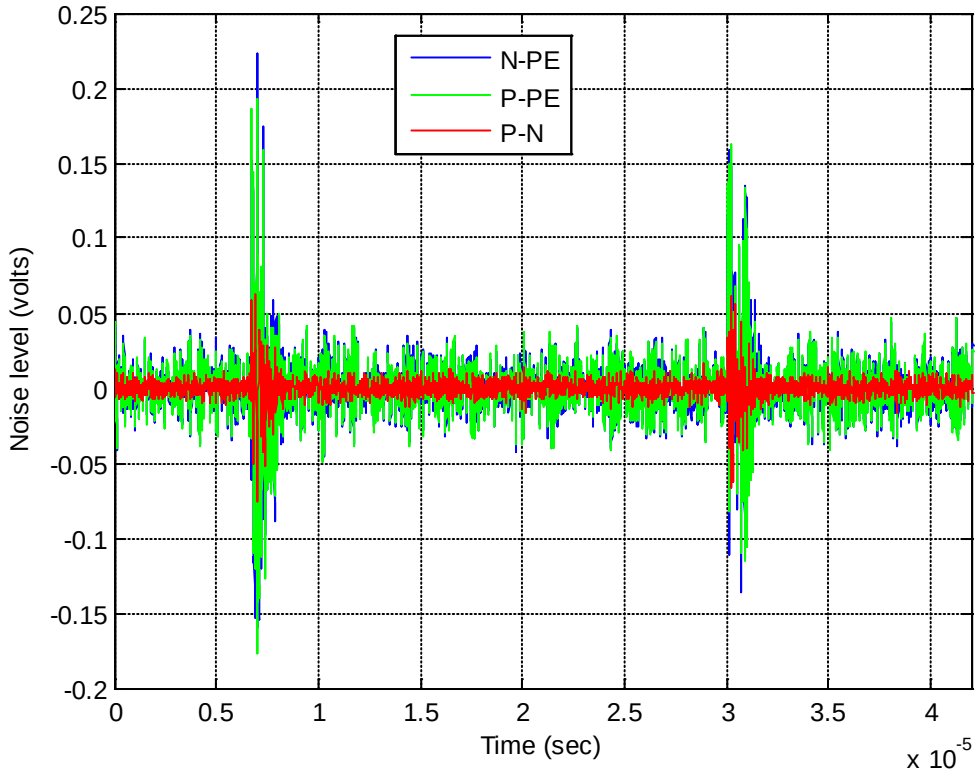

Figure 4.23. MIMO PLC noise obtained by the VAR(15)$_{avg}$ model with N_{in}

4.5.5. **Model Validation**

The validity of the model can be verified through frequency domain cross-correlation and time domain cross-correlation. The MTS generated by VAR(15)$_{avg}$ model should exhibit similar $\Psi_{i,j}$ and $\rho_{ti,j}$ as the measured MIMO PLC channel noise.

1) Time-domain cross-correlation

A comparison between $\rho_{meas,i,j}$ (averaged over 27 sockets) and $\rho_{VAR,i,j}$ obtained from VAR(15)$_{avg}$ model is presented in Table 4.3. It can be observed in Table 4.3 that average VAR(15)$_{avg}$ model achieves similar time-domain correlation as the measured MIMO PLC channel noise. The difference for N-PE & P-PE correlations is 4% and for P-N & P-PE is 1%. In N-PE & P-N case the difference is 18%, however, these correlations are so low that N-PE and P-N can be regarded as uncorrelated anyhow.

	Between N-PE & P-N	Between N-PE & P-PE	Between P-N & P-PE
$\rho_{meas,i,j}$	0.20	0.88	0.30
$\rho_{VAR,i,j}$	0.02	0.92	0.31

Table 4.3 Time-domain correlation between MIMO PLC noises

2) Frequency Domain Cross-Correlation

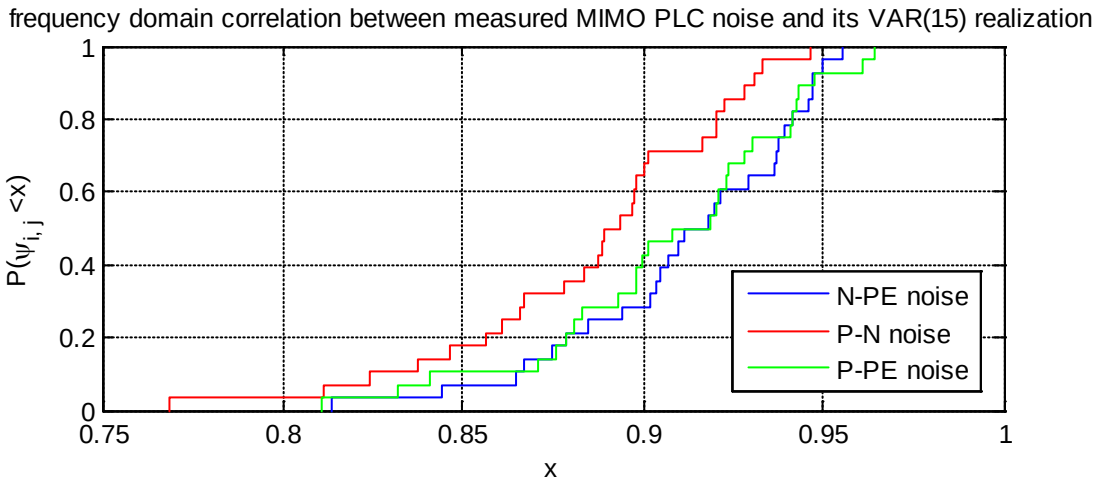

Figure 4.24. CDF of Frequency-domain correlation between measured and VAR(15)$_{socket}$ generated MIMO PLC noises

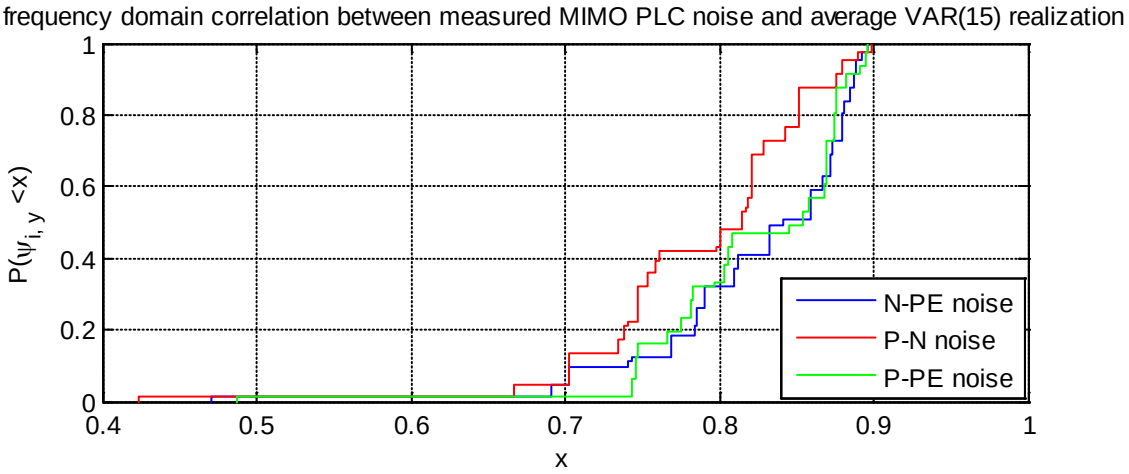

Figure 4.25. CDF of Frequency-domain correlation between measured and VAR(15)$_{avg}$ generated MIMO PLC noises

Figure 4.24 presents the CDF of frequency domain correlation between a given measured MIMO PLC noise and its VAR(15)$_{socket}$ realization. Since VAR(15)$_{socket}$ realization is pertinent to a given socket so it is expected to achieve higher $\Psi_{i,j}$ than VAR(15)$_{avg}$ realization. This effect is clearly visible in the CDFs of Figure 4.24 and Figure 4.25. However, the difference is not significant. For N-PE and P-PE noises, P($\Psi_{i,j}$=0.5) corresponds to $\Psi_{i,j}$ of 0.92 and 0.85, for VAR(15)$_{socket}$ and VAR(15)$_{avg}$ respectively. This amounts to a difference of 7%. Similarly, for P-N noise, the difference is 8%. It can be inferred that the VAR(15)$_{avg}$ model can generate a noise which exhibits nearly similar spectrum as that of the measured MIMO PLC channel background noise.

3) Frequency Domain RMSE

The results for frequency domain RMSE are shown in Figure 4.26 and Figure 4.27. In Figure 4.26, we note that $\varepsilon_{rms,f}$ between a given MIMO PLC noise measurement and its VAR(15)$_{socket}$ realization ranges from 3 to 6 dB. Figure 4.27 shows the CDF of $\varepsilon_{rms,f}$ between MIMO PLC noise measurement and VAR(15)$_{avg}$ model. Here we note that for P(RMSE<50%), $\varepsilon_{rms,f}$ values vary between 4 and 6 dB. This is largely in agreement with the CDF of Figure 4.26 for P(RMSE>50%). However, in Figure 4.27, as we move beyond P(RMSE=50%), $\varepsilon_{rms,f}$ ranges between 6 to 16 dB. It can be argued that $\varepsilon_{rms,f}$ > 12 dB may be inacceptable (i.e. 6 dB or stated otherwise ± 3 dB more than the maxima of Figure 4.26), but this is the price of the simplicity of VAR(15)$_{avg}$ model. One method to reduce $\varepsilon_{rms,f}$ could be to select a higher order of VAR model.

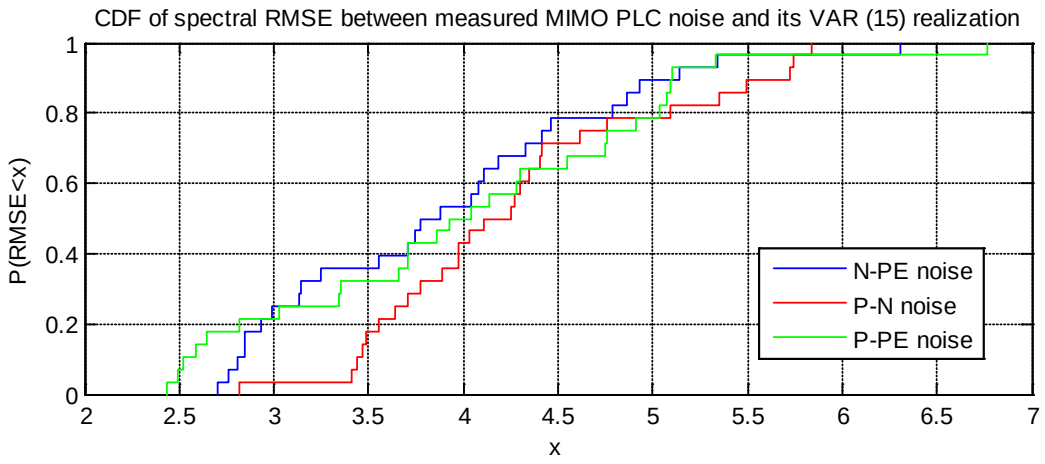

Figure 4.26. CDF of frequency domain RMSE between measured and $VAR(15)_{socket}$ generated MIMO PLC noises

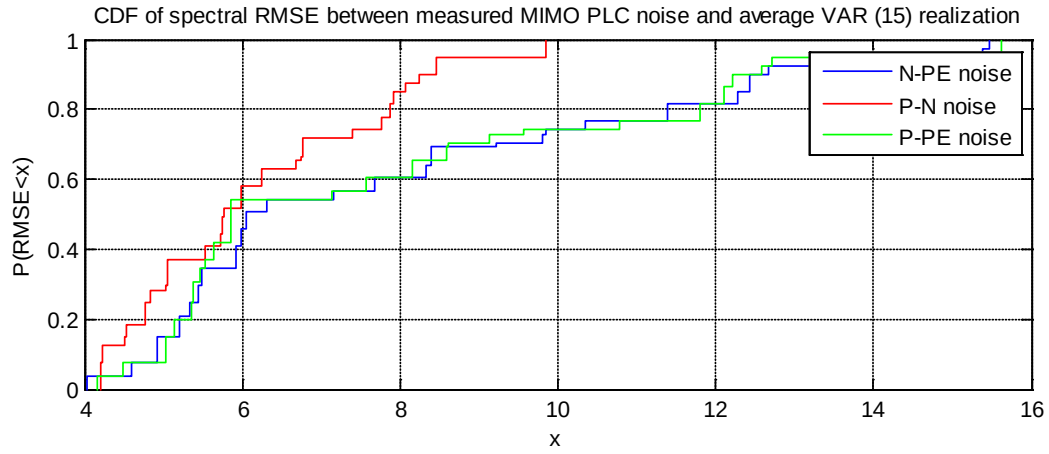

Figure 4.27. CDF of frequency domain RMSE between measured and $VAR(15)_{avg}$ generated MIMO PLC noises

5. Global system model simulation

A global communication system, as demonstrated in Figure 4.28, consists of a transmitter, the channel matrix, a receiver and the channel noise. In Chapter 3 we have proposed a model for the MIMO PLC channel matrix. In this chapter we have presented a complete time domain model for the MIMO PLC noise. It would be interesting to integrate both models to simulate a global MIMO PLC channel.

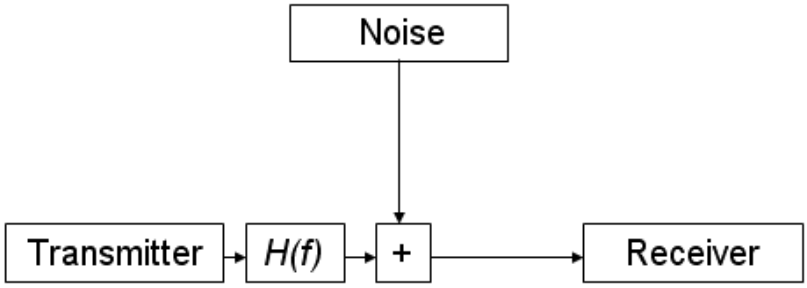

Figure 4.28. A PLC system model

For this purpose RMS delay spread is an appropriate parameter because it includes the effects of the channel impulse response as well as the noise. As mentioned earlier, the CDF of RMS delay spread of measured channels (Figure 3.7) shows more dispersal than that of the modeled channels (Figure 3.15).

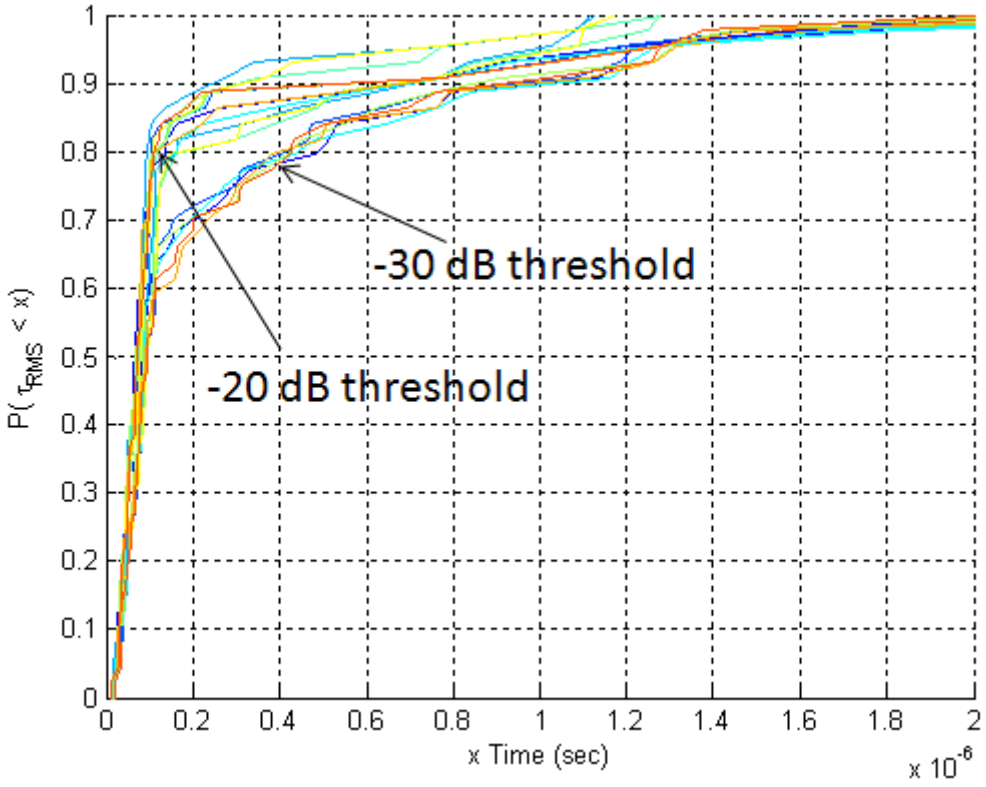

Figure 4.29. CDF of RMS delay spreads of MIMO PLC channels obtained by global system model simulation

This effect has been explained in Section 6.2 of Chapter 3. Adding the modeled noise to the modeled channel matrix should result in RMS delay spread similar to the measured channels. Figure 4.29 shows the CDF of RMS delay spread for MIMO PLC channels obtained by global system model simulation. The similarity between Figure 3.7 and Figure 4.29 demonstrates the global validity of the proposed MIMO PLC channel matrix and noise models.

6. Conclusions

In this chapter frequency domain and time domain models of the MIMO PLC background noise have been presented in the 2-150 MHz range. These models are the first ever MIMO PLC noise models.

The two frequency domain models presented in this chapter are inspired from two existing SISO PLC noise models: the OMEGA model and the Esmailian model. We designed the proposed models by using the measured MIMO PLC noises described in chapter 2. The parameters of the proposed MIMO PLC frequency domain noise models are extracted by fitting the measured MIMO PLC noises to the SISO PLC noise models. It has been illustrated that the frequency domain noise models based on extracted parameters satisfactorily capture the frequency dependent nature of the MIMO PLC background noise. The other important point is that the two models exhibit almost similar performance in accurately reproducing the experimental observations. However, the MIMO PLC noise model based on the OMEGA model is preferable because it uses one parameter less than the Esmailian model.

A detailed and comprehensive time domain model for MIMO PLC noise has also been presented in this chapter. This model is based on multivariate time series analysis. We have shown that the vector auto regressive model satisfactorily captures the mutual time domain correlations among the three constituent sequences of MIMO PLC noise. We have also demonstrated that the spectrum of the MIMO PLC noise generated by the VAR model closely matches the spectrum of the measured noise. In the future, the proposed noise model and the simulation techniques devised in this chapter will form the foundations of a complete digital communication model to assess the performance of comprehensive MIMO PLC transmission systems.

General conclusion

The work presented in this report is a contribution to the field of inhome power lines communication in a MIMO context. First of all the state of the art of the PLC technology is presented. It covers the historical evolution of the PLC technology. We have presented various standards of PLC technology developed over the years. The groups and governing bodies who prepare, inspect and regulate these standards are also introduced. The efforts of various international projects launched for the formulation of research activities and standardization is also mentioned. The role of the industrial groups and the telecom operators in the PLC eco-system is also included in this report. We have provided a brief introduction of the physical inhome PLC network. Major modeling methodologies for the inhome SISO PLC channels are briefly discussed. Various categories of the inhome PLC noises are discussed. After having covered the inhome SISO PLC channels we have discussed various MIMO techniques which are useful to enhance the inhome PLC channel capacity. In this context we have included the brief account of the existing works in the field of MIMO PLC.

First of all we have presented a detailed description of the measurements performed over various MIMO PLC channels during this thesis work. This includes various PLC networks which were selected for the measurements. The measurement setup, measurement equipment and the measurement methodology is mentioned in detail. Afterwards, we have presented the analysis of the measured PLC channel and noise data to obtain some preliminary results about the capacity gain achieved by the MIMO techniques. We observe that on average the capacity of a 2x2 MIMO PLC channel is almost twice the SISO PLC channel. The measurements also provided a first hand knowledge about the frequency dependent and multipath nature of the MIMO PLC channels. The analysis of the measured MIMO PLC noise has revealed the frequency dependent nature of the background noise. Moreover, we observe that the MIMO PLC noise sequences are correlated to each other to a certain degree.

The characterization and modeling of the MIMO PLC channels has been performed during the thesis work. For the characterization of the MIMO PLC channels we have defined some parameters such as channel correlation, RMS delay spread and coherence bandwidth. The statistics of these parameters are extracted from the data obtained in the above mentioned channel measurement campaign. For the modeling of

the MIMO PLC channels we have used a well known and widely accepted multipath PLC channel model as the basis. The attenuation parameters of our model are extracted from the measured data. The statistical properties of the extracted parameters are modeled in form of common statistical distributions. For the generation of the MIMO PLC channels we first generate a SISO PLC channel. The full 3x3 MIMO CTF matrix is obtained by introducing different phase shifts to the modeled SISO channel. We have validated the accuracy of our channel model by comparing the simulated channels with the measured ones.

During the course of this thesis work we have also proposed the MIMO PLC background noise models in the frequency domain as well as in the time domain. By analyzing the measured noise data we have observed the frequency dependent nature of the background noise. We have proposed two frequency domain background noise models based on two existing well known SISO models: the OMEGA noise model and the Esmailian noise model. As mentioned above, the MIMO PLC noises are correlated. To capture the correlation it is necessary to model the noise in the time domain. For this purpose we have visualized the ensemble of the MIMO PLC noises as a multivariate time series. We have used the vector auto-regressive formalism to model the MIMO PLC noises in the time domain. The accuracy of the proposed noise model is validated by comparing the time domain and the frequency domain correlations of the modeled noises to those of the measured ones.

We have also developed a global MIMO PLC channel model by incorporating the above mentioned channel and noise models. For this purpose, we add the modeled noise to the modeled CTFs. The validity of the global PLC model is verified by comparing the statistics of the RMS delay spread of the modeled channels to that of the measured channels.

The future PLC systems will have MIMO functionality. The models and simulation techniques devised during this thesis work are expected to from the foundations of a complete digital communication model that may be used to assess the performance of the MIMO PLC systems. Two international standards recently integrate the MIMO aspects to PLC: the ITU G.9963 standard, approved in December 2011, and the Homeplug AV2 standard, finalized in January 2012. This demonstrates that the MIMO functionality for PLC is highly topical, and shows that there is a need for realistic MIMO PLC channel and noise models to appropriately evaluate the performance of such systems. The EMC issues of the MIMO PLC systems are expected to be studied in detail and this aspect of the future PLC systems will be of particular interest for telecom service providers such as Orange. The ETSI is also

extremely interested to explore the potential of MIMO PLC systems and there is already significant research activity in the field of MIMO PLC channel and noise measurement and characterization. The definition of a MIMO PLC channel model in such standardization organizations would greatly help MIMO PLC system designers by serving as a common basis for the evaluation and comparison of system performance.

Publications

1. **Hashmat R., Pagani P., Chonavel T.** MIMO capacity of inhome PLC links up to 100 MHz. *Workshop on Power Line Communications, WSPLC*. 2009, pp. 4-6.
2. **Hashmat R., Pagani P., Zeddam A., Chonavel T.** MIMO communications for inhome PLC networks: measurements and results up to 100 MHz. *International Symposium on Power Line Communications and its Applications, IEEE ISPLC*. 2010, pp. 120-124.
3. **Hashmat R., Pagani P., Zeddam A., Chonavel T.** Measurement and analysis of inhome MIMO PLC channel noise. *Workshop on Power Line Communications, WSPLC*. 2010, pp. 56-60.
4. **Hashmat R., Pagani P. , Zeddam A., Chonavel T.** Time-reversal for EMC improvement in powerline communicatiosn. *Colloque Internationale et Exposition sur la compatibilité Electromagnétique CEM*. 2010.
5. **Hashmat R., Pagani P., Zeddam A., Chonavel T.** A Channel model for multiple input multiple output in-home power line networks. *International Symposium on Power Line Communications and its Applications, IEEE ISPLC*. 2011, pp. 35-41.
6. **Hashmat R., Pagani P., Chonavel T., Zeddam A.** A time domain model of background noise for inhome MIMO PLC networks. Submitted to *IEEE Transactions on Power Delivery*. 2011.
7. **Hashmat R., Pagani P., Chonavel T., Zeddam A.** Analysis and modeling of background noise for inhome MIMO PLC channels. *International Symposium on Power Line Communications and its Applications, IEEE ISPLC*. 2012.
8. **Pagani P., Hashmat R., Schwager A., Schneider D., Bäschlin W.** European MIMO PLC field measurements: noise analysis. *International Symposium on Power Line Communications and its Applications, IEEE ISPLC*. 2012.
9. **Hashmat R., Pagani P.** Pre-filtration of data signal transmitted over wired media. *Patent No. WO 2011/033217 A1, September* 2009.

10. **Pagani P., Hashmat R.** Noise mitigation method for multi-port transceiver. *Patent No. 10 57924, September* 2010.

Bibliography

[Amir05] **Amirshahi P., Kavehrad M.** Transmission channel model and capacity of overhead multiconductor medium voltage power line for broadband communications. *Consumer communications and networking conference, IEEE CCNC*. 2005. pp. 354-358.

[Avri08] **Avril G., Moulin F.** et al. Impulsive noise detection on masked carriers. *International Symposium on Power Line Communications and its Applications, IEEE ISPLC*. 2008, pp. 369-373.

[Avri08a] **Avril G.** Etude et optimisation des systèmes à courants porteurs domestiques face aux perturbations du réseau électriques. *Doctoral thesis at INSA of Rennes.* 2008, pp. 78-79.

[Baig03] **Baig S., Gohar N.** A discrete Multitone Transceiver at the Heart of the PHY Layer of an In-home Power Line Communication Local Area Network. *IEEE Communications Magazine.* 2003, pp. 48-53.

[Banw05] **Banwel T.** Accurate indoor residential PLC model suitable for channel and EMC estimation. *Signal processing advances in wireless communication, IEEE SPAWC.* 2005, pp. 985-990.

[Banw05a] **Banwel T., Galli S.** A novel approach to the modeling of the indoor power line channel part-I: circuit analysis and companion model. *IEEE Transactions on Power Delivery.* 2005, Vol. 20, No. 2, pp. 985-990.

[Barm06] **Barmada S., Musolino A., Raugi M.** Innovative model for time-varying power line communication channel response evaluation. *IEEE journal on selected areas in communications.* 2006, Vol. 24, No. 7, pp. 1317-1326.

[Beny03] **Benyoucef D.** A New Statistical Model of the Noise Power Density Spectrum for Powerline Communication. *International Symposium on Power Line Communications and its Applications, IEEE ISPLC*. 2003, pp. 136-141.

[Bour98] **Bourke P.** AutoRegression analysis (AR). *http://paulbourke.net/miscellaneous/ar/*. 1998.

[Brow99] **Brown P.** Power line communications- past present and future. *International Symposium on Power Line Communications and its Applications, IEEE ISPLC*. 1999, pp. 1-5.

[Cane02] **Canete J., Diez L.,** et al**.** Broadband modeling of indoor power-line channels. *IEEE Transactions on Consumer Electronics.* 2002, Vol. 48, No. 1, pp. 175-183.

[CEPC] **CEPCA** - Consumers Electronics Powerline Communication Alliance. Website http://www.cepca.org

[Chao08] **Chaouche H., Tlich M.,** et al. Deterministic modelling of powerline channels and impact of domestic appliances impedances. *International Symposium on Power Line Communications and its Applications, IEEE ISPLC*. 2008, pp. 1-5.

[CISP] **IEC CISPR Ed 6.0** – Information Technology Equipment. Radio disturbance characteristics – Limits and methods of measurements 2008-2009.

[Esma03] **Esmailian T.** Multi mega-bit per second data transmission over in-building power lines. *Doctoral thesis at University of Toronto*. 2003, pp. 21-22.

[ETSI] European Telecommunication Standard Institute. Website http://www.etsi.org/Website/Technologies/Powerline

[ETSIa] ETSI TR 101 562-1 V2.1.1, PowerLine Telecommunications (PLT); MIMO PLT; Part 1: Measurement Methods of MIMO PLT.

[ETSIb] ETSI TR 101 562-2 V2.1.1, PowerLine Telecommunications (PLT); MIMO PLT; Part 2: Setup and Statistical Results of MIMO PLT EMI Measurements.

[ETSIc] ETSI TR 101 562-3 V2.1.1, PowerLine Telecommunications (PLT); MIMO PLT; Part 3: Setup and Statistical Results of MIMO PLT Channel and Noise Measurements.

[Fosc98] **Foschini G., Gans M.** On the limits of wireless communications in a fading environment when using multiple antennas. *Wireless Personal Communications*. 1998, vol. 6, pp. 311–335.

[Gall04] **Galli S., Banwell T.** Modeling the indoor powerline channel: new results and modem design considerations.

[Gall06] **Galli S., Banwell T.** A deterministic frequency-domain model for the indoor power line transfer function. *IEEE Journal on Selected Areas in Communications.* 2006, Vol. 24, No. 7, pp. 1304-1316.

[Gall11] **Galli S., Scaglione A.** et al. For the grid and through the grid: the role of power line communications in the smart grid. *Proceedings of the IEEE.* 2011, Vol. 99, No. 6, pp. 998-1027.

[Giov03] **Giovaneli C., Farrel P.** et al. Improved space-time coding applications for power line channels. *International Symposium on Power Line Communications and its Applications, IEEE ISPLC*. 2003, pp. 50-55.

[Giov05] **Giovaneli C., Honary B.** et al. Space frequency coded OFDM system for multi wire power line communication. *International Symposium on Power Line Communications and its Applications, IEEE ISPLC*. 2005, pp. 191-195.

[Gotz04] **Gotz, M., Rapp, M., Dostert, K.** Power line channel characteristics and their effect on communication system design. *IEEE Communications Magazine.* 2004, pp. 78-86.

[Guil10] **Guillet V., Lamarque G.** Unified background model for power line communications. *International Symposium on Power Line Communications and its Applications, IEEE ISPLC*. 2010, pp. 131-136.

[Hash09] **Hashmat R., Pagani P.** et al. MIMO capacity of inhome PLC links up to 100 MHz. *Workshop on Power Line Communications, WSPLC*. 2009, pp. 4-6.

[Hash10] **Hashmat R., Pagani P.** et al. MIMO communications for inhome PLC networks: measurements and results up to 100 MHz. *International Symposium on Power Line Communications and its Applications, IEEE ISPLC*. 2010, pp. 120-124.

[Hash10a] **Hashmat R., Pagani P.** et al. Measurement and analysis of inhome MIMO PLC channel noise. *Workshop on Power Line Communications, WSPLC*. 2010, pp. 56-60.

[Hash11] **Hashmat R., Pagani P.** et al. A Channel model for multiple input multiple output in-home power line networks. *International Symposium on Power Line Communications and its Applications, IEEE ISPLC*. 2011, pp. 35-41.

[Hash11a] **Hashmat R., Pagani P.** et al. A time domain model of background noise for inhome MIMO PLC networks. Submitted to *IEEE Transactions on Power Delivery*. 2011.

[Hash12] **Hashmat R., Pagani P.** et al. Analysis and modeling of background noise for inhome MIMO PLC channels. Submitted to *International Symposium on Power Line Communications and its Applications, IEEE ISPLC*. 2012.

[He04] **He H., Cheng S.** et al. Analysis of reflection of signal transmitted in low voltage power line with complex wavelet. *IEEE Transactions on Power Delivery*. 2004, Vol. 19, No. 1, pp. 8-91.

[Home07] Home Plug Alliance, HomePlug AV specifications. Version 1.1, May 2007.

[HPA] HPA - HomePlug Power Alliance. Website http://www.homeplug.org

[IEEE] **IEEE P1901**, "*Draft Standard for broadband over power line networks: medium access control and physical layer specifications*", 2010

[ITU] **ITU-T G.9960**, "*Transmission systems and media, digital systems and networks*", technical paper, June 2010

[Jaga07] **Jagannathan S.**, **Cioffi M.;** Channel Models for Power Line Communications, *Stanford University Report at France Telecom 2007*

[Kim08] **Kim Y., Choi S.** et al. Closed form expression of Nakagami-like background noise in power line channels. *IEEE Transactions on Power Delivery*. 2008, Vol. 23, No. 3, pp. 1410-1412

[Kita08] **Kitayama M., Abe J.** Channel model simulation technique for power line communication. *IEEE International Symposium on Power Line Communications and Its Applications.* 2008, pp. 351-356.

[Kruz07] **Kruzevac S., Rapajic P.,** et al., Channel capacity estimation for MIMO systems with correlated noise. *IEEE International Symposium on Information Theory*. 2007.

[Kyri03] **P. Kyristi P., D. Cox D.,** et al. Correlation analysis based on MIMO channel measurements in an indoor environment. *IEEE Journal on Selected Areas in Communications*. 2003, vol. 21, no. 5, pp. 713-720.

[Lagu08] **Laguna G., Barron R.** Survey on Indoor Power Line Communication Channel Modeling. *Electronics, Robotics and Automotive Mechanics Conference.* 2008

[Liu08] **Liu L., Cheng T., Yanan L.** Analysis and modeling of multipath for indoor power line channel. *International conference on advanced communication technology.* 2008. pp. 1966-1969.

[Luo05] **Luo C., Cheng S.** et al. A non linear equalization method on multilayer perceptron of OFDM power line communication. *IEEE Transactions on Power Delivery.* 2005, Vol. 20, No. 4, pp. 2437-2442.

[Ma05] **Ma Y., So P.** et al. Performance analysis of OFDM systems for broadband powerline communications under impulsive noise and multipath. *IEEE Transactions on Power Delivery.* 2005, Vol. 20, No. 2, pp. 674-682.

[Ma10] **Ma Y., Liu K.** et al. Modeling the colored background noise for power line communication channel based on artificial neural network. *Wireless and optical communication conference.* 2010, pp. 1-4.

[Maen06] **Maenou T., Katayama M.** Study on signal attenuation characteristics in power line communications. *International Symposium on Power Line Communications and its Applications, IEEE ISPLC.* 2006, pp. 217-221.

[Mell06] **Mello R., Grivet M.** Modeling, simulation and estimation of PLC channels. *International Telecommunication Symposium.* 2006, pp. 201-206.

[Meng04] **Meng H., Chen S., Guan Y.** et al. Modeling of transfer Characteristics for the broadband power line communication channel. *IEEE Transactions on Power Delivery.* 2004, Vol. 19, No. 3, pp. 1057-1064.

[Meng07] **Meng J., Marble A**. Effective Communication Strategies for Noise-Limited Power-Line Channels. *IEEE Transactions on Power Delivery.* 2007, Vol. 22, No. 2, pp. 887-892.

[Mesc10] **Mescco A., Gautier F.** et al. Two models for stationary noise measured on indoor PLC lines up to 500 MHz. *Workshop on Power Line Communications, WSPLC.* 2010, pp. 22-25.

[Neum01] **Neumaier A., Schneider T.,** Estimation of parameters and eigenmodes of multivariate autoregressive models. *ACM Trans. On Math. Softwares.* 2001, vol.27, no.1, pp. 27-57.

[Oh08] **Oh M., Choi S.,** et al. A systemetic approach to analyzing multipath parameters from PLC channel response. *IEEE Transactions on Power Delivery*. 2008, Vol. 23, No. 4, pp. 1921-1929.

[Omega] **OMEGA**. hOME Gigabit Access [website], http://www.ict-omega.org/

[Omega08] **OMEGA Deliverable D3.2.** PLC Channel Characterization and Modelling. 2008, Seventh Framework Programme: Theme 3 ICT 213311.

[Omega08a] **OMEGA Deliverable D3.1.** PState of the art, application scenario and specific requirements for PLC. 2008, Seventh Framework Programme: Theme 3 ICT 213311.

[Oper] **OPERA** website http://www.ist-opera.org/

[Paga12] **Pagani P., Hashmat R.** et al. European MIMO PLC field measurements: noise analysis. *International Symposium on Power Line Communications and its Applications, IEEE ISPLC*. 2012.

[Phil99] **Phillips H.** Modelling of powerline communication channels. *International Symposium on Power Line Communications and its Applications, IEEE ISPLC*. 1999, pp. 14-21.

[Powe] **POWERNET** website, http://ist-powernet.org

[Prah12] **Praho B.** Study of cognitive electromagnetic compatibility in PLC context. *Doctoral thesis at University of Rennes-1*. 2012.

[Robl07] **Roblot S.** Characterization of electromagnetic coupling in the wired copper networks for optimized high data rate transmission. *Doctoral thesis at University of Limoges.* 2007, pp. 107-109.

[Roka05] **Roka R., Dlhan S.** Modeling of transmission channels over the low voltage power distribution networks. *Journal of Electrical Engineering.* 2005, Vol. 56, No. 9-10, pp. 1-9.

[Sabo05] **Sabolic D., Bazant A. Malaric R.** Signal propagation modeling in power-line communication networks. *IEEE Transactions on Power Delivery*. 2005, Vol. 20, No. 4, pp. 2429-2436.

[Schn08] **Schneider D., Speidel J.** et al. Precoded spatial multiplexing MIMO for inhome power line communication. *Global Telecommunications Conference, IEEE Globecom.* 2008, pp. 1-5.

[Schw11] **Schwager A., Schneider D.** et al. MIMO PLC: theory, measurements and system setup. *International Symposium on Power Line Communications and its Applications, IEEE ISPLC*. 2011, pp. 48-53.

[Shan49] **Shannon C.** Communication in the presence of noise. *Proceedings of the IRE.* 1949, Vol. 37, No. 1, pp. 10-21.

[Shiu00] **Shiu D., Foschini G.,** et al. Fading correlation and its effect on the capacity of multi-element antenna systems. *IEEE Transactions on Communications.*2000, vol. 48, pp. 2172-2178.

[Skrz07] **Skrzypczak A., Siohan P.** et al. Application of the OFDM/OQAM Modulation to Power Line Communications. *International Symposium on Power Line Communications and its Applications, IEEE ISPLC*. 2007, pp. 71-76

[Stad08] **Stadelmeier L., Schill D.** et al. MIMO for Inhome Powerline Communication. *7th International ITG Conference on Source and Channel Coding.* 2008, pp. 1-6.

[Tang03] **Tang L., So P.** et al**.** Charecterization and modeling of in building power lines for high speed data transmission. *IEEE Transactions on Power Delivery.* 2003, Vol. 18, No. 1, pp. 69-77.

[Tlic08] **Tlich M., Zeddam A.** et al. Indoor Power-Line Communications Channel characterization Up to 100 MHz—Part I: One-Parameter Deterministic Model. *IEEE Transactions on Power Delivery.* 2008, Vol. 23, No. 3, pp. 1392-1401.

[Tlil03] **Tlili F., Rouissi F.** Precoded for power line broadband communication. *International Symposium on Circuits and Systems, IEEE ISCAS*. 2003, pp. 109-112.

[Tone07] **Tonello A.** Wideband Impulse Modulation and Receiver Algorithms for Multiuser Power Line communications. *EURASIP Journal on Advances in Signal Processing*. 2007, pp.1-14.

[Tone09] **Tonello A., Zheng T.** Bottom-up transfer function generator for broadband PLC statistical channel modeling. *International Symposium on Power Line Communications and its Applications, IEEE ISPLC*. 2009, pp. 7-12.

[Tone10] **Tonello A., Versolatto F.** Bottom-up statistical PLC channel modeling – part II: inferring the statistics. *IEEE Transactions on Power Delivery.* 2010, Vol. 25, No. 4, pp. 2356-2363.

[UPA] Universal Power Association. Website http://www.upaplc.org.

[Vero11] **Veronesi D., Riva R.,** et al. Characetrization of in-home MIMO power line channels. *International Symposium on Power Line Communications and its Applications, IEEE ISPLC*. 2011, pp. 42-47.

[Vers10] **Versolatto F., Tonello M.** Analysis of the PLC channel statistics using a bottom-up random simulator. *International Symposium on Power Line Communications and its Applications, IEEE ISPLC*. 2010, pp. 236-241.

[Vers11] **Versolatto F., Tonello M.** An MTL theory approach for the simulation of MIMO power-line communication channels. *IEEE Transactions on Power Delivery.* 2011, Vol. 26, No. 3, pp. 1710-1717.

[Vers11a] **Versolatto F., Tonello M.** A MIMO PLC random channel generator and capacity analysis. *International Symposium on Power Line Communications and its Applications, IEEE ISPLC*. 2011, pp. 66-71.

[Xi03] **Xi S., Ren L.** et al. On capacity of MIMO systems in fading environments. *International Conference on Communication Technologies, IEEE ICCT*. 2003, Vol. 2. pp. 1152-1156.

[Yoon08] **Yoon S., Bahk S.** Rate adaptation scheme in power line communication. *IEEE International Symposium on Power Line Communications and Its Applications.* 2008

[Yous08] **Yousuf M., Rizvi S.** et al. Power line communication: an overview part II. *International Conference on Information and Communication Technologies, IEEE ICTTA.* 2008, pp. 1-6.

[Yu02] **Yu K., Otterson B.** Models for MIMO Propagation Channels, a Review. *Wiley Journal on Wireless Communications and Mobile Computing Special Issue on Adaptive Antennas and MIMO Systems.* 2002.

[Yu04] **Yu K., Bengtsson M.** et al. Modeling of wide-band MIMO radio channels based on NLoS indoor environment. *IEEE Transactions on Vehicular Technology.* 2004, Vol. 53, No. 3, pp. 655-665.

[Zhan04] **Zhang Z., Cheng S.** A novel multicarrier sugnal transmission systems over multipath channel of low voltage power line. *IEEE Transactions on Power Delivery.* 2004, Vol. 19, No. 4, pp. 1668-1672.

[Zimm02a] **Zimmerman M., Dostert K.** A multipath model for the powerline channel. *IEEE Transactions on Communications.* 2002, Vol. 50, No. 4, pp. 553-559.

[Zimm02b] **Zimmerman M., Dostert K.** Analysis of impulsive noise in broadband power line communications. *IEEE Transactions on Electromagnetic Compatibility.* 2002, Vol. 44, No. 1, pp. 249-258.

Appendix A. Working principle of Vector Network Analyzer (VNA)

The Vector Network Analyzer (VNA) is a measuring instrument based on the principle of a four pole network. It is used to measure the *S*-parameters which correspond to the signal reflection and transmission at different inputs and outputs of the four pole network [Avri08a].

- S_{11}: Reflection measured at port 1.
- S_{21}: Transmission measured from port 1 towards port 2.
- S_{22}: Reflection measured at port 2.
- S_{12}: Transmission measured from port 2 towards port 1.

Figure A.1 presents a simplified block diagram of the working principle of the VNA for the measurement of S_{11} and S_{21}.

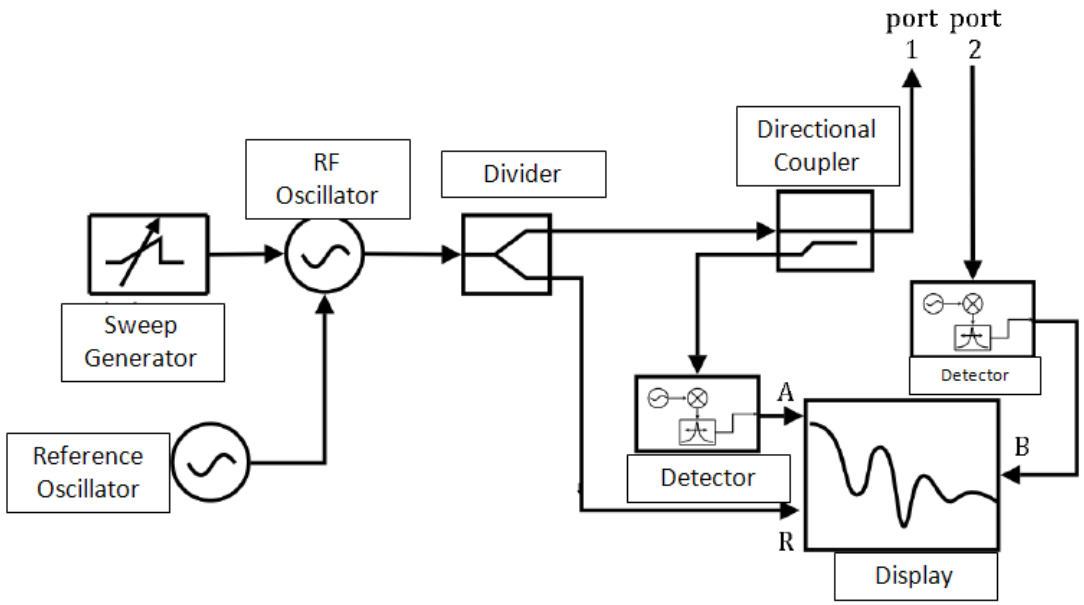

Figure A.1. Simplified working principle of the Vector Network Analyzer [Avri08a].

It can be observed in Figure A.1 that the VNA generates a Radio Frequency (RF) signal whose frequency varies with time. This effect is called frequency sweep. This signal is divided into two parts by a divider. One part of the signal is sent towards the port 1 of the VNA while the other part serves as a reference (R). At port 1, a

directional coupler allows to measure the reflected signal (S_{11} parameter). At port 2, the received signal corresponds to the signal transmission (S_{21} parameter). In both cases it is necessary to use a detector.

A VNA has some merits and demerits: it has a very good spectral sensitivity; however, due to the sweep effect it is not well adapted for temporal events of short duration.

Appendix B. Autoregression (AR) analysis

An autoregressive (AR) model is also known in the filter design industry as an Infinite Impulse Response (IIR) filter or an all pole filter. There is a memory feedback and therefore the model can generate internal dynamics [Bour98].
The AR model is defined as:

$$x_t = \sum_{i=1}^{N} a_i x_{t-1} + \varepsilon_t \qquad \text{(B.2.)}$$

Where a_i are the autoregression coefficients, x_t is the series under investigation, and N is the order or length of the filter which is generally very much less than the length of the series. The noise term or residue ε_t is almost always assumed to be Gaussian white noise. The current term of the series can be estimated by a linear weighted sum of the previous terms in the series. The weights are autoregressive coefficients.

The task in AR analysis is to derive the best values for a_i given a series x_t. The majority of methods assume the series x_t is linear and stationary. By convention the series x_t is assumed to be zero-mean.

A number of techniques exist for computing AR coefficients. The main two categories are least squares and Burg method. Within each of these there are a few variants. The most common least square method is based upon the Yule-Walker equations.

Let us consider an example of AR modeling. The data series x_t is 1000 sample obtained from a sum of 4 sinusoids and is shown in Figure B.1.

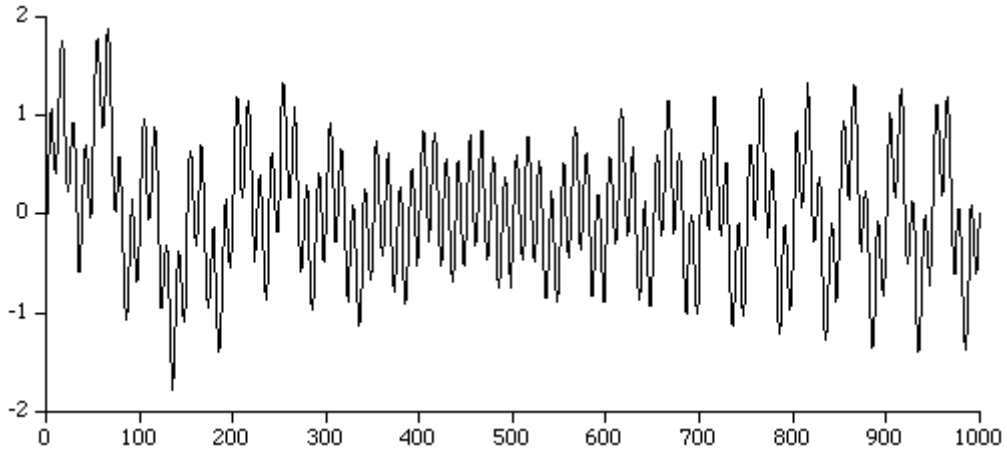

Figure B.1. Data series x_t for AR modeling.

While not particularly useful, an order 1 AR analysis gives a coefficient of 0.94. This is not surprising as it tells that by looking at only one term in the series the next term in the series is almost the same i.e. $x_{t+1} = 0.94\ x_t$. Table B.1. gives the coefficients for a number of model orders for the series shown in Figure B.1.

Order	Coefficients							
	1	2	3	4	5	6	7	8
1	0.941872							
2	1.826156	-0.938849						
3	2.753231	-2.740306	0.985501					
4	3.736794	-5.474295	3.731127	-0.996783				
8	4.259079	-6.232740	2.107323	2.969714	-1.421269	-2.591832	2.614633	-0.704923

Table B.1. AR coefficients for various model orders.

As the order increases the estimates generally improve. It is often useful to plot the RMS error between the series estimated by the AR coefficients and the actual series. Figure B.2 depicts the RMS error between actual x_t and its AR realization as a function of model order. It is evident from Figure B.2 that as the model order increases the RMS error initially drops sharply but then evens out [Bour98].

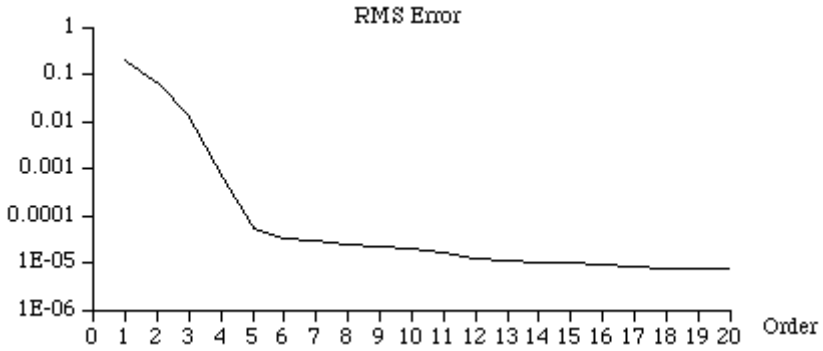

Figure B.2. RMS error between x_t and its AR realization as a function of model order.

There is no straightforward way to determine the correct model order. There are some formal techniques for choosing the model order e.g. the Akaike Information Criterion.